

**ROLE OF THE INOSITOL PHOSPHATASE INPP4B IN THE GENERATION OF
OVARIAN TERATOMAS**

by

Ashwini Balakrishnan

Bachelor of Technology, Anna University, 2006

Submitted to the Graduate Faculty of
the School of Medicine in partial fulfillment
of the requirements for the degree of
Doctor of Philosophy

University of Pittsburgh, School of Medicine

2012

UNIVERSITY OF PITTSBURGH

SCHOOL OF MEDICINE

This dissertation was presented

by

Ashwini Balakrishnan

It was defended on

November 28, 2012

and approved by

Marie C. DeFrances, MD PhD, Department of Pathology

Denise S. O'Keefe, PhD, Department of Urology

Urvashi Surti, PhD, Department of Pathology

William H. Walker, PhD, Department of Obstetrics, Gynecology and Reproductive Sciences

Thesis Director: J.Richard Chaillet, MD PhD, Department of Microbiology and Molecular

Genetics

Copyright © by Ashwini Balakrishnan

2012

**ROLE OF THE INOSITOL PHOSPHATASE INPP4B IN THE GENERATION
OF OVARIAN TERATOMAS**

Ashwini Balakrishnan, PhD

University of Pittsburgh, 2012

Teratomas are a unique class of tumors composed of ecto- meso- and endodermal tissues, all foreign to the site of origin. In humans, the most common teratoma is the ovarian teratoma. Not much is known about the molecular and genetic etiologies of these tumors. Female carriers of the *Tgkd* transgene are highly susceptible to developing teratomas. Ovaries of *Tgkd/+* hemizygous female mice exhibit defects in luteinization, with numerous corpora lutea, some of which contain central trapped, fully-grown oocytes. Genetically, *Tgkd* teratomas originate from mature oocytes that have completed meiosis I, suggesting that *Tgkd* teratomas originate from these trapped oocytes. The insertion of the *Tgkd* transgene 3' of the *Inpp4b* gene is associated with decreased expression of INPP4B and changes in intracellular PI3 Kinase/AKT signaling in follicular granulosa cells. An increase in granulosa cell proliferation and a decrease in apoptosis is also observed in *Tgkd* GCs of late stage follicles. Because INPP4B is not expressed in fully-grown wild-type or *Tgkd* oocytes, these findings suggest that enhanced activation of the PI3K/AKT pathway caused by the decrease in INPP4B in granulosa cells promotes an ovarian environment defective in folliculogenesis and conducive to teratoma formation.

TABLE OF CONTENTS

PREFACE	XIV
ACKNOWLEDGEMENTS.....	XV
NOMENCLATURE	XVII
1.0 INTRODUCTION	1
1.1 STRUCTURE OF THE OVARY AND FOLLICULAR MATURATION.1	
1.1.1 Structure of the ovary	1
1.1.2 Follicular maturation	2
1.2 THE HYPOTHALAMIC-PITUITARY-OVARIAN (HPO) AXIS AND FOLLICLE SELECTION.....	7
1.3 THE HUMAN MENSTRUAL AND MOUSE ESTROUS CYCLE	13
1.4 PROMINENT SIGNALING PATHWAYS DURING FOLLICULAR MATURATION IN THE OVARY.....	15
1.5 OOCYTE MATURATION AND EGG ACTIVATION.....	17
1.6 OVARIAN TERATOMA BACKGROUND & INCIDENCE.....	20
1.7 GENETIC ANALYSIS OF OTS AND TYPES OF ERROR.....	20
1.8 MOUSE MODELS OF OTS	23
2.0 MATERIALS AND METHODS.....	25
2.1 ANIMAL STUDIES	25

2.2	SNP GENOTYPING OF OTS	25
2.3	IDENTIFICATION OF <i>TGKD</i> INSERTION SITE	26
2.4	COLLECTION OF EMBRYOS.....	26
2.5	EMBRYONIC STEM CELL STUDIES	27
2.5.1	Embryonic stem (ES) cell derivation and generation of shRNA clones	27
2.5.2	IGF1 stimulation protocol in ES cells	28
2.5.3	ELISA analysis.....	28
2.6	OVARY STUDIES	28
2.6.1	Collection of ovaries and oocytes.....	28
2.6.2	Ovarian morphometric analysis and follicle counting	29
2.6.3	Oocyte parthenogenetic activation assay	29
2.6.4	Granulosa cell culture	29
2.6.5	Lentiviral transduction of GCs.....	30
2.6.6	Corpora lutea clearance assay	30
2.7	BISULFITE GENOMIC SEQUENCING.....	31
2.8	SOUTHERN BLOT ANALYSIS OF <i>Tgkd</i> METHYLATION	31
2.9	METHYLATION-SENSITIVE PCR.....	32
2.10	PCR FOR DETECTING NOVEL <i>Inpp4b</i> SPLICE ISOFORMS	32
2.11	SINGLE NUCLEOTIDE PRIMER EXTENSION (SNuPE) ANALYSIS	33
2.12	REAL TIME PCR.....	33
2.13	IMMUNOBLOT ANALYSIS	34

2.14	BrDU INCORPORATION ASSAY.....	35
2.15	IMMUNOHISTOCHEMISTRY	35
2.16	RNA <i>IN SITU</i> HYBRIDIZATION (ISH).....	36
2.17	STATISTICAL ANALYSIS.....	37
3.0	THE FVB- <i>Tgkd</i> STRAIN AS A MODEL TO STUDY OVARIAN TERATOMA FORMATION	38
3.1	INTRODUCTION: THE FVB- <i>Tgkd</i> MOUSE STRAIN	38
3.2	ADVANTAGES OF THE FVB- <i>Tgkd</i> OT MODEL	43
3.3	GENOTYPING OF THE <i>Tgkd</i> MOUSE	43
3.4	STRAIN SPECIFICITY OF THE OT PHENOTYPE	46
3.5	CONCLUSIONS	49
4.0	OVARIAN DEFECTS ASSOCIATED WITH THE <i>Tgkd</i> OT MODEL	50
4.1	AIMS OF THESE STUDIES	50
4.2	ABNORMAL FOLLICLE MATURATION AND LUTEINIZED FOLLICLE SYNDROME IN <i>Tgkd</i> OVARIES.....	51
4.3	ABSENCE OF PREMATURE OVARIAN FAILURE IN <i>Tgkd</i> MICE....	54
4.4	OVARIAN TERATOMAS ARISE FROM OOCYTES THAT HAVE COMPLETED MEIOSIS I	57
4.5	PARTHENOGENETIC ACTIVATION OF <i>Tgkd</i> OOCYTES	60
4.6	ROLE OF OOCYTE <i>Tgkd</i> METHYLATION IN DEVELOPMENT OF OTS 62	
4.7	ROLE OF <i>Tgkd</i> METHYLATION IN STRAIN SPECIFICITY OF OT PHENOTYPE.....	64

4.8	CONCLUSIONS	66
5.0	INSERTIONAL EFFECTS OF THE <i>Tgkd</i> TRANSGENE.....	67
5.1	AIMS OF THESE STUDIES	67
5.2	MAPPING OF THE <i>Tgkd</i> TRANSGENE INTEGRATION SITE	68
5.3	ALLELE SPECIFIC TRANSCRIPTION STUDIES ON GENES SURROUNDING <i>Tgkd</i> INSERTION.....	71
5.4	TRANSCRIPTIONAL PROFILE OF INPP4B IN EMBRYONIC BRAIN 84	
5.5	EFFECT OF <i>Tgkd</i> ON INPP4B EXPRESSION IN E13.5 EMBRYONIC BRAIN.....	87
5.6	IMPACT OF THE <i>Tgkd</i> INSERTION ON SPLICE ISOFORMS OF <i>Inpp4b</i>	91
5.7	CONCLUSIONS	92
6.0	ES CELL MODEL TO STUDY EFFECT OF <i>Tgkd</i> ON INPP4B AND DOWNSTREAM SIGNAL TRANSDUCTION PATHWAYS	94
6.1	AIMS OF THESE STUDIES	94
6.2	DEVELOPMENT OF THE <i>Tgkd</i> ES CELL MODEL AND METHYLATION STATUS OF <i>Tgkd</i> IN ES CELLS.....	95
6.3	EFFECT OF <i>Tgkd</i> ON INPP4B IN ES CELLS.....	102
6.4	EFFECT OF <i>Tgkd</i> ON PI3-KINASE/AKT ACTIVATION IN ES CELLS 106	
6.5	ASSESSING THE RELEVANCE OF INPP4B IN ES CELLS	109

6.6	EFFECT OF <i>Tgkd</i> ON METHYLATION OF SURROUNDING GENES	112
6.7	CONCLUSIONS	117
7.0	EFFECT OF <i>Tgkd</i> TRANSGENE ON INPP4B AND DOWNSTREAM PI3-KINASE/AKT PATHWAY IN TGKD OVARIES.....	118
7.1	AIMS OF THESE STUDIES	118
7.2	INPP4B EXPRESSION IN THE OVARY.....	119
7.3	REGULATION OF INPP4B IN <i>Tgkd</i> OVARIES DURING GONADOTROPHIN STIMULATION	124
7.4	REGULATION OF PI3-KINASE/AKT PATHWAY IN <i>Tgkd</i> OVARIES ON GONADOTROPHIN STIMULATION	129
7.5	FUNCTIONAL CONSEQUENCES OF HYPERACTIVATION OF PI3-KINASE/AKT SIGNALING IN <i>Tgkd</i> OVARIES.....	139
7.6	CONCLUSIONS	146
8.0	DISCUSSION AND FUTURE DIRECTIONS	147
8.1	EFFECT OF THE <i>Tgkd</i> TRANSGENE ON OT DEVELOPMENT.....	147
8.2	INPP4B AND REGULATION OF PI3K/AKT PATHWAY	148
8.3	ALTERED KINETICS OF THE PI3K/AKT PATHWAY LEADS TO OT DEVELOPMENT	149
8.4	EFFECT OF INPP4B LEVELS ON OT PHENOTYPE.....	151
8.5	EFFECT OF <i>Tgkd</i> ON INPP4B IN THE ES CELL MODEL	153
8.6	CELL AUTONOMOUS AND NON-AUTONOMOUS ORIGINS OF OTS	154

8.7 STRAIN SPECIFICITY OF THE OT PHENOTYPE	155
8.8 OT DEVELOPMENT IS A MULTIFACTORIAL PROCESS	156
8.9 FUTURE DIRECTIONS	160
APPENDIX A.....	163
APPENDIX B.....	165
APPENDIX C.....	170
BIBLIOGRAPHY.....	171

LIST OF TABLES

Table 1: Analysis of meiotic error in human OTs	22
Table 2: Analysis of viability of hemizygous and homzygous FVB- <i>Tgkd</i> embryos	42
Table 3: Strain specific effects on OT phenotype	48
Table 4: OTs arise from mature oocytes that have completed meiosis I.....	59
Table 5: Analysis of F1 hybrids for allelic specific expression	73
Table 6: Derivation of <i>Tgkd</i> ES cell lines and expected methylation state	97

LIST OF FIGURES

Figure 1: Stages of follicular maturation.....	7
Figure 2: Initial and cyclic recruitment of follicles	10
Figure 3: Positive and negative regulation in the HPO axis.....	12
Figure 4: Serum levels of hormones during the human menstrual cycle	14
Figure 5: Arrests in meiosis during follicular maturation	19
Figure 6: Structure and description of the <i>Tgkd</i> transgene	39
Figure 7: Genotyping of the <i>Tgkd</i> transgene in FVB- <i>Tgkd</i> mice	45
Figure 8: Defects in follicular maturation in <i>Tgkd</i> ovaries.....	54
Figure 9: Fertility studies with <i>Tgkd</i> mice.....	56
Figure 10: Parthenogenetic activation studies in wildtype and <i>Tgkd</i> oocytes.....	61
Figure 11: Role of oocyte <i>Tgkd</i> methylation in OT formation.....	63
Figure 12: <i>Tgkd</i> transgene methylation on the 129 background	65
Figure 13: Schematics of the location of the <i>Tgkd</i> insertion site on chromosome 8.....	70
Figure 14: Representation of the SNUPE Assay.....	74
Figure 15: Imprinting status of the <i>Tgkd</i> transgene in F1 hybrid progeny	76
Figure 16: SNUPE analysis of genes on chromosome 8 centromeric relative to <i>Tgkd</i>	80
Figure 17: SNUPE analysis of genes telomeric relative to the <i>Tgkd</i> insertion	84

Figure 18: Determining <i>Inpp4b</i> levels across gestation	86
Figure 19: Effect of <i>Tgkd</i> on <i>Inpp4b</i> levels in E13.5 embryos	90
Figure 20: PCR genotyping of ES cell lines and maintenance of <i>Tgkd</i> methylation	101
Figure 21: <i>Tgkd</i> induced effects on <i>Inpp4b</i> levels in ES cells	105
Figure 22: Kinetics of the PI3-Kinase/AKT pathway in <i>Tgkd</i> ES cell lines	108
Figure 23: shRNA-mediated downregulation of <i>Inpp4b</i> in mouse ES cells	111
Figure 24: CpG islands examined by HpaII-McrBC PCR	114
Figure 25: CpG island methylation in <i>Tgkd</i> ES cell lines	116
Figure 26: INPP4B expression in the ovary	120
Figure 27: <i>Inpp4b</i> expression in the adult wildtype ovary	123
Figure 28: <i>Inpp4b</i> expression in oocyte and GCs of PD30 ovaries	123
Figure 29: <i>Inpp4b</i> transcript and protein levels in wildtype and <i>Tgkd</i> ovaries	126
Figure 30: INPP4B expression in wildtype and <i>Tgkd</i> GCs	128
Figure 31: Role of INPP4B in regulation of the PI3K/AKT pathway	130
Figure 32: Activation of PI3K/AKT pathway in <i>Tgkd</i> ovaries on PMSG stimulation ...	132
Figure 33: Activation of PI3K/AKT pathway in <i>Tgkd</i> ovaries on HCG stimulation	135
Figure 34: Kinetics of PI3K/AKT activation in <i>Tgkd</i> oocytes and GCs	137
Figure 35: shRNA-mediated downregulation of INPP4B in wildtype GCs.....	138
Figure 36: Comparison of GC proliferation in wildtype and <i>Tgkd</i> ovaries.....	140
Figure 37: Comparison of apoptosis in wildtype and <i>Tgkd</i> ovaries	141
Figure 38: Persistence of corpora lutea in wildtype and <i>Tgkd</i> ovaries	143
Figure 39: FOXO1 localization in wildtype and <i>Tgkd</i> PD30 ovaries	145
Figure 40: Model of <i>Tgkd</i> induced OT formation	160

PREFACE

Chapters of this dissertation contain results from a peer reviewed published manuscript on which I am first author:

Ashwini Balakrishnan and J.Richard Chaillet. Role of the inositol polyphosphate-4-phosphatase type II *Inpp4b* in the generation of ovarian teratomas. *Developmental Biology*. Oct 16 2012. PMID: 23078915

ACKNOWLEDGEMENTS

I would first and foremost like to thank my thesis advisor Dr. Richard Chaillet for his constant support and encouragement during my graduate school years. He gave me the freedom to chose my research area, develop relevant hypotheses, troubleshoot hurdles and shape the direction of the project. With his guidance, I was able to design thoughtful experiments, which gave us exciting insights on the etiology of ovarian teratomas. Most importantly, the time spent in his lab has given me the confidence and ability to approach scientific problems in a rational and independent manner. Thank you Dr. Chaillet!

I thank my thesis committee Drs. Marie DeFrances, Denise O’Keefe, Urvashi Surti, William Walker and Jes Klarlund for all the advice and technical help, which helped make my project more tractable. They motivated me to pursue alternate hypotheses and helped me keep up my morale in the face of negative data. They always encouraged me to improve my technical skills and reasoning abilities, assets that will always remain with me. Thank you for all the advice in my thesis project and all my scientific endeavors. Many thanks to Dr. Anthony Zeleznik for an enormous amount of help with many difficult experiments.

I would like to thank several past and present members of the Chaillet lab for help with troubleshooting and discussions during experimental design. I thank Ben, our lab manager for helping me with numerous experiments, tolerating last minute orders for reagents and the much-needed coffee breaks. I would like to thank Ceci, who was a valuable guide during my initial years in the lab and taught me many of the techniques relevant to my project. Thank you, Kata for the help, encouragement and humor, which made us good-natured even when our experiments refused to co-operate. I also thank Ewa, Mohan and Dino for their advice. Many thanks to fellow grad students Erik and Jim for their help and sharing the Oohs and Aahs of grad school with me. Thank you Chaillet lab for a wonderful and friendly learning environment. I would also like to thank my classmates and friends for many fun-filled times after long days in lab. Special thanks to my friends Kristina and Revati for helping me stay positive and jovial when the times were tough.

I am grateful to my parents and my brother Karthik for their love, support and constant encouragement during my years in graduate school. My parents always encouraged me to dream big and follow my goals with great zeal. Last but not least, I thank grad school for introducing me to my husband Hetu. Life and graduate school has been a fulfilling experience with him. His scientific curiosity and excitement has always motivated me to be a better scientist.

“Sometimes our light goes out but is blown into flame by another human being. Each of us owes deepest thanks to those who have rekindled this light.” Albert Schweitzer

NOMENCLATURE

<i>Tgkd</i> mice – Hemizygous FVB- <i>Tgkd</i> mice	Cyclin-dependent kinase 1 – Cdk1
<i>Tgkd(m)/+</i> – Hemizygous <i>Tgkd</i> (maternal inheritance)	Myelin transcription factor 1 – Myt1
<i>Tgkd(p)/+</i> – Hemizygous <i>Tgkd</i> (paternal inheritance)	Cytostatic factor – CSF
<i>Tgkd/Tgkd</i> – Homozygous <i>Tgkd</i>	Anaphase promoting complex/cyclosome – APC/C
Ovarian teratoma – OT	Single nucleotide polymorphism – SNP
FVB/N – FVB	Embryonic stem cell – ES cell
C57BL/6 – B6	Insulin growth factor 1 – IGF1
129/Sv – 129	Germinal vesicle – GV
Primordial germ cells – PGC	Intra-peritoneal – IP
Embryonic day – E	Hematoxylin and eosin – H&E
Granulosa cell – GC	Short hairpin RNA – shRNA
Follicle stimulating hormone – FSH	Reverse transcription PCR – RT-PCR
Luteinizing hormone – LH	Untranslated region – UTR
Post natal day – PD	Single Nucleotide Primer Extension - SnuPE

Hypothalamic pituitary ovary – HPO	TATA-binding protein – TBP
G protein coupled receptor – GPCR	Beta glucuronidase – GUSB
Gonadotrophin-releasing hormone –GnRH	Bromodeoxyuridine – BrdU
Pregnant mare serum gonadotrophin – PMSG	Immunohistochemistry – IHC
Human chorionic gonadotropin – HCG	<i>In situ</i> hybridization – ISH
Cumulus enclosed oocyte – COC	Rous sarcoma virus – RSV
Small interfering RNA – siRNA	Long terminal repeat – LTR
Cyclic AMP – cAMP	Differentially methylated domain – DMD
Protein kinase A – PKA	Ovarian teratoma susceptibility – Ots
Phosphatidylinositol-3 kinase – PI3K	Phosphorylated-AKT – P-AKT
Acute transforming retrovirus thymoma – AKT	Phosphorylated-FOXO1 – P-FOXO1
Mitogen-activated protein kinase – MAP kinase	Pten – Phosphatase and tensin homolog
Epidermal growth factor – EGF	Maturation promoting factor – MPF
Forkhead box O - FOXO	Metaphase II arrested oocyte –MII oocyte

1.0 INTRODUCTION

1.1 STRUCTURE OF THE OVARY AND FOLLICULAR MATURATION

1.1.1 Structure of the ovary

The ovary is one of the primary organs of the female reproductive system. The ovary is a highly organized composite structure composed of germ cells (oocytes) and somatic cells (granulosa cells, thecal cells and stromal cells). The adult ovary is involved in 2 major processes: release of eggs (oocytes) for fertilization and production of the hormones estradiol and progesterone. The ovary fulfills 2 major objectives, which are generation of fertilizable ova and preparation of the endometrium for implantation of fertilized eggs through secretion of estradiol and progesterone.

Adult human ovaries are 2-5cm in length, 1.5-3cm in width and 0.5-1.5cm in thickness [1]. Paired ovaries lie on either side of the uterus in the pelvic cavity and are connected to the uterus by ovarian ligaments. The ovaries lie close to the posterior and lateral pelvic wall and are attached to the posterior surface by a peritoneal fold called the mesovarium. Blood vessels, nerves and lymphatics traverse the mesovarium and enter the ovary at the hilum. The ovary consists of 3 distinct regions, which are the outer cortex, inner medulla and hilum. The cortex consists of an outer layer of connective tissue called the tunica albuginea covered by a single layer of cuboidal germinal epithelium and an inner zone of ovarian follicles. The inner medulla is

composed of mainly vascularized stromal tissue. Blood vessels, nerves and lymphatics traverse the mesovarium and enter the ovary at the hilum [2]. The ovarian follicle is a basic functional unit of the ovary and consists of a single oocyte surrounded by somatic cells. Follicles at earlier stages of development lie adjacent to the tunica in an avascularized layer while more advanced growing follicles are present at the cortico-medullary border, where they are surrounded by stromal cells and vasculature.

1.1.2 Follicular maturation

During embryogenesis, the mammalian gonad develops between the coelomic epithelium and the mesonephros adjacent to the urogenital ridge. The gonad is designated as a bipotential or indifferent gonad at this stage as development is identical in the male and female lineage. The primordial germ cells (PGCs) migrate from the yolk sac into the indifferent gonad and can be identified as alkaline phosphatase-positive cells. Once the PGCs colonize the female gonad, they proliferate and differentiate into oocytes by entering meiosis by embryonic day 13.5 (E13.5) in the mouse. Development of germ cells into the male or female lineage depends on their interactions with the surrounding somatic cells. Before the formation of the ovarian follicle, the oocytes exist as germ cell clusters or nests due to incomplete cytokinesis after the mitotic proliferation of the PGCs. These germ cell nests break down to form primordial follicles consisting of a single oocyte arrested early in meiosis surrounded by a single layer of flattened squamous pregranulosa cells (Figure 1). Breakdown of the germ cell nests occur prenatally in humans and shortly after birth in the mouse [3]. The formation of primordial follicles is associated with massive apoptosis of germ cells resulting in a decline in this cell population in humans from 6 million to 1 million at birth. The primordial follicle serves as the quiescent

ovarian reserve and recruitment of ovarian follicles for subsequent maturation from this pool constantly depletes the ovarian supply of female germ cells. The two types of recruitment processes in the ovary are initial recruitment of primordial follicles from the quiescent pool and cyclic recruitment of small growing follicles for further maturation and ovulation [4]. The factors that initiate primordial follicle recruitment are not well understood but primordial follicles develop into primary follicles and this is marked morphologically by the differentiation of the squamous pregranulosa cells to cuboidal granulosa cells (GCs). This process is thought to be follicle stimulating hormone (FSH) independent, as these follicles do not possess FSH receptors [5, 6]. Follicle maturation involves 2 simultaneous processes, which are the growth of the oocyte and acquisition of additional layers of GCs. Primordial follicles develop into primary follicles, which develop into secondary follicles when they acquire an additional layer of GCs (Figure 1). Subsequent preantral folliculogenesis involves oocyte growth, acquisition of several layers of GCs and appearance of the outermost layer of thecal cells. Preantral follicles with more than 2 layers of GCs start expressing the FSH receptor, which is required during later stages of maturation. Preantral growth of the recruited follicles occurs 10-12 days after birth in the mouse [7]. Follicle development up until the preantral stage is considered gonadotrophin-independent as in mice deficient for the FSH receptor, healthy preantral follicles are observed but follicles do not progress beyond this stage of development [8]. However morphometric analysis of follicle numbers was not performed in this study and other mouse models with defective gonadotrophin production displayed lower numbers of healthy preantral follicles than controls with many preantral follicles depicting structural abnormalities [9-11]. Preantral folliculogenesis involves complex bidirectional communication between the oocyte and surrounding GCs. The oocyte relies on somatic GCs for growth and development, however the rate of follicular development is

determined by the oocyte. This was demonstrated in an experiment using reaggregated ovaries consisting of oocytes from postnatal day 12 (PD12) mice and somatic cells from ovaries from newborn mice [7]. These reaggregated ovaries showed accelerated folliculogenesis compared to control reaggregated ovaries, when both the somatic cells and oocytes were from newborn mice. The oocytes of PD12 ovaries were at a more advanced stage of growth hence were able to accelerate the rate of folliculogenesis compared to oocytes from newborn ovaries. Once the follicles acquire 3-6 layers of GCs, they acquire an additional outer layer of thecal cells. The theca can be divided into the theca interna and the theca externa, which serve different roles later in folliculogenesis. Maturation of the ovarian follicle from the primordial stage to the preantral stage is classified as the phase of initial recruitment as it can occur in the absence of the cyclical rise in gonadotrophin levels.

Further stages of ovarian follicle maturation and ovulation are dependent on the release of gonadotrophin hormones by the anterior pituitary and these stages of follicle maturation are designated as cyclic recruitment. The exact mechanism by which these hormones regulate follicle survival and selection is defined in the next section. A subset of the preantral follicles in the presence of the gonadotrophin FSH acquire multiple fluid-filled spaces, which eventually coalesce to form a single antral cavity. These antral follicles have 2 types of GCs, those that line the outer wall of the follicle called mural GCs and GCs that surround the oocyte called cumulus GCs (Figure 1) [12]. Mural GCs line the follicle wall and play a vital role in steroidogenesis and ovulation. Cumulus GCs are in close contact with the oocyte through connexin junctions and promote oocyte growth and developmental competence, while maintaining meiotic arrest of the oocyte. Depending on the species, one or more of the early antral follicles is able to promote its growth into the preovulatory stage and are known as graafian follicles. Graafian follicles are

known as dominant follicles as they not only are able to promote their growth but also are able to promote atresia of other early antral follicles [4]. The preovulatory follicle contains an oocyte competent to reenter meiosis and its formation precedes the rapid release or surge of the luteinizing hormone (LH). This surge triggers the completion of meiosis I in the oocyte, which then arrests in the metaphase II (MII) stage of meiosis [13]. The LH surge also triggers ovulation of the mature oocyte and the remnants of the follicles are converted into a steroidogenic structure called the corpus luteum. The GCs of the ovarian follicle show a high rate of proliferation from the preantral stage [14]. Transformation of the preovulatory follicle into the corpus luteum involves cell cycle exit and terminal differentiation of GCs and thecal cells into non-proliferative luteal cells [15]. The main function of the corpus luteum is the production of progesterone, which is required for the initiation and maintenance of pregnancy [2]. In summary, the primordial follicle undergoes a process of initial and cyclical recruitment and matures through the primary, secondary, preantral, antral and preovulatory stages prior to ovulation. The adult ovary is heterogenous organ and multiple follicles in different stages of maturation are observed simultaneously in the ovarian cortex. Pedersen and Peters suggested a more robust classification of ovarian follicles at different stages of maturation, based on the number of GCs present at each stage of maturation (Figure 1) [16].

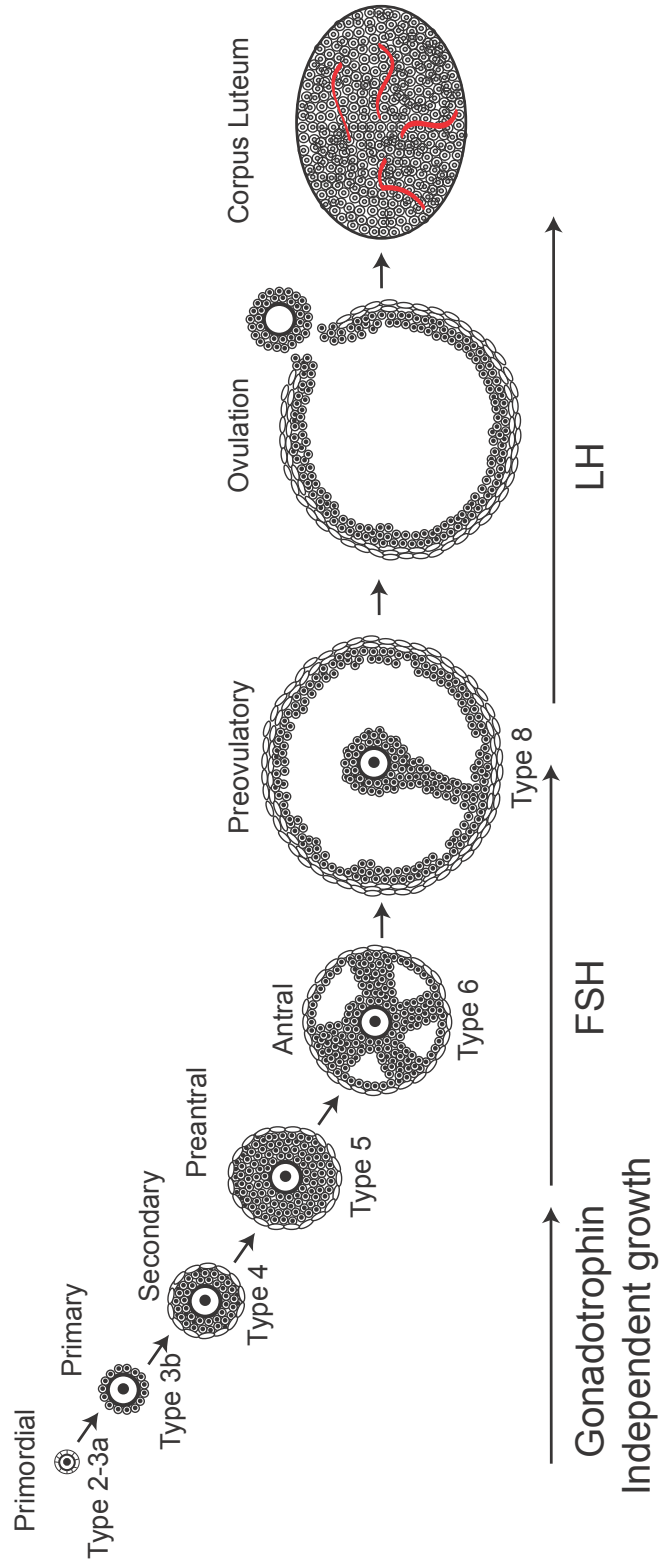


Figure 1: Stages of follicular maturation

The various stages of follicle maturation from primordial follicle recruitment to ovulation and corpus luteum formation are represented in the above figure. The development of the follicle up to the preantral stage is considered gonadotrophin independent. The gonadotrophin hormone FSH is required for acquisition of the antrum and subsequent maturation, while the LH surge is required for ovulation and corpus luteum formation. Type 2 - Type 8 represent the Pedersen and Peters classification [16].

1.2 THE HYPOTHALAMIC-PITUITARY-OVARIAN (HPO) AXIS AND FOLLICLE SELECTION

The selection and survival of early antral follicles to the preovulatory stage is mediated by hormones secreted by the hypothalamus, the anterior pituitary and the ovaries, which play a very vital role in successful ovulation of the oocyte [17, 18]. Because this process is associated with cyclical changes in levels of hormones, the process is considered the cyclical stage of follicle recruitment (Figure 2) [4].

The primary event in the HPO axis in the process of follicle maturation is the pulsatile release of a decapeptide called gonadotrophin-releasing hormone (GnRH) by GnRH secreting-neurons in the hypothalamus [19]. The pulsatile release of GnRH causes the pulsatile release of 2 gonadotrophins from the anterior pituitary namely FSH and LH. The pulsatile nature of GnRH is

important as continuous levels of GnRH during early follicular maturation causes desensitization of the receptors and cessation of FSH and LH production [20, 21]. FSH and LH are glycoprotein hormones consisting of non-covalently bonded α and β subunits. They share a common α subunit but possess unique β subunits, which confer receptor specificity [19]. The receptors of FSH and LH are G-protein coupled receptors (GPCR) with 7 transmembrane domains. The pulsatile generation of GnRH appears to favour the rise in FSH levels during early follicular maturation over LH and this phenomenon may be regulated by the frequency of GnRH release by the hypothalamus [22, 23]. The increase in FSH levels recruits a cohort of early antral follicles to escape atresia and progress in follicular maturation [4]. In humans, one of the follicles manages to grow faster than the rest of the cohort and the reason for the growth advantage is not well understood. This follicle, which is known as the dominant follicle is observed to have an abundance of FSH receptors and abundant well-developed vasculature in the thecal layers [24, 25]. Cells in the theca interna of the dominant follicle have LH receptors and are steroidogenic in nature. The thecal cells respond to LH by upregulating enzymes involved in steroid production and are involved in the production of androstenedione. GCs in the dominant follicle produce the enzyme aromatase (CYP19A1) and convert the secreted androgen from the thecal cells into estradiol [26]. Therefore, the increase in serum FSH seen in the early follicular phase is followed by an increase in the levels of serum estradiol and inhibins produced by the GCs of the dominant follicle. Increasing levels of estradiol exert a negative feedback on the production of FSH and LH from the pituitary and on the pulsatile secretion of GnRH from the hypothalamus [27]. This feedback inhibition by estradiol causes a drop in the levels of serum FSH. FSH acts as a survival factor during late antral folliculogenesis and a drop in FSH levels causes atresia of the recruited antral follicles. The dominant follicle is sensitive to lower levels of FSH possibly due to the

abundance of FSH receptors and the GCs of the dominant follicle begin to express LH receptors [28]. The estradiol produced by the dominant follicle also induces FSH receptor expression in the GCs and promotes follicular growth in the dominant follicle through its mitogenic activity and stimulation of local growth factors. Through these mechanisms, the dominant follicle is able to promote its own follicular growth in low FSH conditions and induce atresia in the other recruited antral follicles. In polyovulatory species such as rodents, the only difference in the mechanism of follicle selection is the lowering of the FSH threshold by the negative feedback through estradiol [4]. Lower levels of negative feedback in polyovulatory species allow multiple follicles to become dominant and develop to the preovulatory stage.

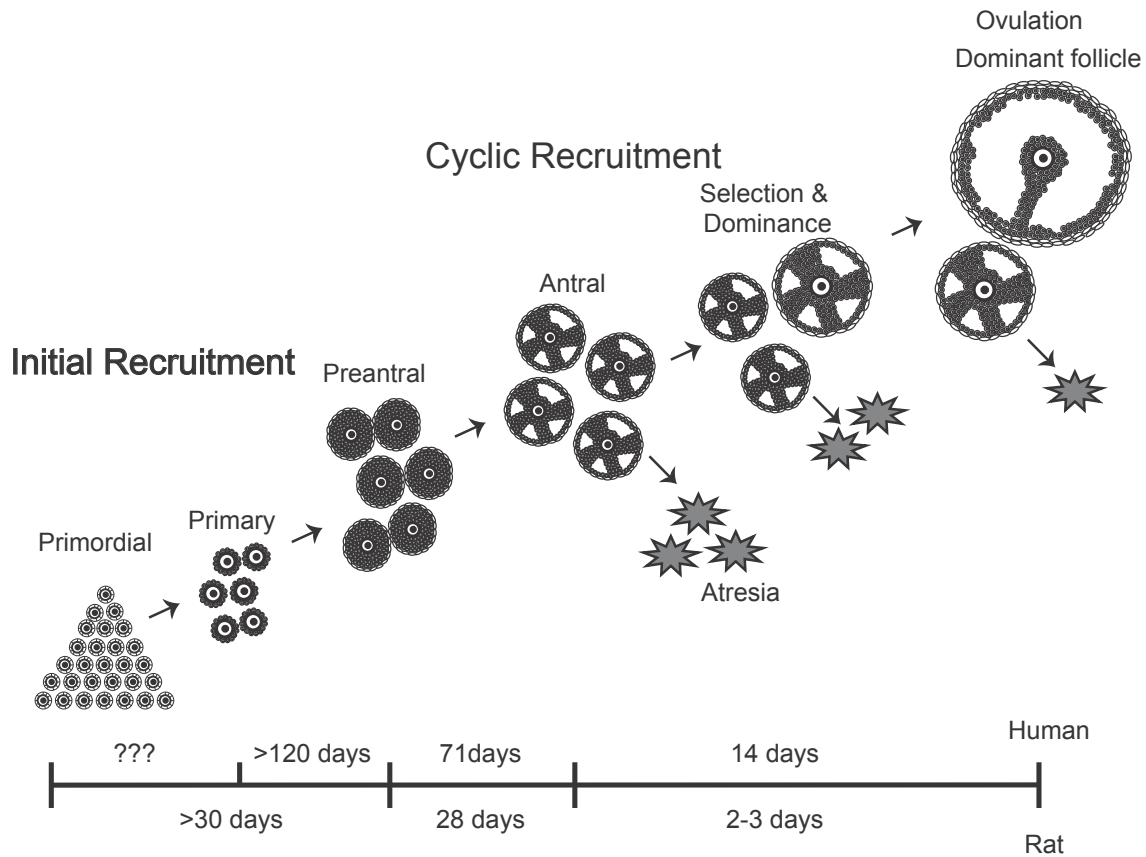


Figure 2: Initial and cyclic recruitment of follicles

The initial and cyclic recruitment phases are represented in the above figure. Initial recruitment of follicles is continuous and independent of the cyclical gonadotrophin surges and involves primordial recruitment to early antral follicle formation. The cyclic recruitment is affected by the cyclic changes of FSH, which induce the processes of dominant follicle selection, non-dominant follicle atresia and ovulation of the dominant follicle. Adapted from [4].

There is a steady increase in estradiol production during the growth of the preovulatory follicle, which reaches a peak just before the LH surge. The high level of estradiol produced by a mature preovulatory follicle with a meiotically competent oocyte acts as a positive feedback on GnRH production causing a continuous surge of GnRH production from the hypothalamus [29]. This GnRH surge is followed by a preovulatory surge in LH levels, which is responsible for initiating the process of ovulation [30]. The LH surge stimulates a series of ovarian gene expression cascades resulting in the production of inflammatory mediators such as prostaglandins and proteolytic enzymes, which cause degradation of the perfollicular matrix of the follicle [3]. The LH surge also triggers the oocyte to complete meiosis I, and the oocyte is ovulated through the ruptured follicular wall. The basal lamina between the GCs and thecal cells breaks down and the vessels in the thecal layer invade the previously avascular GC zone of the follicle. The GCs and thecal cells exit the cell cycle and differentiate into steroidogenic luteal cells, which produce estrogen and progesterone in the newly formed corpus luteum [31]. The progesterone and estradiol produced by the corpus luteum suppresses FSH and LH secretion by the pituitary [18]. In the absence of pregnancy, regression of the corpus luteum in the late luteal phase causes a decrease in progesterone levels allowing an increase in FSH production by the pituitary. This paves way for a new cycle of folliculogenesis causing cyclic recruitment of a new batch of antral follicles. In summary, the hormones of the HPO axis control the phases of follicle maturation and the stage of follicle maturation can be identified by the profile of these hormones (Figure 3).

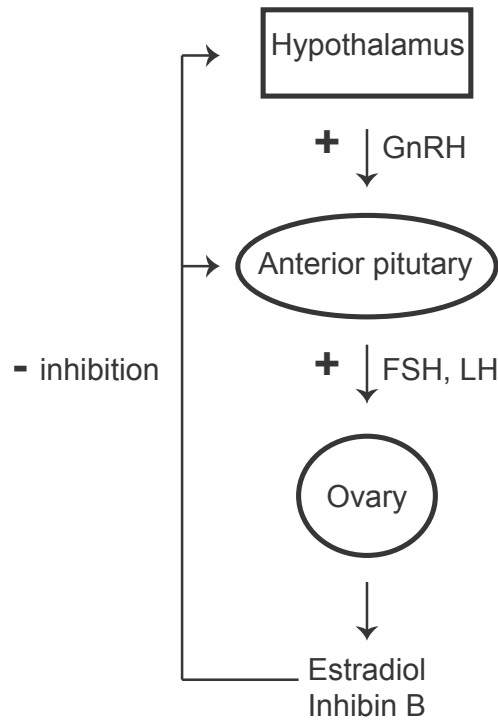


Figure 3: Positive and negative regulation in the HPO axis

The HPO axis plays a major role in the cyclic recruitment of follicles and follicle selection. The hypothalamus secretes GnRH, which induces secretion of FSH and LH from the pituitary. FSH and LH stimulate estradiol production by the GCs of the dominant follicle. Estradiol inhibits the production of FSH and LH, lowering serum FSH levels and promoting atresia in non-dominant antral follicles dependent on FSH for survival.

1.3 THE HUMAN MENSTRUAL AND MOUSE ESTROUS CYCLE

The menstrual cycle in women illustrates the hormonal changes that take place during the process of cyclic follicle recruitment, selection, ovulation and corpus luteum formation (Figure 4). In terms of follicular development, the menstrual cycle is divided into the follicular phase and the luteal phase [32]. The luteal phase is marked by the preovulatory LH surge, which results in ovulation of the oocyte and corpus luteum formation. The corpus luteum produces progesterone and estrogen, which suppress levels of FSH and LH during the luteal phase [4]. Regression of the corpus luteum causes a decrease in progesterone and estrogen levels in the transition between the luteal and follicular phase, which results in an increase in FSH levels in the early follicular phase. Progression through the follicular phase involves follicle maturation and a subsequent increase in estradiol levels and decrease in FSH levels during the process of follicle selection.

The menstrual cycle can also be classified into the menstrual, proliferative and secretory phases based on the lining of the endometrium, which is highly sensitive to ovarian steroid hormones [32]. The most luminal layer of the endometrium called the functionalis is thickened and sloughed off during the menstrual phase due to low levels of estradiol, which coincides with the luteal follicular transition and early follicular phase. The next phase of the cycle is termed as the proliferative phase as the endometrial layer thickens and has proliferation of stromal cells and glands due to the high levels of estradiol during the mid ovarian follicular phase. The luteal phase of follicle maturation is known as the secretory phase as high levels of progesterone cause production of glycogen and mucus, when the endometrium becomes decidualized and receptive to the fertilized embryo. In the absence of pregnancy, there is a drop in progesterone and estrogen levels leading back to the menstrual phase of the cycle (Figure 4).

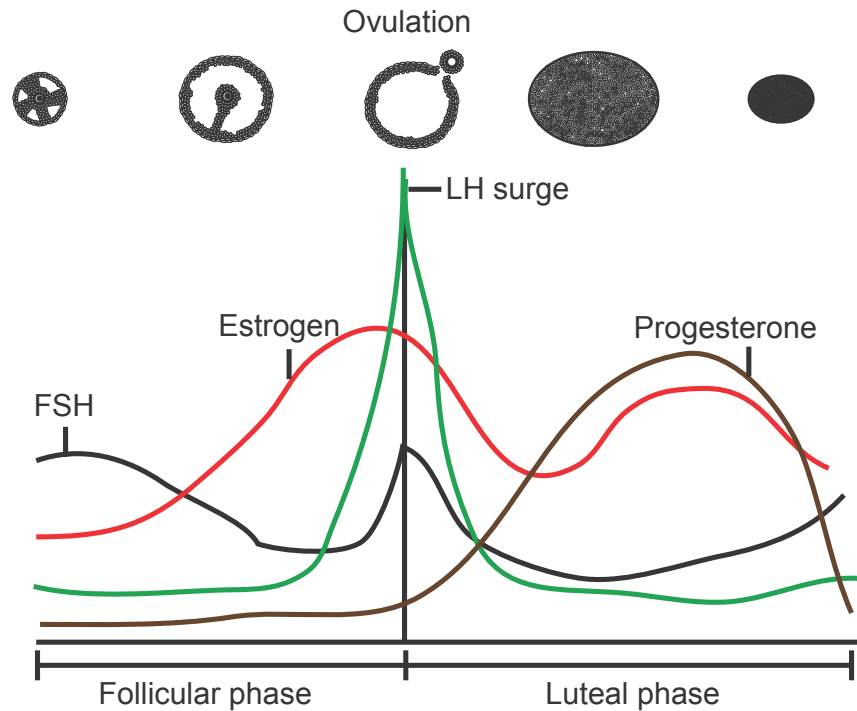


Figure 4: Serum levels of hormones during the human menstrual cycle

The level of different hormones during the menstrual cycle is represented in the above diagram. In the early follicular phase, a rise in FSH levels promotes follicle maturation and increase in estrogen levels, which suppresses the levels of FSH. After the midcycle LH surge, ovulation occurs and the corpus luteum is formed. Progesterone and estrogen secretion by the corpus luteum suppress FSH and LH levels. Regression of the corpus luteum at the end of the luteal phase causes a rise in FSH levels. Adapted from [33].

The main difference between the menstrual cycle and the estrus cycle is the reabsorption of the endometrium in the absence of pregnancy in the estrous cycle. The mouse estrous cycle is 4-6 days in length and consists of 4 stages [34]. The proestrous stage is the first stage when a new batch of follicles reach maturity in the ovarian follicle and serum estrogen levels rise. The estrous stage involves the final stage of selection and ovulation of the fully mature oocytes. The estrous stage is when the female is maximally receptive to the male and estrus begins after midnight lasting 6-8 hours on standard light-dark cycle. Metestrus is the phase during corpora lutea formation and when the mature egg moves through the oviduct and the uterus. If pregnancy does not occur, diestrus is the phase when unfertilized eggs are eliminated and the corpora lutea regress. The proestrous and estrous phase constitute the follicular phase of ovarian maturation while the metestrus and diestrus phases comprise of the luteal phase. The period of gonadotrophin induced cyclic recruitment and follicle selection takes 2-3 days in mice (Figure 2). The process of follicular maturation can be mimicked to induce ovulation in immature mice by single precisely timed intraperitoneal injections of pregnant mare serum gonadotrophin (PMSG) and Human chorionic gonadotropin (HCG), which are analogs of FSH and LH respectively with a long half-life [35].

1.4 PROMINENT SIGNALING PATHWAYS DURING FOLLICULAR MATURATION IN THE OVARY

Numerous transcription factors and signal transduction pathways are involved during the entire process of folliculogenesis from the primordial stage to the formation of the corpus luteum [3, 36]. FSH binds to its receptor in GCs, which is a GPCR and activates a classical adenylyl cyclase/

cAMP/PKA signal transduction pathway that directly regulates many target genes such as aromatase, inhibin and the LH receptor. FSH also activates independently or through cAMP mediated mechanisms many signal transduction molecules such as PI3-kinase/AKT, SRC, RAS and MAP kinase and their downstream pathways [36, 37]. FSH induces a pro-proliferative pathway in GCs, whereas LH induces cell cycle exit. LH binding to the LH receptor also stimulates PKA, PI3K/AKT, RAS signaling cascades, which are critical for ovulation. The LH surge triggers release of EGF-like factors, which is critical for cumulus cell expansion and ovulation [3, 36]. The LH surge turns off the FSH gene expression program in preovulatory GCs and turns on genes controlling matrix formation and inflammation.

One of the primary signal transduction pathways activated in GCs by FSH is the phosphatidylinositol-3 kinase (PI3K)/acute transforming retrovirus thymoma (AKT) signal transduction pathway. The PI3K/AKT pathway plays a vital role during many stages of folliculogenesis. The PI3K/AKT pathway regulates PGC migration, survival and primordial follicle recruitment [38-40]. The pathway has also been shown to be critical for gonadotrophin mediated-GC differentiation, cumulus cell expansion and resumption of oocyte meiosis [41-45]. This pathway is necessary but not sufficient for the induction of many FSH target genes in GCs such as LH receptor, 3 β -hydroxysteroid dehydrogenase, aromatase, and inhibin [44]. One of the main functions of this pathway in GCs is to promote G1/S phase transition in the cell cycle. Activation of the PI3K/AKT pathway promotes phosphorylation and degradation of the transcription factor FOXO1 relieving transcriptional repression on the S phase Cyclin D2 [46]. An increase in Cyclin D2 levels is seen after PMSG stimulation, while Cyclin D2 null ovaries depict defective GC proliferation and block in folliculogenesis [47]. Deletion of the *Pten* (negative regulator of PI3K/AKT pathway) gene in GCs led to hyperactivation of AKT on

gonadotrophin stimulation in GCs [48]. Increased phosphorylation of AKT was associated with degradation of FOXO1, higher levels of Cyclin D2 and an increase in GC proliferation in this model. This was associated with increased rate of ovulation and litter sizes from females with *Pten*^{-/-} GCs. The PI3K/AKT pathway also appeared to play a role in corpora lutea clearance in this model as persistent non-functional corpora lutea were observed in females with *Pten*^{-/-} GCs. In summary, the PI3K/AKT pathway is one of the primary signal transduction pathways that promote the proliferative effects of FSH in GCs. Components of the PI3K/AKT pathway are examined in detail in this thesis.

1.5 OOCYTE MATURATION AND EGG ACTIVATION

During the process of folliculogenesis, oocytes arrest early in meiosis in the diplotene stage prior to completion of meiosis I in the embryonic gonad around E14.5 (Figure 5). The oocyte acquires competence to resume meiosis at the antral stage due to achieving a threshold in the accumulation of the complex maturation promoting factor (MPF) complex, which consists of the proteins CDK1 and cyclin B [49]. The oocyte resumes meiosis only after the LH surge, hence this complex is maintained in the inactive state in the antral follicle. It is known that the follicular milieu specifically the mural GCs maintain meiotic arrest of the oocyte as removal of cumulus enclosed oocytes (COCs) from antral follicles causes meiotic resumption of the oocyte. Further high cAMP levels in oocytes are required to maintain meiotic arrest as phosphodiesterase inhibitors prevent a decrease in intra-oocyte cAMP levels and meiotic resumption [50]. The activity of CDK1 of MPF is negatively regulated by phosphorylation on Threonine 14 and Tyrosine 15 residues by the protein kinases WEE1/MYT1 [3, 51]. The phosphatase CDC25

dephosphorylates these residues thereby activating CDK1. During meiotic arrest, high cAMP levels in the oocyte activate PKA, which phosphorylates CDC25 and sequesters it in the cytoplasm in association with the protein 14-3-3 [52]. The LH surge causes a decrease in intra-oocyte cAMP levels resulting in dephosphorylation of CDC25. The CDC25 phosphatase activates CDK1 causing activation of MPF and reentry into meiosis. The first morphological change in the oocyte is the breakdown of germinal vesicle (GV) or nuclear membrane followed by asymmetric division of the cytoplasm and extrusion of the first polar body. A decline in MPF activity is required for progression into anaphase and telophase of meiosis I and increase in MPF levels is seen at metaphase II [53].

After completion of meiosis I, the ovulated oocyte is arrested at metaphase II due to the activity of the cytostatic factor (CSF). The MOS serine/threonine kinase is a vital component of CSF and causes oocyte metaphase II arrest by stabilizing MPF [54]. CSF stabilizes MPF by inhibiting the E3 ubiquitin ligase anaphase promoting complex/cyclosome (APC/C), which targets cyclin B for degradation [55]. Oocytes from *mos*^{-/-} mice demonstrate an inability to maintain metaphase II arrest and thereby undergo parthenogenetic cleavage [56, 57]. The oocyte completes the final stage of meiosis after fertilization, after introduction of phospholipase C into the oocyte cytoplasm by the sperm [55, 58]. This triggers calcium oscillations in the oocyte activating APC/C leading to cyclin B degradation and completion of meiosis.

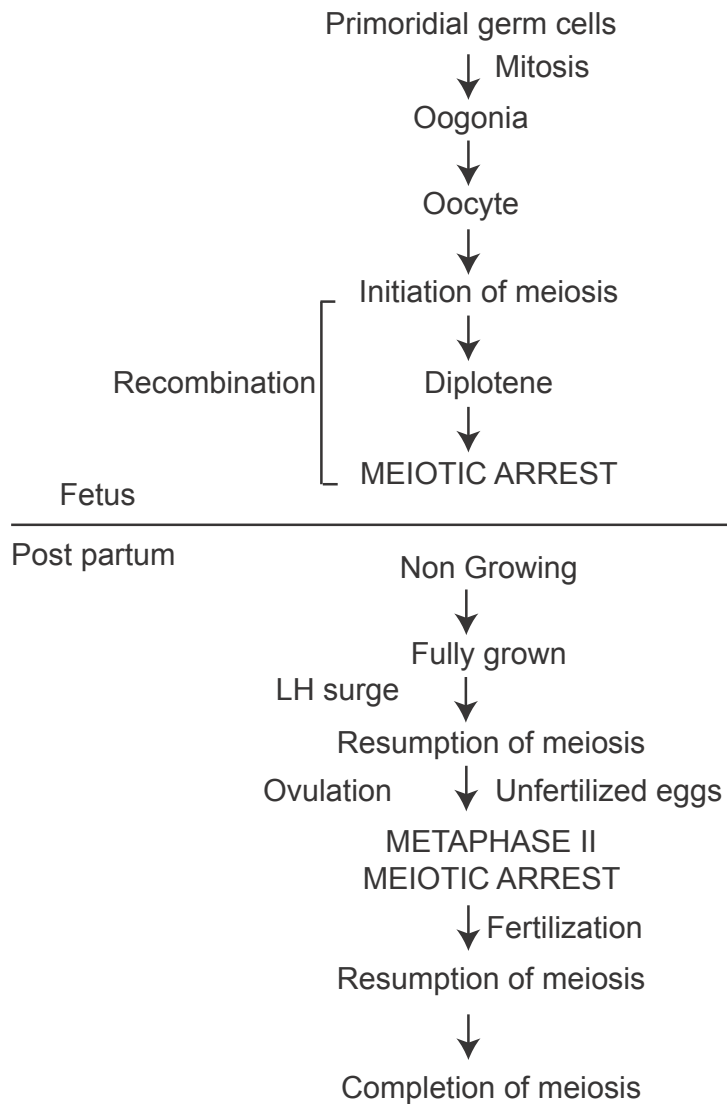


Figure 5: Arrests in meiosis during follicular maturation

The landmark phases in oocyte maturation are represented. Oocytes arrest in meiosis I prior to birth and resume meiosis in the preovulatory follicle after the LH surge. Following completion of meiosis I, the oocyte arrests at metaphase II and completes meiosis after fertilization. Adapted from [19].

1.6 OVARIAN TERATOMA BACKGROUND & INCIDENCE

Ovarian teratomas (OTs) are tumors of the ovary derived from non-ovulated female germ cells that have undergone parthenogenetic activation and display a disorganized pattern of cellular differentiation [59, 60]. Human OTs are relatively common, constituting 95% of all ovarian germ cell tumors [60]. Most OTs are benign but a small percentage (1-2%) transform into malignant tumors [61]. OTs contributed to 1.5% of the invasive ovarian cancer cases in the United States between 2004 and 2008 [62]. OTs are also seen at a low frequency in other mammalian species, including the mouse [63]. Most OTs are benign and are composed of differentiated ectodermal, mesodermal and endodermal tissues, proportions varying from teratoma to teratoma. Immature OTs contain undifferentiated cells (primarily immature neuroepithelium or embryonal carcinoma cells) in addition to the differentiated tissues and have malignant potential.

1.7 GENETIC ANALYSIS OF OTS AND TYPES OF ERROR

Human OTs arise due to the parthenogenetic activation of an oocyte caused by errors in meiosis or initiation of OT formation at a follicular stage prior to the resumption of meiosis. Oocytes as described are arrested in prophase of meiosis I until ovulation and are arrested in metaphase II until fertilization. Five mechanisms have been proposed to explain the origin of human OTs. These mechanisms can be distinguished by analyzing a series of pericentric and distal markers on different chromosomes in the teratoma DNA, which are identified as heterozygous in the host tissue (Table 1) [64].

Human OTs originate from oocytes at all meiotic stages, although most develop by Type II error from oocytes that have completed meiosis I [64-69]. Rarely, benign cystic ovarian teratoma and specific malignant germ cell tumor cases have been observed within families, suggesting one or more underlying genetic etiologies [70-75]. However, the majority of OTs occur sporadically. No associations with known genetic loci have been established in either familial or sporadic OT cases. The absence of a clear genetic association raises the possibilities that mutations in many different genes can cause OTs or that non-genetic etiologies are common.

Table 1: Analysis of meiotic error in human OTs

Heterozygous pericentric and distal markers are identified as informative in the somatic tissue from the OT patient. By analyzing the genotype of informative pericentric and distal markers in the OT tissue, the stage of meiotic failure of the oocyte resulting in an OT can be determined. Het – Heterozygous marker, Hom –Homozygous marker. Adapted from[64].

Types of Error	Mechanism of OT development	Ovarian Teratoma Genotype	
		Pericentric marker	Distal marker
Type I	Failure to complete meiosis I or fusion of oocyte with first polar body	Het	Het/Hom
Type II	Failure to complete meiosis II or fusion of oocyte with second polar body	Hom	Het/Hom
Type III	Duplication of genome of mature ovum	Hom	Hom
Type IV	Failure to complete meiosis I & II in PGC	Het	Het
Type V	Fusion of two ova	Het/Hom	Het/Hom

1.8 MOUSE MODELS OF OTS

Mouse strains predisposed to developing OTs have provided insight into the genes involved in OT development. LT/Sv is an inbred mouse strain in which approximately 50% of the females develop OTs by 90 days of age [63]. These OTs originate from parthenogenetically activated oocytes that have completed meiosis I [76]. LT/Sv oocytes experience a prolonged period of meiotic arrest at metaphase I [77]. This arrest (delayed metaphase to anaphase I transition) has been linked to the sustained activity of MPF [53]. Normally, a decrease in MPF activity is required for metaphase I to anaphase I transition, and sustained MPF activity and metaphase I arrest may predispose unfertilized LT/Sv oocytes to spontaneous cell division (parthenogenesis) and OT formation. Prolonged metaphase I arrest and parthenogenetic activation of oocytes have been reported to be necessary but not sufficient for OT formation [78]. Other requirements for OT formation have been revealed in an analysis of crosses between C57BL/6 (B6) and LT/Sv mice, which identified OT susceptibility loci, including a prominent locus (*Ots1*) on chromosome 6 [79].

Targeted mutagenesis in mice has also produced mouse strains susceptible to developing OTs. The *c-mos* gene encodes the cytostatic factor responsible for metaphase II arrest. Consequently, oocytes of homozygous *c-mos*-null mice fail to maintain metaphase II arrest and spontaneously initiate parthenogenetic embryonic development in the absence of fertilization. Approximately 40% of *c-mos*-null mice develop OTs [56, 57]. Mutations in the coding region of the human *c-mos* gene have not been reported, suggesting that mutations in the *c-mos* gene do not play a role in the genesis of human OTs [80]. The *MommeRI* mouse strain with a missense mutation in the transcription factor *Foxo3a* is predisposed to developing OTs; one-sixth of homozygous *MommeRI* females develop OTs [81]. The missense mutation was found to cause a

decrease in the transactivation potential of the transcription factor FOXO3A. Notably, both FOXO3A and c-MOS proteins are primarily expressed in the oocyte, with little expression in somatic cells of the ovary [82, 83].

Genetic defects in genes expressed in follicular GCs, but not in oocytes, also lead to OT formation in mice. One fifth of mFshr^{D580H} transgenic mice expressing a constitutively active form of the FSH receptor in GCs develop OTs [84]. Similarly, overexpression of the *Bcl-2* gene in mouse GCs led to a 20% incidence of OTs [85]. Hence alteration in normal cell signaling within the GCs can predispose to OTs. Transgenic mice expressing small interfering RNAs (siRNAs) targeting the *Gata4* (*siGata4*) gene also developed OTs [86]. In the mouse ovary GATA4 is primarily expressed in GCs [87]. Although the mechanism of OT formation in this model is presently unknown, it is possible that a decrease in granulosa-cell GATA4 indirectly influences oocyte function, leading to OT formation. Taken together, the molecular and functional abnormalities observed in the various OT mouse models suggest that several distinct cell-signaling or cell-cycle defects in cells of the ovarian follicle can mediate OT development.

We have previously reported that 15-20% of hemizygous female carriers of the imprinted *Tgkd* transgene develop OTs in the inbred FVB/N (FVB) strain [88]. Because numerous other transgenic mouse lines with the same or related imprinted transgenes did not develop teratomas, we postulated that the development of OTs in FVB-*Tgkd* females is due to disruptions in one or more genes near the genomic site of transgene integration on mouse chromosome 8. In this study, I have examined the mechanism by which the transgene *Tgkd* predisposes FVB mice to OT formation.

2.0 MATERIALS AND METHODS

2.1 ANIMAL STUDIES

The *Tgkd* transgene was maintained on the inbred FVB as described previously and on the OT non-permissive 129/Sv (129) background [88]. All experiments were performed in compliance with guidelines established by the Institutional Animal Care and Use Committee of the University of Pittsburgh. For determining the onset of puberty, females were examined daily for vaginal opening from day 22 postpartum. Primers and conditions for PCR genotyping of +/+ and *Tgkd* mice are provided in Appendix B.

2.2 SNP GENOTYPING OF OTS

Spleen and teratoma DNA samples were collected from female progeny of the backcross of F1 (FVB-*Tgkd* X B6) to FVB mice. 20 pericentric and 20 distal SNPs (one per chromosome) were examined in the spleen DNA for evidence of heterozygosity. This was performed by PCR amplification and DNA sequencing of the region surrounding the single nucleotide polymorphism (SNP) allele. The heterozygous SNPs in the spleen were examined in the teratoma to determine the last meiotic stage completed by the oocyte before initiating OT formation [64].

Detailed information of SNP locations and sequence in the spleen and OT are provided in Appendix A.

2.3 IDENTIFICATION OF *TGKD* INSERTION SITE

This was accomplished by identifying the two *Tgkd*-genome junctional fragments on Southern blots of FVB-*Tgkd* DNA probed with fragments of the *Tgkd* transgene, constructing *Tgkd* subgenomic libraries in the λ FixII vector (Stratagene, La Jolla, CA), and identifying clones containing the two junctional fragments. DNA sequencing of the junctional fragments containing *Tgkd* and endogenous genomic sequence was used for mapping of the insertion site.

2.4 COLLECTION OF EMBRYOS

Crosses were set up between hemizygous *Tgkd*/+ and +/+ animals so that the parental origin of the *Tgkd* transgene was known. The day on which the plug was observed was noted as day 0.5. E9.5 embryos, E13.5 and E16.5 embryo heads were collected 9, 13 and 16 days after observation of the plug respectively. The samples were frozen at -80°C until RNA extraction or protein extraction. Tail DNA was isolated from these embryos and used to determine presence or absence of *Tgkd*.

2.5 EMBRYONIC STEM CELL STUDIES

2.5.1 Embryonic stem (ES) cell derivation and generation of shRNA clones

129-*Tgkd*(maternal) ES cell lines were derived from 129-*Tgkd* X 129 crosses and 129-*Tgkd*(paternal) ES cell lines were derived from 129 X 129-*Tgkd* crosses. Homozygous *Tgkd* ES cell lines were derived from 129-*Tgkd* X 129-*Tgkd* crosses. ES cell lines were generated by collection of E3.5 blastocysts and ES cell lines were established using previously published methods [89]. Briefly, blastocysts were seeded on 24 well dishes (coated with gelatin) with irradiated feeder cells in ES cell media containing Leukemia inhibitory factor (LIF) (1000U/ml). After 5 days, the inner cell mass was dissociated from blastocysts that had attached to the bottom of the well into clumps of 6-12 cells. The dissociated inner cell mass was transferred to a new plate with feeder cells. ES cell colonies began to grow in a subset of wells and these wells were passaged into new wells with feeder cells every 3-4 days. After 2-3 passages, the established ES cell lines were frozen down until further use.

Stable knockdown clones of INPP4B were obtained by the electroporation of linearized shRNA plasmid constructs TRCN0000080645 and TRCN0000080646 (Open Biosystems, Huntsville, AL) followed by isolation of puromycin-resistant colonies. The extent of knockdown of INPP4B was determined by immunoblot analysis.

2.5.2 IGF1 stimulation protocol in ES cells

ES cells were passaged twice without feeders and then plated on 12 well plates coated with 0.1% gelatin. The cells were serum starved for 34 hours and then stimulated with 1 μ g/ul of mouse insulin growth factor-1 (IGF1) (Sigma-I8779) for indicated periods.

2.5.3 ELISA analysis

Phospho-AKT activation was measured in ES cell lysates using the PathScan® Phospho-Akt1 (Ser473) and Total Akt1 Sandwich ELISA Kit (Cell signaling: 7160 & 7170) according to manufacturer instructions.

2.6 OVARY STUDIES

2.6.1 Collection of ovaries and oocytes

Whole ovary, GV-stage oocytes and GCs were collected from immature females (21-23 day post partum) at designated time points following intra-peritoneal (IP) injection of 5IU PMSG (Calbiochem- 367222, LaJolla, CA) and 5IU of HCG (Sigma- C5297, St Louis, MO) injection 48 hours later. GCs and oocytes were collected in M2 medium (Millipore-MR-015-D, Temecula, CA) following needle puncture of the ovaries. The oocytes were collected and the remaining GCs were pelleted and lysed in 1X Laemmli sample buffer.

2.6.2 Ovarian morphometric analysis and follicle counting

Ovarian morphology was examined in hematoxylin and eosin (H&E)-stained paraffin sections of ovaries fixed overnight in 4% paraformaldehyde. Follicle counting and classification were performed on every fifth adjacent section of 5 μ m thickness according to an established system described by Pederson and Peters [16].

2.6.3 Oocyte parthenogenetic activation assay

Parthenogenetic activation of FVB-*Tgkd* oocytes was examined by isolating COCs from immature PD23 FVB and FVB-*Tgkd* mice after 48 hours of PMSG stimulation. Oocytes were separated from surrounding cumulus cells after 17 hours of *in-vitro* maturation and the frequency of 2-cell embryos was determined after 24 hours of additional culture in KSOM (Embryomax-MR-106-D, Millipore) as described previously [78].

2.6.4 Granulosa cell culture

This experiment was performed as described previously with minor modifications [90]. This protocol enables selective enrichment of GCs by isolating and culturing GCs from ovaries and excludes oocytes, and the ovarian capsule from the analysis. Ovaries were harvested from immature females (day 21-23 postpartum) and incubated in 6mM EGTA and 0.5M Sucrose in DMEM/F12 (Cellgro-10-092-CV, Herndon, VA). The ovaries were punctured with needles to release GCs in DMEM/F12. The GCs were pelleted at 100g for 10 minutes and resuspended at a density 0.5 X 10⁶ cells /well in DMEM/F12 +10%FBS. After overnight culture the cells were

stimulated for indicated time points with DMEM/F12+ recombinant human FSH (LER-4161B) (50ng/ μ l-final concentration) (Kind gift from Dr. Anthony Zeleznik) and the cells were subsequently lysed in 1X Laemmli sample buffer.

2.6.5 Lentiviral transduction of GCs

For lentiviral infections, 10^6 GCs were subjected to centrifugation and then resuspended in DMEM/F12 containing 8 μ g/ml polybrene (hexadimethrin bromide – Sigma H9268). The GCs were infected with lentivirus expressing short hairpin RNA (shRNA) constructs to *Inpp4b*, either TRCN0000080645 or TRCN0000080646 (Open Biosystems) at an MOI (multiplicity of infection) of 10. The GCs and the lentiviral suspension tubes were subjected to centrifugation at 1200g at 35°C for 2 hours (4X30 minutes) and the lentivirus-cell suspension was plated in DMEM/F12 +10%FBS. After 48 hours of culture, the cells were stimulated with DMEM/F12+ FSH (50ng/ μ l) for the indicated times.

2.6.6 Corpora lutea clearance assay

Immature females were given an IP injection of 5IU PMSG and 5IU of HCG (Sigma- C5297, St Louis, MO) 48 hours after PMSG stimulation. The ovaries were collected 7 days after HCG stimulation. Presence and size of corpora lutea was examined in H&E stained paraffin sections of ovaries fixed overnight in 4% paraformaldehyde.

2.7 BISULFITE GENOMIC SEQUENCING

Bisulfite genomic sequencing was performed using the EpiTect Bisulfite Kits (Qiagen-59104, Valencia, CA) [91]. Following bisulfite treatment, the RSV sequence was amplified with PCR primers flanking the RSV DMD (within the *Ig* and *c-myc* sequences). Primer sequences are provided in Appendix B. The PCR products were cloned into the Topo-TA cloning vector (Invitrogen -K4550-40) and transformed into electrocompetent cells. Individual plasmid clones were isolated and sent for sequencing with the M13 forward sequencing primer.

2.8 SOUTHERN BLOT ANALYSIS OF *Tgkd* METHYLATION

To assess the extent of *Tgkd* methylation, genomic DNA was digested with the methylation sensitive restriction enzyme BstUI [92]. The digested DNA was subjected to electrophoresis on a 0.7% agarose gel, transferred onto Genescreen nylon filters (NEN, Boston, MA). The filter membrane was hybridized with the *Ca* probe 42°C and subsequently washed with 2X SSC and 0.1X SSC at 65°C. The *Ca* probe is a 1.75kb EcoRI – XbaI fragment of the *Ca* region in the *RSV Igmyc* transgene (Figure 6). DNA probes were prepared from gel-purified fragments. 100ng of DNA was denatured at 100°C and annealed with random primers on ice. Synthesis of a ³²P *Ca* probe was done in the presence of (α -³²P) dCTP and the Klenow fragment. The labeled probe was purified using the Probe Quant G50 microcolumns (Amersham Bioscience, Piscataway, NJ). Bands were visualized by autoradiography and quantified using Image J analysis software.

2.9 METHYLATION-SENSITIVE PCR

Genomic DNA was isolated from ES cell lines and digested with the restriction enzyme *AseI*. The cut genomic DNA was purified by phenol/chloroform extraction, precipitated and subjected to another round of restriction digest by the methylation sensitive restriction enzymes *HpaII* or *McrBC* or the enzyme *MspI*. The DNA from this round was once again purified and PCR primers were used to amplify 10 CpG islands identified by the program CpG island searcher in a 2 Mb region surrounding the *Tgkd* insertion. Primer sequences are provided in Appendix B.

2.10 PCR FOR DETECTING NOVEL *Inpp4b* SPLICE ISOFORMS

RNA from FVB and homozygous *Tgkd/Tgkd* E13.5 brains were converted to cDNA. A series of reverse transcription PCRs (RT-PCRs) were done on the cDNA samples to span the entire coding region and transcribed but untranslated region (UTR) of *Inpp4b* α and β isoforms. The PCR primers were designed to generate approximately 1kb amplicons and successive PCR products had overlap regions greater than 200bp. The PCR amplified amplicons were cloned followed by sequencing of 4 clones per amplicon from FVB E13.5 brains and 8 clones from *Tgkd/Tgkd* brains. The sequence from FVB and *Tgkd/Tgkd* embryos were compared for differences in cDNA sequence or novel splice isoforms. Primer sequences are provided in Appendix B.

2.11 SINGLE NUCLEOTIDE PRIMER EXTENSION (SNUPE) ANALYSIS

RNA was isolated from adult tissues and converted to cDNA. RT-PCR was performed on the cDNA with primers amplifying the region surrounding the SNP allele difference between FVB and 129 strains for each gene (Appendix B). The RT-PCR product was gel extracted and resuspended in water before performing the SNUPE reaction. Each SNUPE reaction was performed in a 10ul reaction mix containing (³²P) dNTP (appropriate nucleotide), 2mM MgCl₂, 50mM KCl, 10mM Tris-HCl at pH 8.3, 0.001% gelatin, 1μM of the appropriate SNUPE primer, approximately 10ng of RT-PCR product and 0.75 units of Taq polymerase (Invitrogen). Samples were incubated at 95°C for 30s, 42°C for 30s and 72°C for 1 minute in a thermocycler. After separating the products on a 15% denaturing polyacrylamide gel, the ratio of the SNP alleles were determined by autoradiography and quantified using a phosphoimager. RT-PCR primers and the SNUPE primer sequence for each gene are provided in Appendix B [93].

2.12 REAL TIME PCR

RNA was extracted using the RNeasy Micro kit (Qiagen). 1μg of RNA was converted to cDNA using the high capacity cDNA reverse transcription kit (Applied Biosystems, Foster City CA) in a reaction volume of 20μl. 2μl of the cDNA was used in a 10μl Real time PCR reaction. Real time PCR was performed using the SYBR Green master mix (Applied Biosystems) on the 7900HT Fast Real-Time PCR System machine (Applied Biosystems). Steady-state transcript levels were measured by real-time PCR using oligonucleotide primers located across exons 23 and 24 of *Inpp4b* mRNA, a region common to all known forms of *Inpp4b* transcripts. The α and

β isoforms were assayed separately by amplification of their alternative terminal exons. The Pfaffl method was used to determine fold changes and the fold changes were determined as fold change over wildtype levels [94]. TATA-binding protein (TBP) (E13.5 embryo studies) and beta glucuronidase (GUSB) (Ovary studies) were selected as housekeeping control genes. Primer sequences are provided in Appendix B and efficiency curves in Appendix C.

2.13 IMMUNOBLOT ANALYSIS

E13.5 heads, ovaries and ES cell proteins were extracted using RIPA lysis buffer supplemented with complete protease inhibitor and PhosSTOP phosphatase inhibitor (Roche, Basel, Switzerland). Oocytes and GCs were lysed in 1X Laemmli sample buffer. Immunoblot analysis was performed as described previously [95]. In brief, samples were denatured by heating at 100°C for 5 minutes and then separated by electrophoresis on SDS-7% polyacrylamide gels. Afterwards, they were transferred to PVDF membranes (Immobilon-P, Millipore). Membranes were blocked in 5% dry skim milk in 0.1% Tween-20 TBS (TBS-T) for 1 hour and probed with the indicated antibodies overnight at 4°C according to manufacturer's instructions. Following 5 washes of 5 minutes each in TBS-T, the membranes were incubated for 1 hour in the respective secondary antibody in blocking solution. Membranes were washed as above. Bound antibody was detected using the chemiluminescence detection kit ECL Plus (Amersham, Piscataway, NJ). When a blot was reprobed with a different primary antibody, the first antibody was removed by incubation with stripping solution (100 mM 2-Mercaptoethanol, 2% SDS, 62.5 mM Tris-HCl pH 6.8) at 50°C for half hour, washed for an hour in TBS-T and then the blot was blocked for 1 hour at room temperature.

Membranes were probed with the following antibodies: INPP4B (Brain and ES cells - Santa Cruz-sc12318, Santa cruz, CA), INPP4B (Ovary and GCs - 106), Phospho-AKT (Ser-473) (9271), phospho-FOXO1 (Ser-256) (9461), E2F1 (3742), Cyclin D2 (3741) (Cell Signaling technology, Beverly, MA) and Actin (Abcam, Cambridge, MA). The blots were stripped and reprobed with FOXO1 (2880), AKT (9272) (Cell Signaling technology) and P27^{KIP} (Santa cruz-sc528). Anti-rabbit (GE healthcare: NA934V, Piscataway, NJ) or anti-goat (sc-2020) secondary antibodies were diluted in blocking solution (5% milk). Protein levels were determined by comparison of intensity on autoradiography films using the BioSpectrum 500 imager and VisionWorks®LS analysis software (UVP, LLC, Upland, CA).

2.14 BrDU INCORPORATION ASSAY

PD30 mice received an IP injection of 100mg/kg of bromodeoxyuridine (BrdU) (Sigma -B9285) and were killed 2 hours after injection. Ovaries were isolated and the BrdU incorporation was detected by immunohistochemistry.

2.15 IMMUNOHISTOCHEMISTRY

Ovaries were fixed in 4% PFA and embedded in paraffin. Immunohistochemistry (IHC) was performed on 5µm sections using the Vectastain Elite ABC Kit (Vector laboratories, Burlingame, CA) according to manufacturer instructions. Mouse anti-BrdU (Sigma- B2531) was used to evaluate cell proliferation and rabbit anti-cleaved caspase3 (Cell Signaling Technology-

9664) was used to determine the rate of apoptosis in follicles. IHC was performed on 4 non-adjacent sections and positive cells were counted in 25 follicles containing a clear oocyte. Rates of proliferation and apoptosis per follicle were determined by the number of positive cells in each preantral (Type 5) and antral follicle divided by the total number of cells in the follicle. FOXO1 IHC was performed on wildtype and *Tgkd* PD30 ovaries using the FOXO1 antibody (Cell Signaling - 2880) and the Vectastain Elite ABC Kit.

2.16 RNA *IN SITU* HYBRIDIZATION (ISH)

RNA in situ hybridization (ISH) was performed using digoxigenin-labelled cRNA riboprobes. The unique terminal exon (exon 25) of *Inpp4b* α and β isoforms were amplified by RT-PCR from E13.5 brain cDNA and cloned into the pBluescript vector (Primers for RT-PCR – Appendix B). The resultant vectors were linearized and antisense plus sense riboprobes were prepared by in vitro transcription using the Riboprobe Combination System-T3/T7 RNA Polymerase (Promega –P1450) and DIG RNA Labeling Mix (Roche – 11277073910). Ovaries from 7-week-old mice were dissected in M2 media, washed in 1X PBS and fixed in fresh 4% paraformaldehyde. Paraformaldehyde-fixed samples were immersed in 10%, then 20% sucrose in PBS, followed by OCT embedding. Cryosections (10 μ m) of the OCT-embedded placentas were used for ISH as previously described [96]. Briefly, sections were fixed in 4%PFA, washed in PBS (3 X 5 min), acetylated for 10 minutes at room temperature and washed again in PBS. Prehybridization (Hybridization solution - 50% Formamide, 5X SSC, 5X Denhardts solution, 0.25mg/ml tRNA, 0.5mg/ml Herring sperm DNA) was performed in a humidified chamber for 2 hours at room temperature. Hybridization (denatured riboprobe in hybridization solution) was

performed at 65°C overnight in a humidified chamber. Sections were stained overnight with anti-digoxigenin antibody conjugated to alkaline phosphatase (Roche - 11093274910). Detection was performed with nitro blue tetrazolium chloride (NBT) and 5-bromo-4-chloro-3-indolyl-phosphate, toluidine-salt (BCIP) and levamisole (Roche 11681451001) reagent solutions. The slides were subsequently dehydrated and mounted in cytooseal.

2.17 STATISTICAL ANALYSIS

Each experiment was repeated a minimum of 3 times. A mean and standard error was calculated. Significance was assessed using the Wilcoxon Rank-sum test. Results were considered significant (*) if the p value was less than 0.05.

3.0 THE FVB-*Tgkd* STRAIN AS A MODEL TO STUDY OVARIAN TERATOMA FORMATION

3.1 INTRODUCTION: THE FVB-*Tgkd* MOUSE STRAIN

The FVB-*Tgkd* mouse strain carries a randomly inserted transgene *Tgkd* on the FVB mouse strain background. The *Tgkd* transgene is a genomically imprinted transgene that is methylated in offspring when inherited from the mother and unmethylated on paternal inheritance [92]. The *Tgkd* transgene is imprinted irrespective of the location of genomic integration. The *Tgkd* transgene is a modified version of the *RSVlgmyc* transgene, which also exhibits maternal allele specific methylation [97]. The *RSVlgmyc* transgene was originally designed to express the *c-myc* oncogene in the mouse. The *Tgkd* transgene consists of the Rous Sarcoma Virus (RSV) Long Terminal Repeat (LTR) sequence and the *Igα/c-myc* Burkitt-like fusion gene product from the S107 plasmacytoma cell line in which the 5' region of the switch recombination sequences of *IgA (Sa)* has translocated into the 5' region of *c-myc* [92, 98] (Figure 6A). The *c-myc/Igα* regions within the transgene are organized such that the constant and switch regions of the immunoglobulin locus are immediately followed by the *c-myc* gene having a truncated exon 1. The RSV LTR serves as the differentially methylated domain (DMD) of the *Tgkd* transgene and the *Tgkd* transgene is not genomically imprinted in the absence of the RSV LTR sequence (Figure 6B).

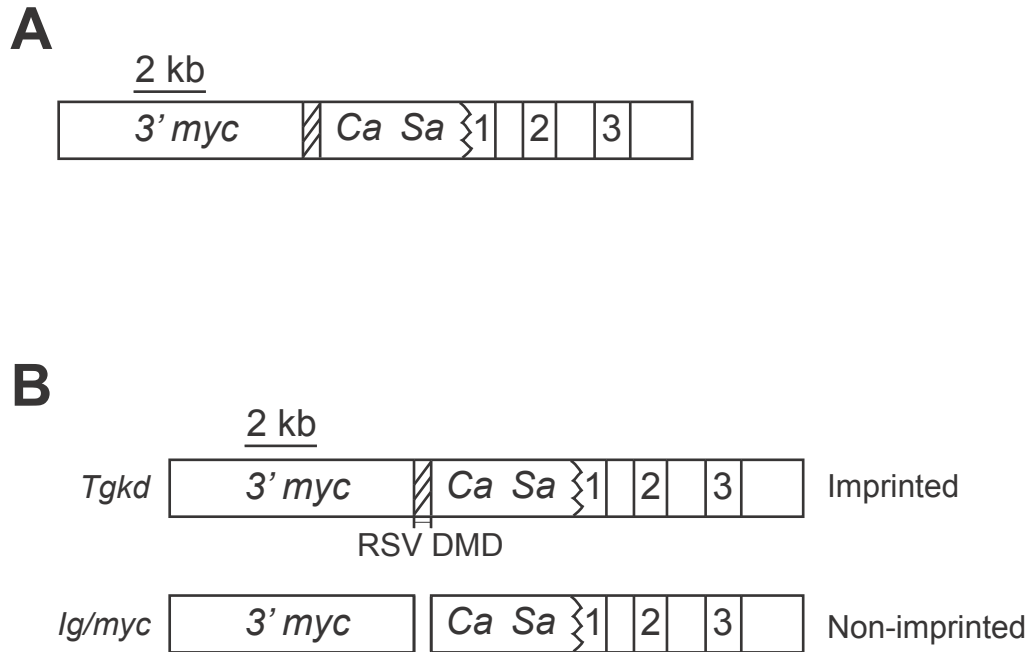


Figure 6: Structure and description of the *Tgkd* transgene

Figure and legend adapted from [92] (A) The *Tgkd* transgene is a fusion gene product composed of the *IgA/c-myc* translocation with the switch region (*Sa*) of the immunoglobulin locus adjacent to the truncated exon 1 of *c-myc*. Numbers 1-3 represent exons 1-3 of the endogenous *c-myc* gene. *Sa* and *Ca* represent the switch recombination sequences and constant region coding exons of the endogenous immunoglobulin *Igα*. The hatched region is a 440bp fragment of the LTR of the RSV of the Schmidt-Ruppin strain (subgroup D). (B) The RSV region constitutes the DMD of the *Tgkd* transgene. The *Tgkd* transgene is methylated on maternal inheritance and *Tgkd* loses this genomic imprinting property in the absence of the RSV region.

Hemizygous carriers of the *Tgkd* transgene on the FVB strain background (FVB-*Tgkd* mice) are observed to develop OTs at a frequency of 15-20% between 12-22 weeks of age [88]. The OTs in the FVB-*Tgkd* mice exhibit a malignant mixed germ cell phenotype (teratocarcinoma) with evidence of metastases to the mesenteric lymph node and lung. The tumors contain areas of well-differentiated benign teratoma structures such as keratinizing squamous epithelium, respiratory epithelium, cartilage, sebaceous glands, hair follicles, intestine, bone, fat, smooth muscle and nerves which constitute derivatives of the embryonic layers: ectoderm, mesoderm and endoderm. The FVB-*Tgkd* OTs also contain immature malignant components such as areas of undifferentiated highly mitotic embryonal carcinoma cells, embryoid bodies, Schiller-Duval bodies (characteristic of endodermal sinus tumors) and malignant trophoblasts (characteristic of choriocarcinoma). The central areas of the larger tumors also exhibited substantial amounts of necrosis [88].

Homozygous carriers of the *Tgkd* transgene on the FVB strain exhibit perinatal lethality. To determine the time of death of homozygous FVB-*Tgkd* mice, embryos from crosses between hemizygous FVB-*Tgkd* mice were genotyped at various time points during gestation (Table 2) [88]. The observed percentages of the different genotypes of embryos were equivalent to the expected mendelian ratios from the cross at days 8.5 and 10.5 of embryogenesis. However at birth, the expected number of homozygous *Tgkd/Tgkd* embryos was one-half of the expected mendelian ratio and adult *Tgkd/Tgkd* mice were absent at 3 weeks of age (Table 2). Both the OT phenotype in hemizygous *Tgkd* mice and the perinatal lethality phenotype of *Tgkd/Tgkd* mice on the FVB strain are integration-site dependent as other independently derived transgenic lines with the *Tgkd* transgene construct do not develop OTs or exhibit perinatal lethality, even though the *Tgkd* transgene is imprinted in all these lines [88, 92]. In initial studies, the *Tgkd* transgene

array was found to be inserted on chromosome 8 in the FVB-*Tgkd* strain [88]. Hence, the development of the OT phenotype is most likely due to the disruption or interference by *Tgkd* of genes surrounding the genomic integration site on chromosome 8.

Table 2: Analysis of viability of hemizygous and homozygous FVB-*Tgkd* embryos

Crosses were set up between hemizygous FVB-*Tgkd* males and females. 78 carrier offspring out of 115 tested were hemizygous *Tgkd* mice when analyzed at 3 weeks of age. The ratio of hemizygous to wildtype offspring (78:37) is close to the expected mendelian ratio of 2:1 confirming normal viability of hemizygous offspring at this age. However homozygous *Tgkd/Tgkd* offspring were absent at 3 weeks of age. Further at birth, the number of *Tgkd/Tgkd* offspring observed was half the expected value (wildtype=15, *Tgkd/Tgkd*=7) indicating perinatal lethality of homozygous FVB-*Tgkd* embryos. +/+ - Wildtype embryos, *Tgkd/+* - Hemizygous FVB-*Tgkd* embryos, *Tgkd/Tgkd* - Homozygous FVB-*Tgkd* embryos. Data adapted from [88].

Embryonic Stage	Embryo Genotype		
	+/+	<i>Tgkd/+</i>	<i>Tgkd/Tgkd</i>
Day 8.5	5	14	5
Day 10.5	5	13	5
Birth	15	40	7
Adult	37	78	0

3.2 ADVANTAGES OF THE FVB-*Tgkd* OT MODEL

The aim of these studies was to characterize the process by which the insertion of the *Tgkd* transgene leads to the development of OTs on the FVB strain background. The FVB-*Tgkd* mouse strain is an excellent model to study teratoma formation as the defined insertion of the *Tgkd* transgene array at a single genomic integration site causes the OT-free FVB females to become susceptible to formation of teratomas. This suggests that OT formation in this model may be linked a limited set of gene/genes close to the site of the transgene insertion on chromosome 8. The integration site (characterized later on in the thesis) is distinct from previously described OT susceptibility loci or genes; hence the evaluation of the FVB-*Tgkd* OT model may provide new insights into distinct pathways to OT formation.

Another important aspect in the FVB-*Tgkd* model is the requirement of the FVB strain background for the development of the OT phenotype. We have presented some preliminary experiments in this section that illustrate the strain specific features of the OT phenotype and have aimed to identify chromosomal regions associated with the strain specific modifier alleles that confer susceptibility to this phenotype (Eicher et al., manuscript in preparation).

3.3 GENOTYPING OF THE *Tgkd* MOUSE

To identify carriers of the *Tgkd* transgene, genotyping studies were performed with primers designed across the *Igα/c-myc* translocation of the *Tgkd* transgene (Figure 7A). The design of these primers across the translocation prevented PCR amplification from the endogenous *IgA* or *c-myc* genomic sequence. Further primers were designed to be complementary to endogenous

sequences lost by the insertion of *Tgkd* on chromosome 8. These primers were used to detect the wildtype allele as PCR amplification occurred only when the *Tgkd* transgene array was absent. Using a combination of the wildtype allele and *Tgkd* transgene PCR, I was able to distinguish wildtype (+/+), homozygous (*Tgkd/Tgkd*) and hemizygous (*Tgkd/+*) *Tgkd* genotypes (Figure 7B).

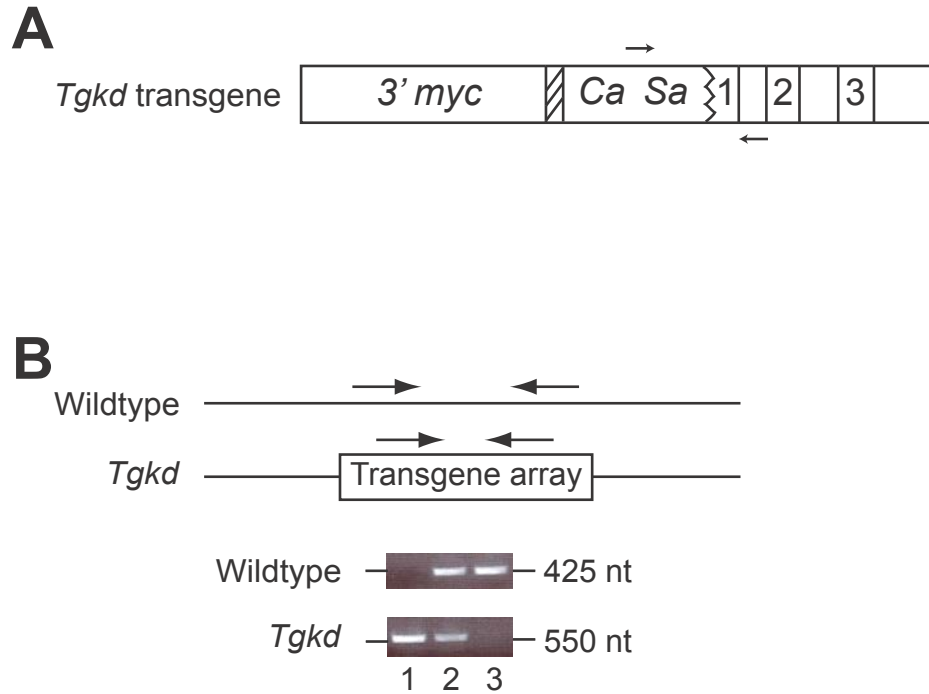


Figure 7: Genotyping of the *Tgkd* transgene in FVB-*Tgkd* mice

The above figures illustrate **(A)** PCR primers to detect the *Tgkd* transgene were designed across the *c-myc/Igα* translocation to obtain a specific PCR product for the transgene and avoid amplification from the endogenous *c-myc* and *Igα* genomic sequence. **(B)** Two sets of primers were used for genotyping mice containing the *Tgkd* transgene. The first set of primers was designed to detect endogenous sequences present only on the wild-type allele; PCR amplification occurred only in the absence of the *Tgkd* transgene array. The *Tgkd* transgene primers represented in 7A were used to detect the *Tgkd* transgene array. Using these 2 sets of primers, I could distinguish between a homozygous *Tgkd* genotype (1), hemizygous *Tgkd* genotype (2) and wildtype allele (3).

3.4 STRAIN SPECIFICITY OF THE OT PHENOTYPE

The OT phenotype in the FVB-*Tgkd* strain is observed to be highly dependent on the FVB strain background. As described before, 17% of the hemizygous female carriers of *Tgkd* develop OTs on the FVB strain background. However none of the females carrying the *Tgkd* transgene (at the same genomic integration site) develops OTs on the B6 or 129 strain background (Table 3). This data suggests that besides the gene disrupted by the *Tgkd* insertion, there are additional FVB modifier alleles required for the OT phenotype.

Further studies to characterize the FVB strain specific effect on *Tgkd* induced OTs were performed by Dr. Eva Eicher at Jackson Laboratories (Bar Harbor, Maine). In these studies, FVB-*Tgkd* females were crossed to B6 males and no OTs were observed in the *Tgkd* females of the F1 generation (Table 3). The absence of the OT phenotype was also observed in the *Tgkd* females of the reciprocal cross. When the *Tgkd* females from the F1 cross (FVB-*Tgkd* X B6) were backcrossed to FVB males, 8% of the F2 *Tgkd* females developed OTs by 120 days of age (Table 3) (Eicher et al., manuscript in preparation). These experiments illustrate two aspects of the FVB strain effect on OT development in FVB-*Tgkd* mice. The first aspect is that there is an absolute requirement of the FVB strain background for *Tgkd* induced teratoma development. Further, the gene/genes promoting OT development in the FVB background are recessive in nature and have to be in the homozygous state to promote teratoma formation in *Tgkd* females. The genomic region/regions carrying the FVB strain specific modifier alleles for the OT phenotype was designated as ovarian teratoma susceptibility region 2 (*Ots2*). Lee et al identified a similar susceptibility locus in OT-susceptible LT/Sv mice, which has a semi-dominant effect on OT development in this strain. This locus was designated as ovarian teratoma susceptibility

region 1 (*Ots1*) and linkage analysis studies identified an OT susceptibility region on mouse chromosome 6 [79].

Linkage analysis studies were also performed on *Tgkd* positive females that developed OTs to identify the FVB strain specific modifier alleles required for the phenotype. Linkage analysis was performed on DNA isolated from 31 OT positive females from the *Tgkd* progeny of the backcross [(B6 X FVB-*Tgkd*) F1 X FVB]. Besides the region on chromosome 8 associated with the *Tgkd* insertion, a significant linkage score was associated with markers between 20-50 cM on mouse chromosome 6 (Eicher et al., manuscript in preparation). These results indicate that both *Ots1* and *Ots2* loci reside on chromosome 6.

To investigate whether *Ots1* and *Ots2* involve the same susceptibility genes, FVB-*Tgkd* mice were crossed with LT/Sv mice and the progeny were scored at 120 days for the presence of OTs (Table 3). 43 out of 48 *Tgkd* positive F1 progeny (89.5%) from the above cross developed OTs indicating that *Ots1* and *Ots2* loci may involve the same subset of genes or the two loci complement each other to increase the penetrance of the *Tgkd* induced OT phenotype (Eicher et al., manuscript in preparation). These studies indicate in addition to the genes disrupted by the insertion of *Tgkd* transgene on chromosome 8, additional modifier alleles exist on mouse chromosome 6 of the FVB strain that contribute to the development of OTs. The identity of these genes is not known; however, they may constitute susceptibility loci that are common to different OT mice models. These susceptibility loci may be necessary but not sufficient for OT formation. Identification of these loci may help identify common processes involved in OT formation.

Table 3: Strain specific effects on OT phenotype

Data for table adapted from Eicher et al., manuscript in preparation. The table illustrates that *Tgkd* females develop OTs only on the permissive FVB strain background. A heterozygous FVB/B6 background is not permissive to OT formation in F1 females between FVB-*Tgkd* and B6 mice. However on backcrossing these F1 progeny to FVB mice, half of the F2 mice possess homozygous FVB loci and the frequency of the OT phenotype (8%) is correspondingly reduced to about half of that in the FVB-*Tgkd* frequency (17%). On crossing the FVB-*Tgkd* mice to the OT susceptible LT/Sv mice, 89.5% of the *Tgkd* positive mice develop OTs.

Mouse Strain	OT incidence (%)
FVB- <i>Tgkd</i>	17
B6- <i>Tgkd</i>	0
129- <i>Tgkd</i>	0
(B6 X FVB) F1 – <i>Tgkd</i>	0
[(B6 X FVB) F1 X FVB] F2 – <i>Tgkd</i>	8
(LT/Sv X FVB) F1 – <i>Tgkd</i>	89.5

3.5 CONCLUSIONS

This section summarized the abnormalities observed in the FVB-*Tgkd* strain of mice. Hemizygous carrier females of the imprinted *Tgkd* transgene developed OTs at a frequency of 17-20% while homozygous *Tgkd* mice exhibited perinatal lethality. These phenotypes were consistent with the notion of the *Tgkd* disrupting one or more genes surrounding the insertion site on chromosome 8.

In addition to the *Tgkd* insertion, there was a strain specific modifier effect on the *Tgkd* induced OT phenotype. *Tgkd* positive females only developed OTs on the FVB strain background and homozygosity of the FVB background was required for teratoma formation. The only other strain background with predisposition to OT formation was the LT/Sv strain background, which appeared to enhance the frequency of OT formation in FVB-*Tgkd* mice.

In this thesis, I have focused on the genetic and molecular effects of the *Tgkd* transgene on OT formation in hemizygous FVB-*Tgkd* (henceforth designated *Tgkd*) mice.

4.0 OVARIAN DEFECTS ASSOCIATED WITH THE *Tgkd* OT MODEL

4.1 AIMS OF THESE STUDIES

The aims of these studies are to characterize the defects present in *Tgkd* ovaries and assess how they may relate to OT formation. Many OT models exhibit several follicular defects such as oocyte growth asynchronous with ovarian follicle growth, alterations in the distribution of various follicle types, depletion of the primordial follicle pool and associated decrease in reproductive fitness [81, 84]. I wanted to evaluate whether there were any alterations in ovarian follicle development between FVB (wildtype) and *Tgkd* ovaries or whether the defects leading to OT development are confined to the oocyte.

Further studies also aimed to evaluate the properties of wildtype and *Tgkd* oocytes in terms of potential of parthenogenetic activation as oocyte parthenogenetic activation has been reported to be a necessary requirement but not sufficient for OT formation [78]. Additionally, I have analyzed the type of error or the last stage of meiosis completed by *Tgkd* oocytes before initiating OT formation. In terms of oocyte requirements for OT formation, I evaluated whether methylation on the *Tgkd* transgene is required for the OT phenotype and whether this methylation plays a role in the strain specificity of the OT phenotype. In summary, I have evaluated the contribution of various aspects of ovarian development to the OT phenotype.

4.2 ABNORMAL FOLLICLE MATURATION AND LUTEINIZED FOLLICLE SYNDROME IN *Tgkd* OVARIES

The ovarian follicle comprising of the oocyte and the surrounding GCs form the main developmental component of the ovary. The ovarian follicle goes through various stages of development and all these stages can be seen in serial sections of the whole mouse ovary. The earliest stage of the follicular development is the quiescent ovarian reserve of primordial follicles, which consist of oocyte surrounded by a single layer of squamous GCs. Once a follicle is recruited from the primordial follicle pool towards further development, the follicle either successfully ovulates the oocytes or undergoes atresia during development. A reliable way of assessing follicular function is by counting the number of different follicle types in the ovary and defects in follicle development are manifested as significant changes in one or more follicle stages. Recruited follicles were classified as primary (1 layer of cuboidal GCs – Type 3b), secondary (2 layers of GCs – Type 4), preantral (3 or more layers of GCs – Type 5) and antral follicles (Type 6-8) according to Pedersen and Peters method of classification [16]. Primordial follicles quantification is presented along with fertility studies in the next section. In these studies, I have quantified the different activated follicular types in pre-pubertal PD23 mice and just after puberty at PD30 to evaluate if the gonadotrophin hormones play a role in promoting follicular defects. Both wildtype and *Tgkd* mice attained puberty on PD28 (n=4 mice) consistent with normal gonadotrophin signaling during puberty in *Tgkd* female mice.

The distribution of follicle types differed in PD23 wildtype and *Tgkd* mice, although the total number of activated follicles was not significantly different. Absolute numbers of primary (Type 3b) and secondary follicles (Type 4) were similar in wildtype and *Tgkd* ovaries, but there were twice the number of preantral (Type 5) follicles in *Tgkd* ovaries (Figure 8A, $p < 0.05$). This

was accompanied by a decrease in the absolute number of early and late antral (Type 6-8) follicles per ovary. Similar defects in folliculogenesis were seen in post-pubertal PD30 *Tgkd* female mice. Specifically, I observed a significant 1.6-fold increase in the number of preantral follicles in PD30 *Tgkd* mice, which was accompanied by a 0.4-fold decrease in the number of antral follicles (Figure 8A). A subset of large preantral follicles without antrum formation was observed in PD30 *Tgkd* ovaries, which may contribute to the increase in the number of preantral follicles and decrease in the number of antral follicles (# - Figure 8C). The cause for this lag in antrum formation in these follicles is not known but these follicles manifest defects in follicle maturation.

PD30 *Tgkd* ovaries showed additional follicular defects, not present in age-matched wildtype mice, which are indicative of perturbed follicle maturation. An average of 4.4 corpora lutea were observed, whereas no corpora lutea were observed in control wildtype mice (Figure 8B). In addition, trapped oocytes were observed in many PD30 *Tgkd* corpora lutea (& - Figure 8C); one examined ovary contained four corpora lutea with trapped oocytes. A corpus luteum is formed from the remnants of the follicle after ovulation of the oocyte; hence a trapped oocyte indicates that the follicle has luteinized prior to ovulation of the oocyte. These luteinized, unruptured follicles are a further indication of defective ovarian follicle maturation in *Tgkd* mice that may be directly relevant to teratoma formation as the associated OTs may form via parthenogenetic activation of these trapped oocytes.

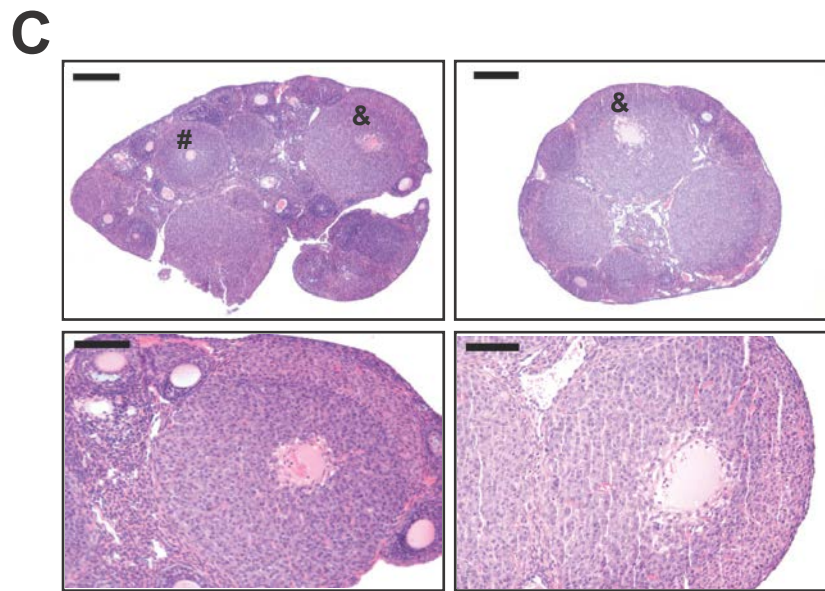
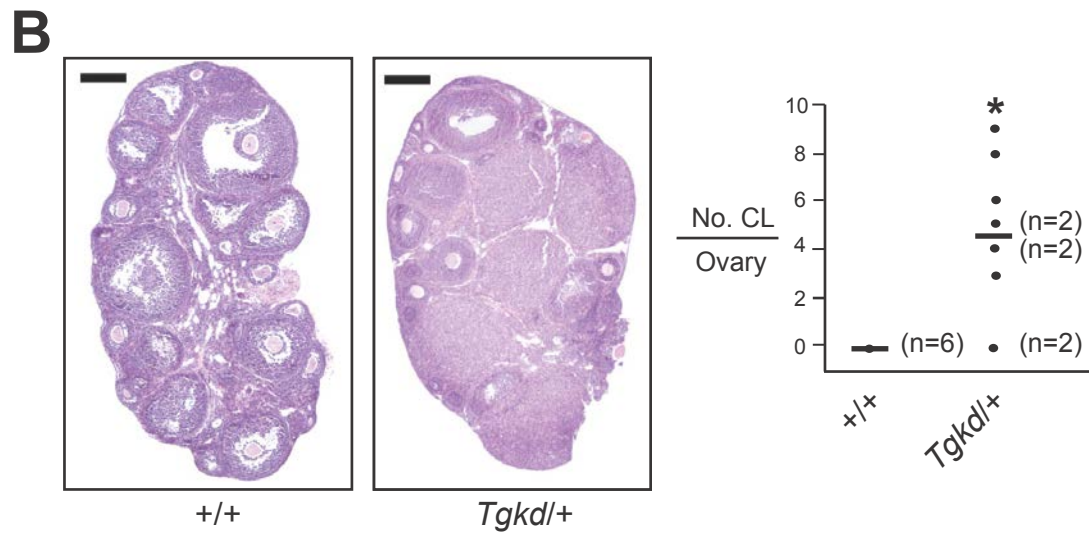
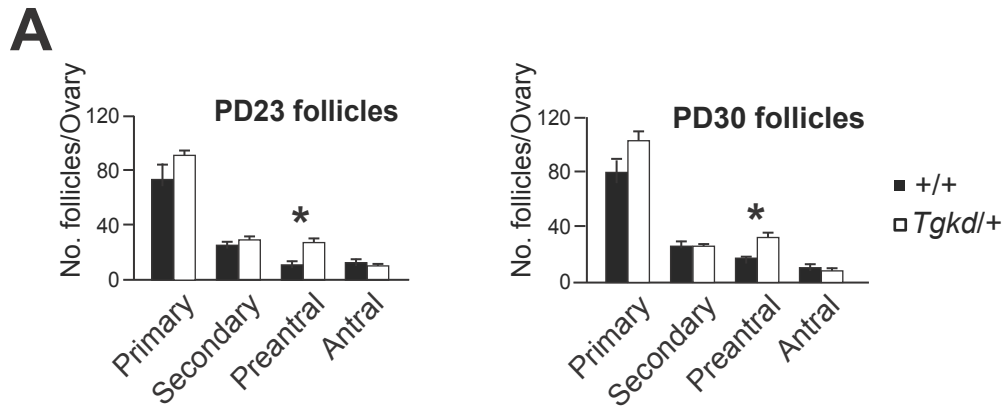


Figure 8: Defects in follicular maturation in *Tgkd* ovaries

Premature corpora lutea formation and luteinized unruptured follicles were observed in OT susceptible *Tgkd* mice. **(A)** Classification and numbers of ovarian follicles in the OT susceptible *Tgkd* strain compared to wildtype mice (n>6 ovaries). **(B)** Corpora lutea formation was observed in the *Tgkd* strain (n=10 ovaries) at PD30 but not in wildtype PD30 mice (n=6) (Scale bar: 200µm). **(C)** Depicts follicular defects observed in *Tgkd* ovaries not observed in wildtype ovaries such as large preantral follicles (#) and unruptured luteinized follicles (&), which consist of corpora lutea with oocytes trapped within them (scale bar in upper panels 200µm; scale bar in lower panels 100µm). * - p<0.05.

4.3 ABSENCE OF PREMATURE OVARIAN FAILURE IN *Tgkd* MICE

In addition to the follicular defects, alterations in reproductive fitness have been reported in many OT models. Homozygous *MommeR1* mice carrying a missense mutation in the *Foxo3a* gene exhibit infertility in early adult hood consistent with the phenotype of premature ovarian failure (POF) [81]. Mice developing OTs due to expression of constitutively active FSH receptor (mFshr^{D580H}) are either infertile due to irregular estrous cycles or mice with regular estrous cycles depict an initial increase in litter size followed by premature ovarian failure [84]. Female infertility can be caused by defective maturation at any stage of folliculogenesis, however premature ovarian failure is characterized by depletion of the primordial follicle reserve due to

excessive recruitment, which leads to a sudden decrease in fertility in early adulthood. Some OT models such as the mice overexpressing *Bcl-2* in GCs (*Inh α -bcl2*) display an increase in litter size compared to wildtype controls [85].

These reports on the relationship of the OT phenotype with female fertility led me to examine the effect of the *Tgkd* transgene on the reproductive fitness of the *Tgkd* mice. Further I have evaluated the effect of *Tgkd* on the number of primordial follicles in PD23 and PD30 ovaries to assess for premature follicle depletion. Despite the observed abnormalities in *Tgkd* ovary morphology, there was no evidence of a significant reduction in the fertility of hemizygous *Tgkd* females, and no differences in primordial follicle numbers between wildtype and *Tgkd* mice at both PD23 and PD30 (Figure 9A and 9B). A decrease in fertility in older *Tgkd* females was seen due to the death of OT positive females set up for mating. Once the OTs reached a large size, the females died or were sacrificed due to the large size of the teratomas. When the fertility data was examined only in the *Tgkd* females without palpable OTs, there was no difference in fertility from wildtype controls. Consequently there was no evidence of premature ovarian failure (POF) in *Tgkd* females, which is associated with OT formation in other mouse strains.

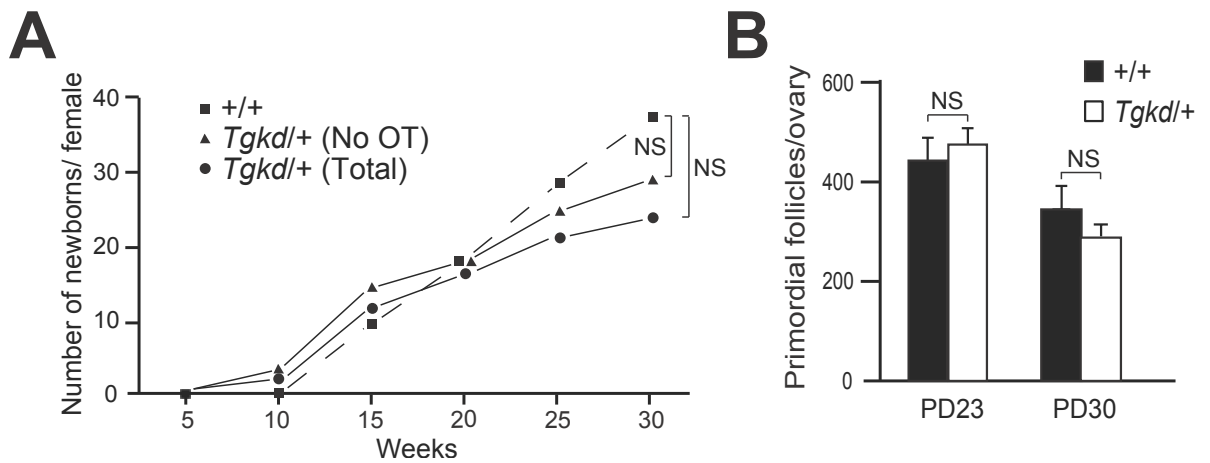


Figure 9: Fertility studies with *Tgkd* mice

Reproductive fitness and primordial follicle reserve in *Tgkd* mice was comparable to that in wildtype mice. **(A)** Litter sizes were recorded in wildtype (n=4) and *Tgkd* (n=5) females crossed with *Tgkd* males till the mother was 30 weeks of age or *Tgkd* females developed OTs (n=2). *Tgkd* females with palpable OTs were killed. **(B)** Number of primordial follicles in immature PD23 and post pubertal PD30 ovaries of *Tgkd* mice compared to wildtype mice. NS – non-significant

4.4 OVARIAN TERATOMAS ARISE FROM OOCYTES THAT HAVE COMPLETED MEIOSIS I

Both follicle luteinization and meiotic maturation of fully-grown oocytes require the LH surge. Therefore if trapped oocytes were postulated to give rise to OTs, we would expect the OTs to develop from mature oocytes that have completed meiosis I. To test this hypothesis and more definitively determine the cellular etiology of *Tgkd* OTs, I studied genomic DNA samples from *Tgkd* OTs and paired host spleens obtained from *Tgkd* transgenic offspring of F1 (FVB-*Tgkd* x B6) hybrid male mice backcrossed to inbred FVB female mice. Genotypes of paired OT and spleen DNA samples were compared using pericentric and distal single nucleotide polymorphisms (SNPs) between FVB and B6 strains for each autosome and the X chromosome. If OTs arise from oocytes that have failed to complete meiosis I, pericentric markers of the OTs would be genetically identical to the paired spleen. However if they arise from oocytes that have completed meiosis I, the pericentric markers (FVB/B6) heterozygous in the host spleen would become homozygous in the OT. For the majority of informative (heterozygous FVB/B6) pericentric markers in each spleen DNA sample, genotypes of the paired OT DNA sample were homozygous (Table 4). In contrast, the majority of the informative distal SNPs in each spleen DNA sample remained heterozygous in the OT, consistent with frequent meiotic recombination between a distal SNP marker and the centromere of the same chromosome. Detailed description of the SNPs and their chromosomal location are provided in Appendix A. The small number of pericentric SNPs that were heterozygous in both paired OT and spleen DNA was likely due to a low frequency of recombination events near the centromere. These studies are consistent with OTs arising from oocytes through Type II meiotic error (Table 1)[64]. I could conclude from

these findings that each of the seven examined *Tgkd*⁺ OTs originated from a single mature oocyte that had completed meiosis I.

Table 4: OTs arise from mature oocytes that have completed meiosis I

Heterozygous pericentric and distal SNPs were identified in the spleens of 7 females with OTs from the cross between F1 (FVB-*Tgkd* X B6) and FVB mice. Genotypes (heterozygous or homozygous FVB) of these SNPs were then determined in each of the paired OTs. SNP information and location are provided in Appendix A.

<i>Tgkd</i> ovarian teratoma	Genotype (b/a)	
	Pericentric	Distal
1	0/11	6/7
2	0/11	7/7
3	1/12	6/6
4	2/11	4/4
5	0/7	5/5
6	1/7	6/8
7	0/8	6/8
a – Number of heterozygous SNPs in spleen of mouse with OT		
b – Number of SNPs heterozygous in both OT and spleen of host <i>Tgkd</i> /+ female		

4.5 PARTHENOGENETIC ACTIVATION OF *Tgkd* OOCYTES

From the above studies, it is clear that abnormal follicular development, specifically the presence of luteinized unruptured follicles (trapped oocytes), may play a crucial role in OT formation. Trapped oocytes have been observed in other OT models such as the constitutively active FSH receptor (mFshr^{D580H}) mice, however all mouse models with luteinized unruptured follicles do not develop OTs [3]. This observation indicates that some property of oocytes may have a role in increasing the propensity of OT development.

Parthenogenetic activation of oocytes has been reported to be necessary for OT formation [78]. Given this, I measured spontaneous parthenogenetic activation in cultured unfertilized *Tgkd* oocytes by measuring the frequency of oocytes that progressed to the 2-cell stage [78]. COCs were collected and matured for 17 hours in vitro after which the oocytes were separated from the surrounding cumulus cells. Parthenogenetic activation was scored as the number of oocytes that progressed to the 2-cell stage after an additional 24 hours of culture [78]. Approximately 30% of cultured *Tgkd* oocytes underwent cell division, similar to the percentage of 2-cell embryos seen in cultured wildtype FVB oocytes (Figure 10). The presence of the *Tgkd* transgene did not seem to significantly increase the rate of parthenogenetic activation seen in FVB oocytes. However the rate of parthenogenetic activation of FVB oocytes was much greater than that reported in B6 oocytes (3%) and even the OT susceptible LT/Sv mice (18%) (Eppig et al., 1996), suggesting that mature oocytes in inbred FVB mice have a propensity toward parthenogenetic activation. The absence of OTs in inbred FVB female mice however indicates that the FVB strain background alone is not sufficient for OT formation reiterating a previously reported observation that parthenogenetic activation is necessary but not sufficient for OT formation [78]. In this

regard, we speculate that the strain-specific modifier alleles (e.g. *Ots2*) promoting *Tgkd*-induced OT development in the FVB background also promote oocyte parthenogenetic development.

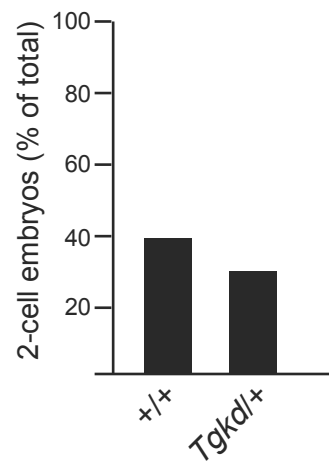


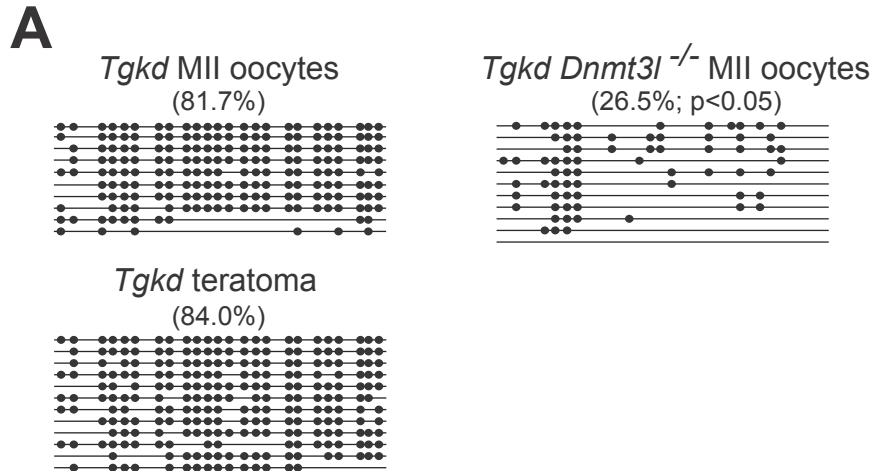
Figure 10: Parthenogenetic activation studies in wildtype and *Tgkd* oocytes

Parthenogenetic activation and development to 2-cell stage was examined in wildtype (43 COCs from 4 females) and *Tgkd* oocytes (37 COCs from 4 females). Both wildtype and *Tgkd* oocytes of the FVB strain exhibited a high rate of parthenogenetic activation, which was not increased in the presence of the *Tgkd* transgene.

4.6 ROLE OF OOCYTE *Tgkd* METHYLATION IN DEVELOPMENT OF OTS

Because the *Tgkd* transgene is maternally imprinted in *Tgkd* mice, I determined whether the loss of *Tgkd* transgene methylation influenced the formation of *Tgkd* OTs. The RSV sequences of *Tgkd* are methylated on the maternal and unmethylated on the paternal *Tgkd* alleles [92]. To assess the importance of *Tgkd* methylation on OT formation, *Tgkd* mice were crossed to *Dnmt3l*^{-/-} mice (FVB strain) in order to obtain *Dnmt3l*^{-/-}*Tgkd* females as DNMT3L protein is vital to the establishment of genomic methylation, including imprinted methylation, during development of mouse oocytes [99]. As expected, RSV sequences were highly methylated in *Tgkd Dnmt3l*^{+/+} MII oocytes (82%) and *Tgkd* OTs (84%), but poorly methylated in *Tgkd Dnmt3l*^{-/-} MII oocytes (26%) (Figure 11A).

OTs were correspondingly found in *Tgkd* and *Tgkd Dnmt3l*^{+/-} heterozygous female mice, but not in *Tgkd, Dnmt3l*^{-/-} female mice (Figure 11B). These findings support the notion that *Tgkd* transgene methylation may be required for OT formation in *Tgkd* female mice. However since the phenomenon of genomic imprinting is perturbed in *Dnmt3l*^{-/-} oocytes, I cannot exclude the possibility that abnormal maternal imprints and not the unmethylated *Tgkd* transgene precludes OT formation in these mice.



B

Genotype	OT incidence (%)
<i>Tgkd, Dnmt3l</i> ^{+/+}	12/80 (15)
<i>Tgkd, Dnmt3l</i> ^{+/-}	5/31 (16)
<i>Tgkd, Dnmt3l</i> ^{-/-}	0/14 (0)

Figure 11: Role of oocyte *Tgkd* methylation in OT formation

Loss of oocyte *Tgkd* methylation is associated with the loss of the OT phenotype in the *Tgkd* strain. **(A)** Methylation of RSV region of *Tgkd* in MII oocytes (from 4 *Tgkd* mice), teratomas (from 2 *Tgkd* mice) and MII oocytes (from 2 *Tgkd, Dnmt3l*^{-/-} mice) determined by bisulfite genomic sequencing. Filled circles – Methylated CpGs and absence of circle – Unmethylated CpGs **(B)** The OT phenotype is present in 15% of *Tgkd* hemizygous females but is lost in the *Dnmt3l*^{-/-} background. *- p value < 0.05.

4.7 ROLE OF *Tgkd* METHYLATION IN STRAIN SPECIFICITY OF OT PHENOTYPE

Since the loss of *Tgkd* methylation in FVB-*Tgkd Dnmt3l*^{-/-} MII oocytes was associated with lack of OTs, I assessed whether strain permissiveness for OT formation was a function of *Tgkd* methylation. To do this, I examined whether the *Tgkd* transgene was genomically imprinted (methylated on maternal allele) in the OT non-permissive 129 strain background. The FVB-*Tgkd* strain was backcrossed to the 129 strain for several generations (n>10) and 129-*Tgkd* females did not develop OTs.

Methylation of genomic imprints that are established in the female oocyte are maintained post fertilization and during adult development of most somatic tissues [100]. Hence I analyzed the methylation of *Tgkd* in the genomic DNA of F1 mice that either inherited the *Tgkd* transgene from the mother or from the father. The methylation of the *Tgkd* transgene in F1 progeny that inherit *Tgkd* only from the female recapitulate the state of *Tgkd* methylation in the oocytes of 129-*Tgkd* mother. On assessing the methylation state of the RSV sequences in the maternal *Tgkd* allele and the paternal *Tgkd* allele in genomic DNA from adult spleen, I found that the *Tgkd* transgene methylation is intact on the maternal allele and the *Tgkd* transgene is more highly methylated on the maternal allele (62.3%) than on the paternal allele (41.1%) (Figure 12). The methylation of maternally inherited *Tgkd* on the 129 background (62.3%) is lower than the level in *Tgkd* oocytes on the FVB background (81.7%), however *Tgkd* methylation is not depleted to levels observed in *Tgkd Dnmt3l*^{-/-} MII oocytes (26%), where OTs are absent. These studies led me to conclude that a high level of *Tgkd* methylation exists in 129-*Tgkd* oocytes and the non-permissiveness of the OT phenotype on this background is not connected to the loss of *Tgkd* methylation.

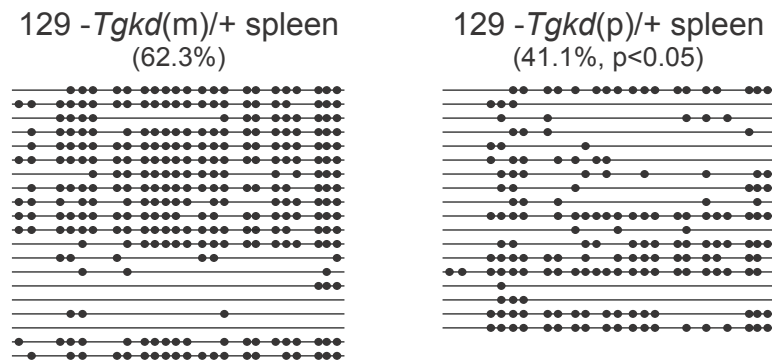


Figure 12: *Tgkd* transgene methylation on the 129 background

The methylation on the RSV sequence on the *Tgkd* transgene was measured in adult spleen DNA of F1 progeny that inherit *Tgkd* either maternally or paternally by bisulfite genomic sequencing. The maternal allele reflects the methylation state of *Tgkd* in 129-*Tgkd* oocytes. The methylation of maternally inherited *Tgkd* is maintained on the 129 strain and is higher than the methylation of paternally inherited *Tgkd* transgene. Filled circles – Methylated CpGs and absence of circle – Unmethylated CpGs.

4.8 CONCLUSIONS

In this chapter, I have examined the development defects in *Tgkd* ovaries. The *Tgkd* OT model is a complex model with several features contributing to the OT phenotype. I have observed a number of dramatic follicular defects such as premature corpora lutea formation and the presence of trapped oocytes in a subset of these follicles in *Tgkd* ovaries. OTs in *Tgkd* mice arise from mature oocytes that have completed meiosis I supporting the hypothesis that a subset of the trapped oocytes may develop into OTs. The oocytes of these mice display a high frequency of parthenogenetic activation, which is independent of the *Tgkd* transgene but highly dependent on the FVB strain. The parthenogenetic activation property may be linked to *Ots2* alleles on chromosome 6, which is associated with the FVB strain specificity of the phenotype. Previous studies by Lee et al also suggested that oocyte parthenogenetic development in the OT susceptible LT/Sv mice might be linked to *Ots1* alleles on chromosome 6 [79]. Surprisingly I found that OT development in *Tgkd* mice was not associated with fertility defects or premature ovarian failure observed in other reported OT mouse models.

Another important aspect in the *Tgkd* model was the requirement of the oocyte DNMT3L protein for subsequent OT formation. This observation indicated that either oocyte *Tgkd* methylation or the presence of intact maternal imprints was necessary for OT development. *Tgkd* methylation in oocytes was maintained in the non-permissive strains such as the 129 strain. Therefore strain specific OT non-permissiveness was not connected to the inherited methylation of *Tgkd* in the 129 strain.

I have characterized the ovarian follicular and oocyte defects that are associated with the OT phenotype [101]. In the next sections, I aim to identify the molecular and signaling defects that lead to these maturation defects in *Tgkd* ovaries.

5.0 INSERTIONAL EFFECTS OF THE *Tgkd* TRANSGENE

5.1 AIMS OF THESE STUDIES

The aim of these studies was to identify the gene or genes affected by the *Tgkd* insertion in order to explain the molecular and signaling defects that lead to OT formation in *Tgkd* females. To explore this possibility, we first mapped the precise insertion site of the *Tgkd* transgene array and surveyed the effect of the *Tgkd* insertion on the transcription of the surrounding genes. Because OTs arise from oocytes and the quantity of oocytes from female mice is limited (20 oocytes/mouse), each gene was characterized in tissues where the gene was highly expressed. The tissues of interest to study the expression of each gene was chosen on the basis of expression data curated in Mouse Genome Informatics (<http://www.informatics.jax.org/>) website. These gene transcription studies were performed on the assumption that the effect of the transgene *Tgkd* on the surrounding genes would be similar in the tissue analyzed and the *Tgkd* oocyte that leads to OTs. I also separated the tissues based on parental inheritance of *Tgkd* to analyze whether methylation of the transgene contributing to its effect on gene transcription. Alterations of gene transcription observed in *Tgkd* tissues would be independently confirmed in *Tgkd* oocytes that lead to the OT.

5.2 MAPPING OF THE *Tgkd* TRANSGENE INTEGRATION SITE

To explore the molecular basis of *Tgkd* OTs, we first identified the genomic location into which the *Tgkd* transgene array had inserted. The integration site of *Tgkd* was determined by identifying the genomic fragments flanking both sides of the *Tgkd* insertion by Dr. Richard Chaillet (University of Pittsburgh, Pittsburgh, PA). This was accomplished by identifying single copy junction fragments on southern blots of DNA from FVB-*Tgkd* mice probed with *Tgkd* transgene fragments. Two junctional fragments, one from either side of the *Tgkd* insertion were cloned from sub-genomic libraries of FVB-*Tgkd* DNA. Sequences of the endogenous genomic ends of both junctional fragments containing endogenous and *Tgkd* transgene sequences aligned with sequences on mouse chromosome 8, between the *Inpp4b* and *Il5* genes.

Further analysis of the junctional fragments indicated that approximately one kilobase of endogenous genomic DNA was deleted from the insertion site in *Tgkd* mice. The *Tgkd* transgene is located ~65 kilobases 3' of the known 3' end of the inositol polyphosphate-4-phosphatase type II (*Inpp4b*) gene and ~120 kilobases 5' of the known 5' end of the Interleukin 15 (*Il5*) gene (Figure 13A). The location of the large *Tgkd* transgene array in the intergenic region of *Inpp4b* and *Il5* suggested that the phenotypic abnormalities in *Tgkd* mice were due to disruption of one or more unidentified genes in the intergenic region or due to effects on the gene function of surrounding genes on chromosome 8. No spliced or unspliced transcripts have been reported in the *Inpp4b-Il5* intergenic region and multiple attempts to recover exons in this intergenic region using exon-trapping strategies failed. Therefore we postulated that the abnormalities observed in *Tgkd* mice were due to effects of the transgene on transcription of surrounding genes. In terms of the genes surrounding the integration site, I hypothesized that the novel inositol phosphatase *Inpp4b* was more likely to play a role in the etiology of OTs for a number of reasons. The first

reason was that the *Tgkd* insertion site was closest to the 3' end of the *Inpp4b* gene. Secondly the gene downstream of the *Tgkd* insertion *Il15* has been mainly reported to be involved in the control of the innate immune system and neither *Il15*^{-/-} mice nor mice that overexpress IL15 have been reported to develop OTs [102, 103]. However there have been reports of long-range transcriptional effects of DNA hypermethylation on surrounding genes [104, 105]. Therefore to perform an unbiased survey of the effect of the *Tgkd* transgene on genes surrounding the insertion site, I assessed the effect of *Tgkd* on transcription of protein-coding genes in a 2Mb region (1Mb on either side) on chromosome 8 surrounding the *Tgkd* insertion site (Figure 13B).

Two genes *4930579O11Rik* and *Gm9725* encoding long intergenic non-coding RNAs (lincRNA) have been reported to be present 0.5Mb and 1Mb centromeric to the *Tgkd* transgene on chromosome 8, but no function has been attributed to either lincRNA transcript (<http://www.informatics.jax.org/>). The effect of the *Tgkd* transgene in altering the levels of these lincRNA transcripts was not examined in this thesis.

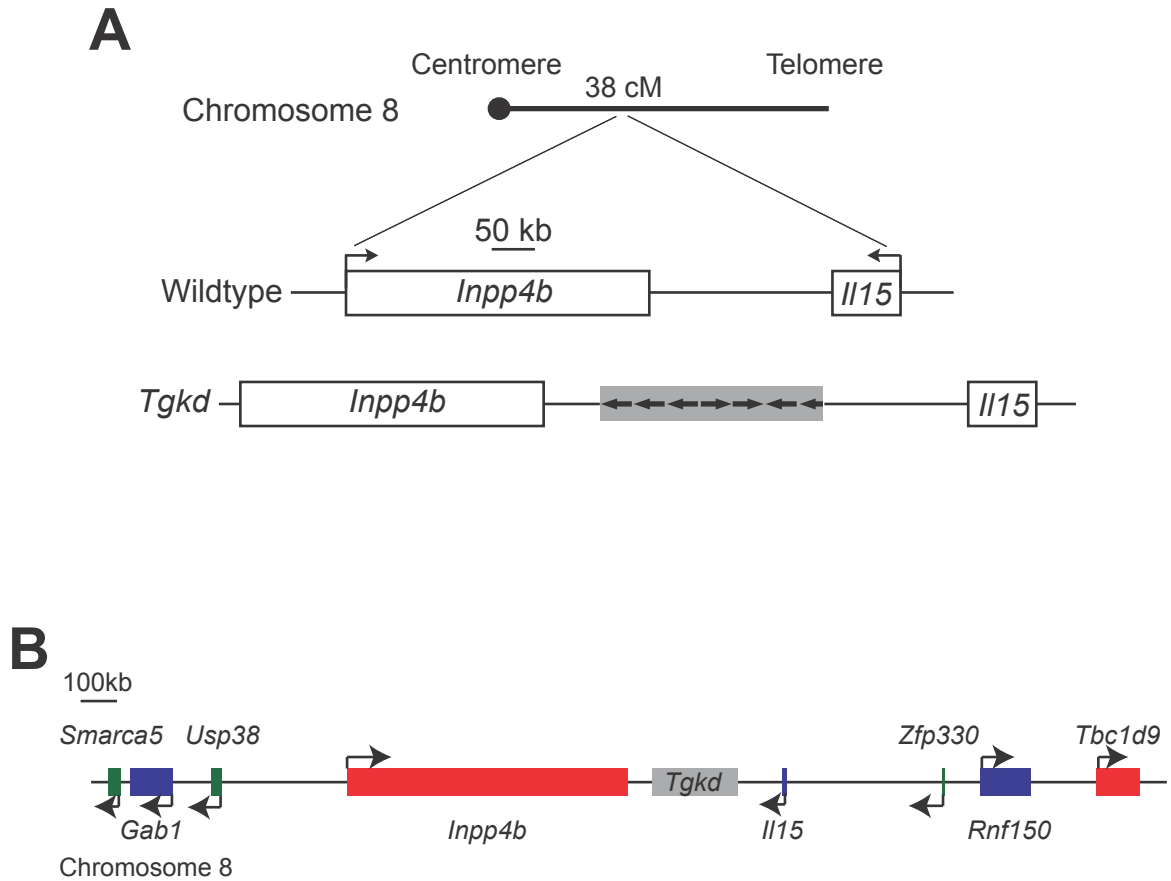


Figure 13: Schematics of the location of the *Tgkd* insertion site on chromosome 8

Representation of the insertion site of *Tgkd* transgene and surrounding genes on chromosome 8

(A) The *Tgkd* allele is inserted on chromosome 8 between the genes *Inpp4b* and *Il15* as a transgene tandem array in head-head, tail-tail or head-tail orientation. Each arrow represents a single copy of the transgene. (B) Genes located on chromosome 8 in a 2Mb region surrounding the insertion of the *Tgkd* transgene array. The effect of the *Tgkd* insertion on the transcription of the genes represented in the figure was analyzed in adult *Tgkd* tissues. Description of the

function and nomenclature of each of the genes are provided in subsequent sections. Arrow on each gene indicates sense or antisense transcription from the genomic strand.

5.3 ALLELE SPECIFIC TRANSCRIPTION STUDIES ON GENES SURROUNDING *Tgkd* INSERTION

The hemizygous *Tgkd* transgene on the FVB strain causes the OT phenotype in 15-20% of mice. Therefore, if we envision a cis-acting effect of *Tgkd* on the surrounding genes on chromosome 8, we would expect only the allele on the chromosome with the transgene to be affected by the insertion. As a result, we would expect an affected locus to have a normal wildtype allele on chromosome 8 without the *Tgkd* insertion and an altered allele on the copy of chromosome 8 with the *Tgkd* transgene. If we presume that *Tgkd* completely suppresses the expression of a gene by 100%, the overall reduction in the cellular levels of the gene product would be 50% due to the contribution of the wildtype allele in hemizygous *Tgkd* mice.

I first decided to examine whether the *Tgkd* transgene array affected the transcription of the genes surrounding the insertion site. To magnify the difference in gene expression caused by the *Tgkd* transgene and eliminate the contribution of the wildtype allele, we decided to use allele specific expression studies to specifically analyze cis-acting effects of *Tgkd* in a 2Mb region only on the copy of chromosome 8 where it is inserted. I analyzed the expression of each gene in the presence and absence of *Tgkd* in adult tissues, where they have previously been reported to be

highly expressed (<http://www.informatics.jax.org/>). To distinguish the gene expression between the 2 parental copies of chromosome 8, I utilized previously described SNP differences between mouse strains in the transcribed but untranslated UTRs or the coding exons of the gene. I set up crosses between FVB and 129 mice and analyzed allelic differences in the tissues of the F1 hybrid progeny. Further the crosses were set up such that the *Tgkd* transgene was always on the FVB copy of chromosome 8 and we could modify the parental inheritance of the transgene *Tgkd* and accordingly modify the methylation of the transgene by the design of the parental cross (Table 5).

I was able to subsequently analyze allele specific transcription in F1 hybrid tissues by the use of the method Single Nucleotide Primer Extension (SNUPE) assay (Figure 14) [93]. In this technique, RNA isolated from the F1 hybrid tissues was converted to cDNA and subsequently reverse transcriptase PCR was performed on the converted cDNA. Both the FVB allele and 129 allele of the specific gene are amplified by the RT-PCR, however they are amplified in proportion to the expression level in the tissue. Therefore if the *Tgkd* transgene has an effect on the FVB allele of the specific gene, the contribution of the FVB allele would be unequal to that of the 129 allele in the RT-PCR product. To measure this bias in the RT-PCR product, a single cycle of PCR is performed with a common primer (SNUPE primer) exactly 5' of a reported SNP in the RT-PCR product and radioactive nucleotides corresponding to the respective SNPs of the FVB and 129 alleles (Figure 14). The extent of radioactive incorporation of the FVB SNP is a measure of the transcript levels of the FVB allele. When both alleles are equally transcribed as in wildtype (+/+) F1 hybrids, the FVB to 129 allele incorporation ratio is 1:1. Significant deviations from this ratio of 1:1 indicate the effect of the *Tgkd* transgene on the FVB allele of the gene as it is normalized to the unaffected 129 allele. Since we are analyzing cis-acting effects of the *Tgkd*

transgene, I restricted the allele specific expression studies to a 2Mb region surrounding the *Tgkd* insertion on chromosome 8.

Table 5: Analysis of F1 hybrids for allelic specific expression

Allele specific expression was analyzed in adult tissues of F1 progeny obtained from the following crosses. The crosses were set up such that the *Tgkd* transgene was always on the FVB chromosome in the progeny. Further *Tgkd* transgene was inherited maternally in the progeny of the first cross and paternally in the progeny of the second cross.

Cross (Female X Male)	Transgene Inheritance	Expected Methylation of <i>Tgkd</i>
FVB- <i>Tgkd</i> X 129	Maternal	Highly Methylated
129 X FVB- <i>Tgkd</i>	Paternal	Relatively Unmethylated
FVB X 129	None	None

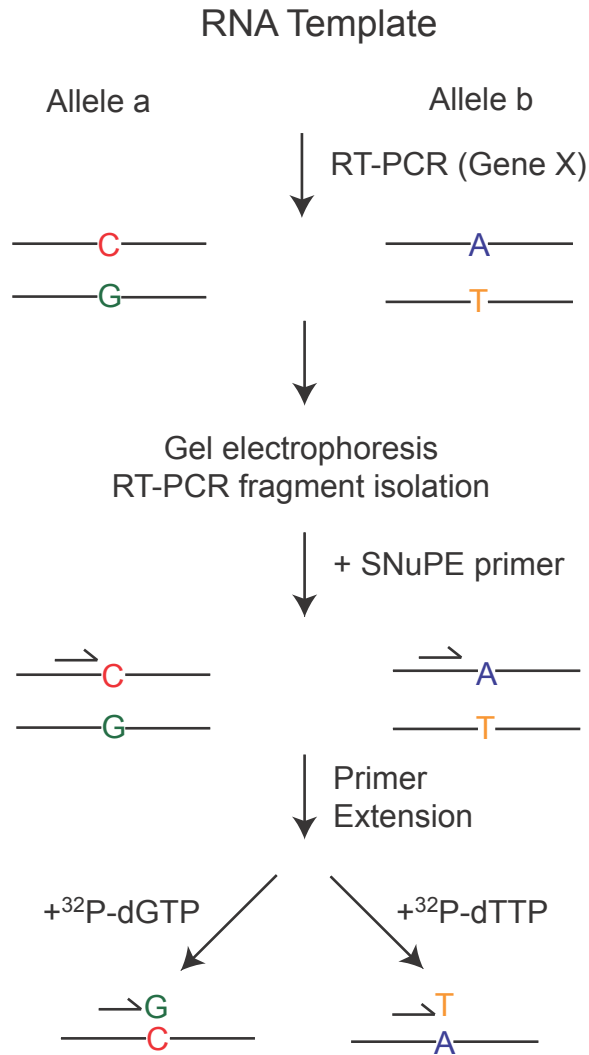


Figure 14: Representation of the SNuPE Assay

The SNuPE assay was used to detect allele specific gene expression from the FVB allele on chromosome 8 with the *Tgkd* transgene insertion. RT-PCR for each gene was performed on cDNA from equal quantities of RNA. A single round of primer extension on the RT-PCR product with radioactive nucleotides revealed allele specific differences in transcription.

Once we obtained progeny from the F1 crosses described in Table 5, I wanted to first confirm that the imprinted methylation of the *Tgkd* transgene is maintained in the F1 hybrid background. *Tgkd* as previously described in methylated on maternal inheritance and relatively unmethylated on paternal inheritance in both the FVB and 129 strain (Figure 12) [92]. I used a Southern blot approach with a probe located in the *Tgkd* transgene to confirm the imprinted status of *Tgkd* in the F1 hybrids [92].

The *Tgkd* transgene was heavily methylated on maternal inheritance (F1 *Tgkd*(m)/+) and relatively unmethylated on paternal inheritance (F1 *Tgkd*(p)/+) in F1 hybrid progeny from crosses between FVB-*Tgkd* and 129 mice (Figure 15). The specificity of the probe is confirmed by the absence of *Tgkd* methylated and unmethylated bands in the F1 hybrid (+/+) mice (Figure 15). The 129 strain also depicted an imprinted methylation state similar to FVB-*Tgkd* mice as determined by Southern blot and bisulfite genomic sequencing analysis.

Since I have confirmed that the methylation of *Tgkd* can be altered by parental inheritance in F1 hybrid mice, I subsequently analyzed the effect of *Tgkd* methylation on the transcription of the FVB allele of each of the genes analyzed on chromosome 8.

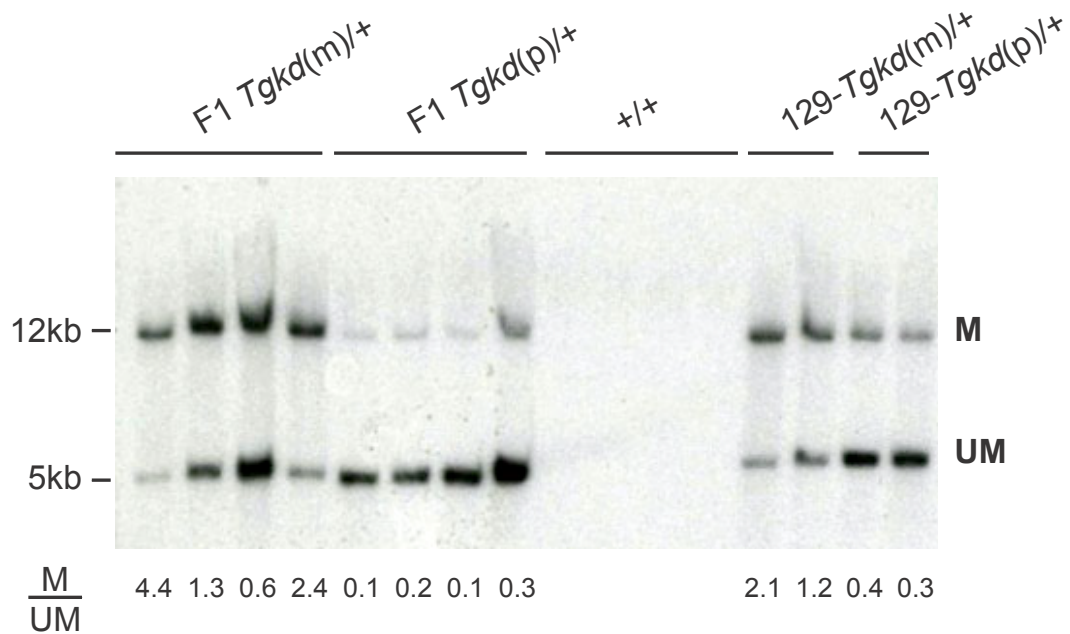


Figure 15: Imprinting status of the *Tgkd* transgene in F1 hybrid progeny

The methylation of the *Tgkd* transgene was analyzed by Southern blot analysis as previously described [92]. Spleen DNA was digested with the methylation sensitive enzyme BstUI and the southern blot was hybridized with the *Ca* probe located in the *Tgkd* transgene (Described in methods section). The *Tgkd* transgene in F1 hybrid progeny from the FVB-*Tgkd* and 129 cross is methylated on maternal inheritance and unmethylated on paternal inheritance as in the parent FVB and 129 strain. Lanes 1-4 – F1 progeny (*Tgkd* –Maternal inheritance), Lanes 5-8 – F1 progeny (*Tgkd* –Paternal inheritance), Lanes 9-12 – F1 progeny (*Tgkd* absent), Lanes 13-14 – Controls 129-*Tgkd* (Maternal inheritance) and Lanes 15-16 – Controls 129-*Tgkd* (Paternal inheritance). M - Methylated *Tgkd* band. UM - Unmethylated *Tgkd* band.

Allele specific expression studies using SNUPE analysis were performed on F1 hybrid tissue on 8 genes located either 1Mb upstream or downstream of the *Tgkd* insertion site (Figure 13B). Expression studies for each gene were performed on a tissue reported to have a high level of expression. We assumed that the *Tgkd* transgene would have the same effect on gene transcription in all tissues with sufficient expression and I would subsequently confirm alterations in oocytes, which give rise to OTs. The SNP differences between the FVB and 129 allele were confirmed in the RT-PCR product by sequencing prior to SNUPE analysis. RT-PCR primers and the SNUPE reaction primer for each gene are provided in Appendix B.

On the centromeric side of the *Tgkd* transgene, I analyzed 4 genes – SWI/SNF related, matrix associated, actin dependent regulator of chromatin, subfamily a, member 5 (*Smarca5*), growth factor receptor bound protein 2-associated protein 1 (*Gab1*), ubiquitin specific peptidase 38 (*Usp38*) and inositol phosphatase *Inpp4b*. *Smarca5* and *Inpp4b* were previously reported to depict high expression in the adult brain [106, 107]. *Gab1*, *Usp38* and *Inpp4b* were reported be highly expressed in the adult spleen. I analyzed allele specific expression of *Inpp4b* in brain and spleen, as it is located closet to the *Tgkd* insertion site [108]. For each SNUPE experiment, FVB and 129 control samples were used to depict the specificity and quantitative nature of the SNUPE analysis. The radioactive incorporation of the FVB specific SNP was quantitated using phosphoimager analysis and this was normalized to the level of 129 specific SNP. The 129 chromosome 8 did not have the *Tgkd* transgene insertion, hence was used as normalization control between the different groups.

I analyzed 3 different regions in the gene *Smarca5* for SNP differences between the FVB and 129 alleles, but none of the reported SNPs were true SNPs. In each case, the FVB SNP was also present on the 129 allele. Since, I could detect only the FVB cytosine SNP as depicted in

Figure 16A, I could not perform allele specific expression analysis on this gene. Since *Smarca5* was located farthest away (1.36Mb) from the *Tgkd* transgene, I did not pursue further SNUPE experiments on this gene.

Both *Gab1* and *Usp38* had SNP differences in the 5'UTR and coding exon 9 respectively (Figure 16B and C). On performing SNUPE analysis in adult spleens of F1 hybrids, I obtained a G/C ratio for *Gab1* and T/C ratio for *Usp38* when the FVB allele expression was normalized to the 129 allele. The G/C ratio for *Gab1* was similar in wildtype (+/+) F1 hybrids and F1 hybrids with the *Tgkd* transgene irrespective of parental inheritance (*Tgkd(m)/+* and *Tgkd(p)/+*) (Figure 16B). The T/C ratio for *Usp38* from SNUPE analysis was also similar among the various groups (Figure 16C). On performing SNUPE analysis on the *Inpp4b* gene in adult brain tissue, I observed a statistically significant 2 fold decrease in the levels of the FVB allele expression (C/T ratio) in maternal *Tgkd(m)/+* F1 hybrids compared to wildtype F1 hybrids (Figure 16D). This decrease was a *Tgkd* parent of origin specific effect as it was not observed in paternal *Tgkd(p)/+* hybrids. I observed a similar trend in adult spleen tissue but the effect of *Tgkd* on FVB *Inpp4b* expression was not as pronounced as that observed in the brain (Figure 16E). This parent specific decrease in *Inpp4b* is consistent with the importance of *Tgkd* methylation on the transgene-induced decrease of *Inpp4b* levels. Further an increase in CpG methylation has been correlated with a decrease in transcription of nearby genes, therefore we can hypothesize that the array of CpG methylation on *Tgkd* may cause transcriptional suppression of *Inpp4b*.

A*Smarca5* 3'UTR - Brain

ATAATTTTCTATGCATATTT[C/T]

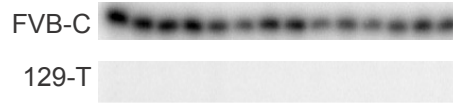
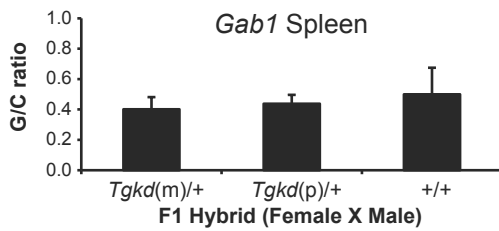
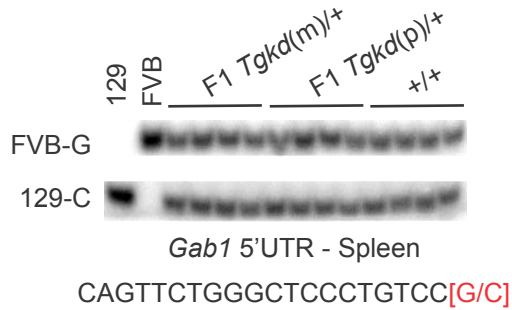
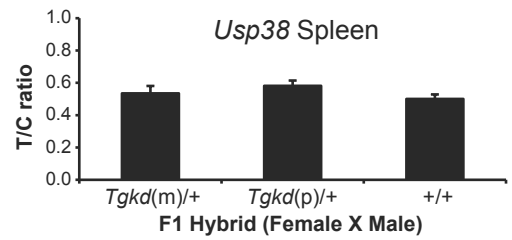
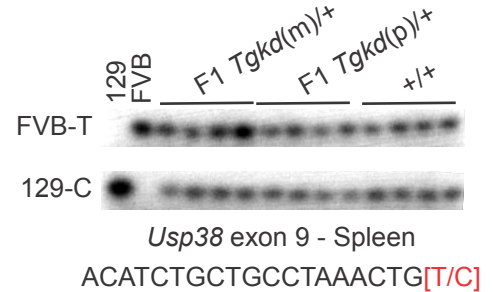
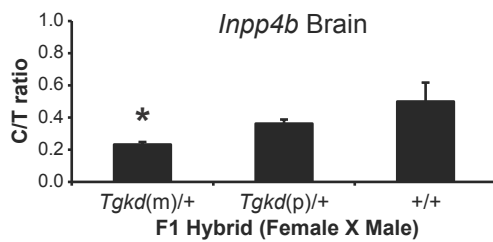
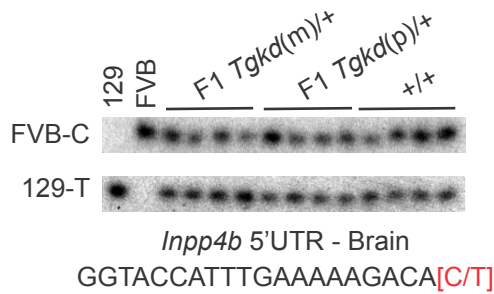
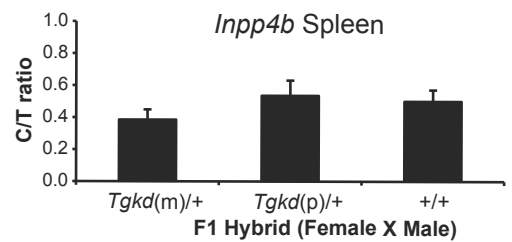
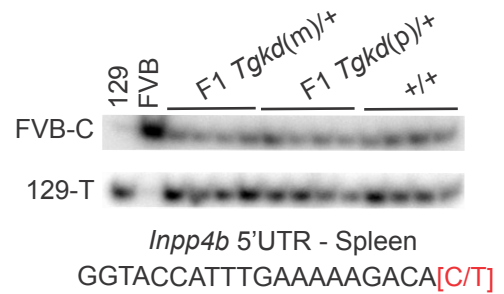
**B****C****D****E**

Figure 16: SNUPE analysis of genes on chromosome 8 centromeric relative to *Tgkd*

Allele specific expression studies were performed on the FVB allele, which contained the *Tgkd* transgene on genes in a 1Mb region centromeric of the transgene array. **(A)** SNPs differences between the FVB and 129 strain were not found in the cDNA of the *Smarca5* gene. Hence SNUPE analysis could not be performed. **(B)** SNUPE analysis was performed using G/C SNPs in the 5'UTR of the *Gab1* gene in spleen tissue. **(C)** SNUPE analysis was performed using T/C SNPs in coding exon 9 of the *Usp38* gene in spleen tissue. **(D&E)** SNUPE analysis was performed using C/T SNPs in the 5'UTR of the *Inpp4b* gene in brain and spleen tissue. SNUPE primer sequence for the single round of extension is indicated in each case along with the SNPs used for allele specific quantitation. SNP alleles are indicated as [FVB/129] SNP pairs. +/+ - wildtype F1 hybrid, *Tgkd(m)/+* - maternal inheritance of *Tgkd* in F1 hybrid and *Tgkd(p)/+* - paternal inheritance of *Tgkd* in F1 hybrid. n=4/genotype

For investigations on the telomeric side of the *Tgkd* insertion, I surveyed 4 genes, which are within 1Mb downstream of the *Tgkd* transgene. The 4 genes are interleukin 15 (*Il15*), zinc finger protein 330 (*Zfp330*), ring finger protein 150 (*Rnf150*) and TBC1 domain family, member 9 (*Tbc1d9*) (Figure 13B). The gene *Il15* was reported to be highly expressed in adult thymus, while the genes *Zfp330*, *Rnf150* and *Tbc1d9* were all reported to be highly expressed in the brain [109, 110].

The genes *Il15*, *Zfp330* and *Rnf150* had SNP differences in the 3'UTR of the gene, while *Tbc1d9* had SNP differences in the 5'UTR between the FVB and 129 strains (Figure 17A-D). On

performing SNUPE analysis in adult thymus of F1 hybrids, I obtained a T/C ratio for *Il15* when the FVB allele expression was normalized to the 129 allele. Similarly, on performing allele specific expression studies on F1 hybrid brains, I was able to determine a T/C, C/T and T/C ratio for *Zfp330*, *Rnf150* and *Tbc1d9* respectively to quantitate FVB allele expression. The T/C ratio of *Il15* in the thymus tissue of F1 hybrids was not significantly different in the presence or absence of the *Tgkd* transgene (Figure 17A). The FVB allele expression or T/C ratio of *Zfp330* showed a small but significant increase on both maternal (*Tgkd(m)/+* - 1.7 fold of *+/+*) and paternal (*Tgkd(p)/+* - 1.4 fold) inheritance of *Tgkd* compared to the wildtype F1 hybrid in adult brain (Figure 17B). The gene *Rnf150* also depicted a small (0.8 fold) but significant decrease in the C/T ratio in adult brain only on maternal inheritance of *Tgkd* (Figure 17C). The T/C ratios obtained from allele specific expression studies on *Tbc1d9* were not significantly different in the presence or absence of the *Tgkd* transgene (Figure 17D).

This survey of allele specific expression of genes in a 2Mb region surrounding *Tgkd* yielded 3 potential gene candidates to pursue, with significant transcription differences in the presence of *Tgkd*: *Inpp4b*, *Zfp330* and *Rnf150*. Since the transcription changes in *Rnf150* were small even in allele specific expression studies, I decided to exclude the gene from further analysis. Between *Inpp4b* and *Zfp330*, I postulated that *Inpp4b* would be better potential candidate involved in OT formation for several reasons. The first reason is that *Inpp4b* is closest to the *Tgkd* integration site, therefore is more likely to be influenced by the insertion. Secondly *Inpp4b* has the highest fold change (2 fold decrease) in the presence of maternal *Tgkd* and a decrease in expression would be consistent with the role of *Tgkd* methylation in transcriptional suppression. I also observed a *Tgkd* parent of origin effect on *Inpp4b* in adult brain and this effect is consistent with the notion that the heavily methylated maternal *Tgkd* is more effective at

transcriptional suppression of nearby genes (*Inpp4b*) than the unmethylated paternal *Tgkd* transgene. In summary, the allele specific expression studies led us to focus on the effect of *Tgkd* on *Inpp4b* levels and the mechanism by which transcriptional suppression of *Inpp4b* could lead to OT formation.

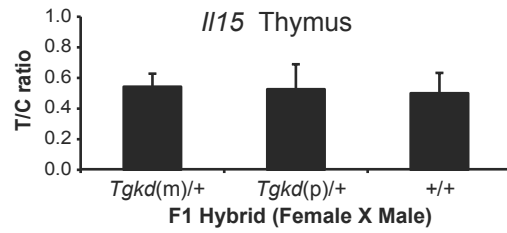
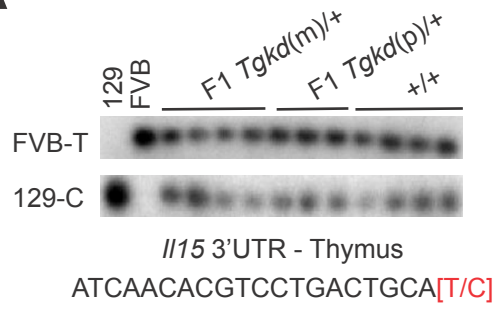
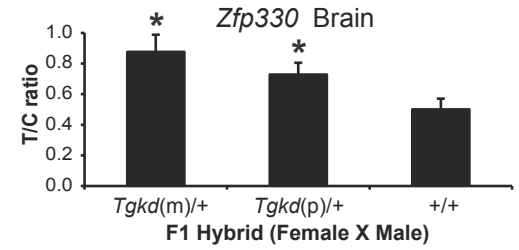
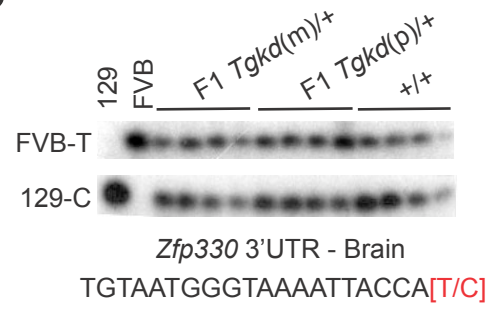
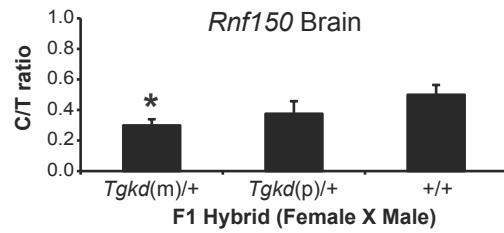
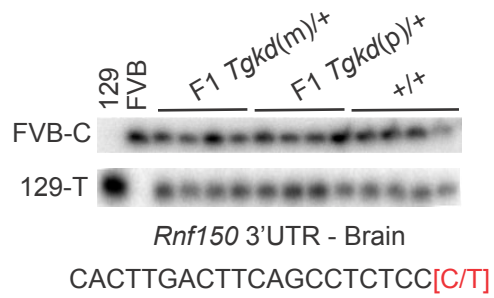
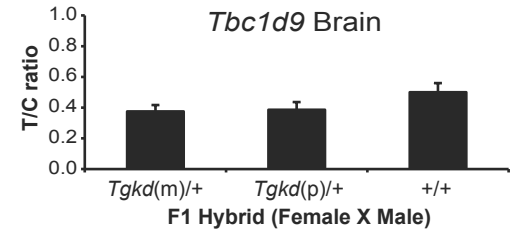
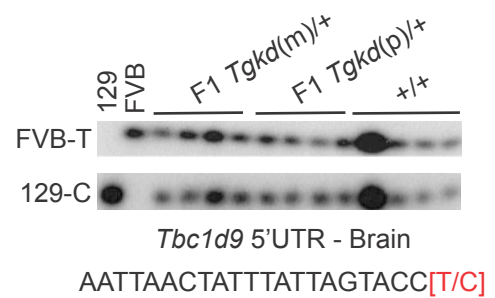
A**B****C****D**

Figure 17: SNUPE analysis of genes telomeric relative to the *Tgkd* insertion

Allele specific expression studies were performed on the FVB allele with the *Tgkd* insertion on genes in a 1Mb region telomeric of the transgene array. **(A)** SNUPE analysis was performed using T/C SNPs in the 3'UTR of the *Il15* gene in thymus tissue. **(B)** SNUPE analysis was performed using T/C SNPs in the 3'UTR of the *Zfp330* gene in brain tissue. **(C)** SNUPE analysis was performed using C/T SNPs in 3'UTR of the *Rnf150* gene in brain tissue. **(D)** SNUPE analysis was performed using T/C SNPs in the 5'UTR of the *Tbc1d9* gene in brain tissue. SNUPE primer sequence for the single round of extension is indicated in each case along with the SNPs used for allele specific quantitation. SNP alleles are indicated as (FVB/129) SNP pairs. +/+ - wildtype F1 hybrid, *Tgkd(m)/+* - maternal inheritance of *Tgkd* in F1 hybrid and *Tgkd(p)/+* - paternal inheritance of *Tgkd* in F1 hybrid.

5.4 TRANSCRIPTIONAL PROFILE OF INPP4B IN EMBRYONIC BRAIN

The *Tgkd* transgene on the FVB background leads to 2 phenotypes: adult hemizygous *Tgkd* females develop OTs and homozygous *Tgkd* mice die around birth. The perinatal death of homozygous *Tgkd* mice led us to hypothesize that both the maternal and paternal copy of *Tgkd* may have an effect on the surrounding genes and the additive effect of both copies of *Tgkd* in homozygous *Tgkd* mice causes the death of the mice. Therefore I decided to perform a 4-way comparison between wildtype (+/+), maternal *Tgkd* (*Tgkd(m)/+*), paternal *Tgkd* (*Tgkd(p)/+*) and

homozygous *Tgkd* (*Tgkd/Tgkd*) embryos to assess the effect of *Tgkd* on *Inpp4b* levels. I decided to perform this analysis on embryos earlier in gestation to avoid biases due to developmental defects later in gestation that eventually lead to the perinatal lethality of *Tgkd/Tgkd* mice.

I initially measured the levels of *Inpp4b* transcript in +/+, *Tgkd(m)/+*, *Tgkd(p)/+* and *Tgkd/Tgkd* E9.5 FVB embryos using real-time PCR analysis. I found that the levels of *Inpp4b* in all four groups were similar to each other independent of the presence of the *Tgkd* transgene (Figure 18A). However on evaluating the levels of *Inpp4b* transcript across gestation by real-time PCR, I found that *Inpp4b* was not highly expressed in E9.5 embryos (Figure 18B). *Inpp4b* has been reported to be expressed in the adult brain and I found that *Inpp4b* expression increases 8 fold in E13.5 wildtype embryo brains and 14 fold in E16.5 wildtype embryo brains compared to the levels in E9.5 wildtype embryos (Figure 18B) [106]. Since E16.5 embryos were closer to the time point of perinatal lethality, I decided to evaluate the effect of *Tgkd* on *Inpp4b* levels in E13.5 embryonic brains.

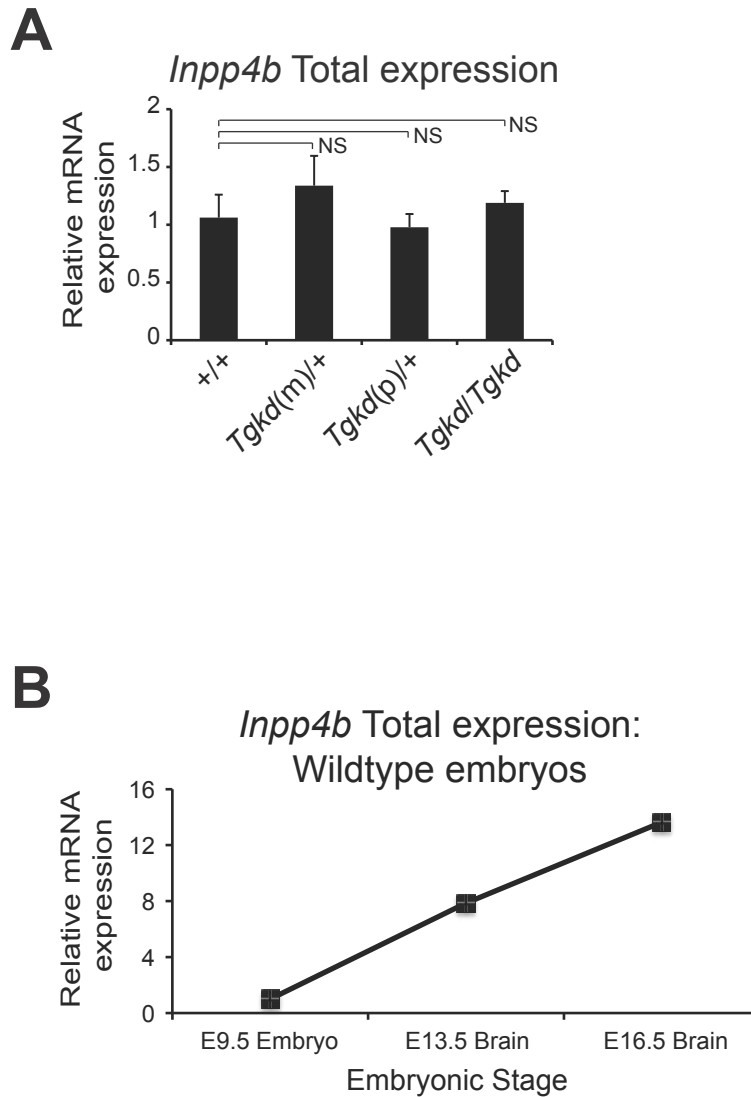


Figure 18: Determining *Inpp4b* levels across gestation

Inpp4b levels were determined in embryos across gestation by real-time PCR analysis. **(A)** *Inpp4b* levels were determined in hemizygous and homozygous *Tgkd* embryos at E9.5 during gestation by real-time PCR analysis (n=3 embryos/group). Relative mRNA expression or fold change was determined relative to wildtype (+/+) embryos. **(B)** *Inpp4b* transcript levels were

measured across gestation in wildtype FVB E9.5 embryos, E13.5 brain and E16.5 brain (n=1 at each stage). Fold change was determined relative to the expression measured in E9.5 embryos.

Inpp4b levels were normalized to the housekeeping gene TBP. NS – non-significant

5.5 EFFECT OF *Tgkd* ON INPP4B EXPRESSION IN E13.5 EMBRYONIC BRAIN

Since *Inpp4b* transcripts are highly expressed in the adult and embryonic brain, I first explored the effect of the *Tgkd* insertion on *Inpp4b* transcript and protein levels in the heads of E13.5 embryos (Figure 18B) [106]. This enabled us to perform a 4 way comparison of *Inpp4b* levels between wildtype (+/+), maternal *Tgkd* (*Tgkd*(m)/+), paternal *Tgkd* (*Tgkd*(p)/+) and homozygous *Tgkd* (*Tgkd*/*Tgkd*) embryos on the FVB strain. I was also able to perform an in-depth comparison on the role of methylation and homozygosity of *Tgkd* in altering *Inpp4b* transcript and protein levels. At the level of *Inpp4b* transcription, I also analyzed the effect of the *Tgkd* transgene on known splice isoforms of *Inpp4b*.

The two well-characterized *Inpp4b* transcripts, *Inpp4b* α and *Inpp4b* β are produced by alternative splicing of the 3' end of *Inpp4b* and are translated into the INPP4B α and INPP4B β proteins respectively [106]. A comparison of *Inpp4b* transcript levels was performed among wild-type, *Tgkd*(m)/+, *Tgkd*(p)/+ and *Tgkd*/*Tgkd* E13.5 embryos (Figure 19A). The level of *Inpp4b* β was found to be most affected by the *Tgkd* insertion; *Tgkd*/*Tgkd* and *Tgkd*(m)/+

embryos expressed ~50% of wild-type *Inpp4bβ*, whereas *Tgkd(p)/+* embryos showed an ~20% decrease in *Inpp4bβ* expression ($p < 0.05$).

Inpp4ba (includes *Inpp4bas*, a short α -like transcript) was less affected in *Tgkd* embryo heads. Homozygous *Tgkd/Tgkd* embryos showed the most downregulation (20%) compared to wildtype controls, and *Tgkd(m)/+* embryos had comparable *Inpp4ba* expression as *Tgkd/Tgkd* embryos ($p < 0.05$). Levels of *Inpp4ba* in *Tgkd(p)/+* embryos were somewhat lower than wildtype embryos but this difference was not statistically significant. Total *Inpp4b* followed a pattern of expression similar to the *Inpp4ba* transcript because the level of *Inpp4bβ* was approximately 10-fold lower than the total levels of *Inpp4b* in adult brain.

INPP4B protein levels were correspondingly affected in E13.5 embryonic heads. Individual *Tgkd/Tgkd* heads had a significant reduction of ~50% of the wildtype protein concentration (Figure 19B). Individual *Tgkd(m)/+* and *Tgkd(p)/+* heads had somewhat lower concentrations of INPP4B, although collectively, levels of INPP4B in hemizygous mice were not statistically different than wild-type mice (Figure 19B). The combination of small effects on the normally highly expressed *Inpp4ba* transcripts, and large effects on the normally poorly expressed *Inpp4bβ* transcript from both parental *Tgkd* alleles accounts for the significant differences in INPP4B expression between *Tgkd/Tgkd* and control wildtype embryos. I was surprised to observe that the transcriptional differences observed between *Tgkd(m)/+* and *Tgkd(p)/+* embryo heads did not manifest in the levels of total INPP4B protein. We cannot distinguish between INPP4B α and β protein isoforms with the currently available antibodies, which are targeted to the N-terminus of the INPP4B protein. The absence of significant differences between *Tgkd(m)/+* and *Tgkd(p)/+* embryo heads is most likely due to the low levels of the INPP4B β protein compared to the INPP4B α protein. In summary, in E13.5 embryonic

brains, the *Tgkd* transgene has parent-specific effects on *Inpp4b* transcription, however the effect on INPP4B protein levels is similar in hemizygous *Tgkd* brains to wildtype levels and an additive decrease is seen in homozygous *Tgkd* brains.

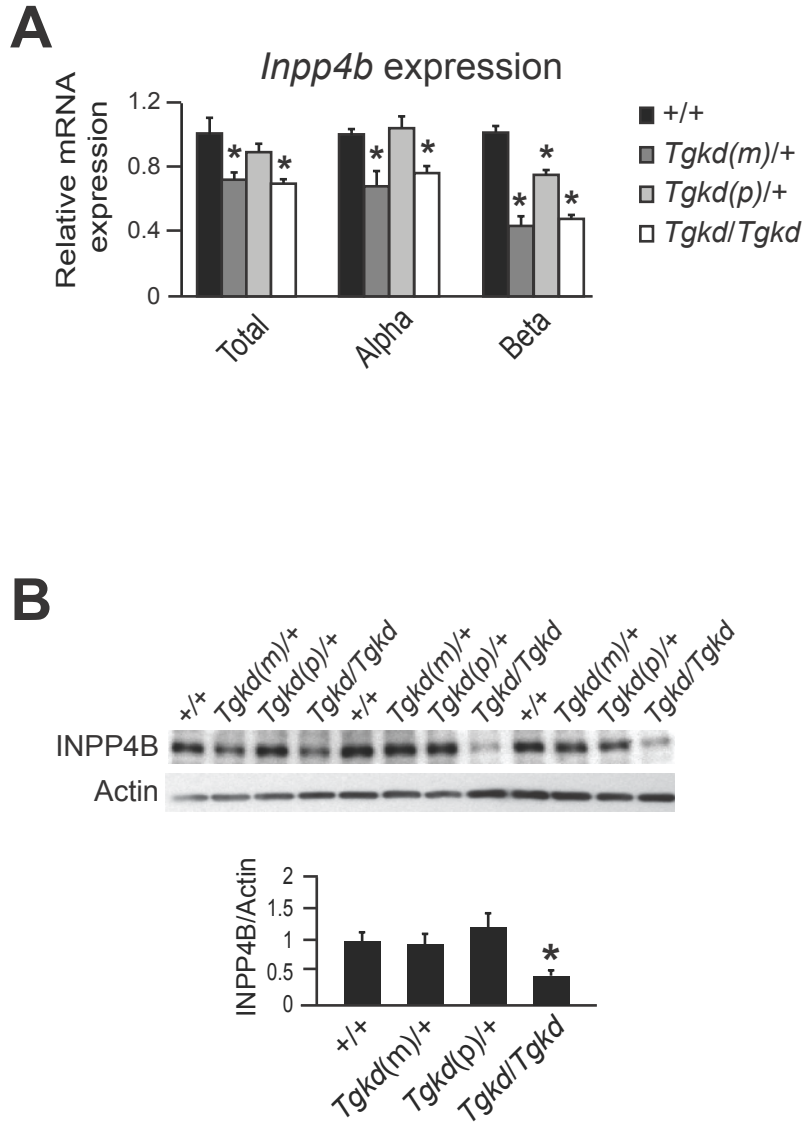


Figure 19: Effect of *Tgkd* on *Inpp4b* levels in E13.5 embryos

Expression of *Inpp4b* in E13.5 *Tgkd* embryonic brain. (A) *Inpp4b* total transcript and levels of α and β isoforms were measured in *Tgkd* E13.5 embryo heads (+/+ - wildtype, *Tgkd(m)/+* - maternally inherited *Tgkd*, *Tgkd(p)/+* - paternally inherited *Tgkd*, and *Tgkd/Tgkd* - homozygous *Tgkd*) (n>3 mice/genotype). *Inpp4b* levels were normalized to the housekeeping gene TBP and

fold changes were expressed relative to +/+ embryos. **(B)** INPP4B protein levels in homozygous and hemizygous *Tgkd* E13.5 embryo heads (n=3). * - p value <0.05

5.6 IMPACT OF THE *Tgkd* INSERTION ON SPLICE ISOFORMS OF *Inpp4b*

In the analysis of the effect of *Tgkd* on *Inpp4b* transcription, I found that the *Tgkd* transgene had a more pronounced effect on *Inpp4bβ* compared to the *Inpp4bα* splice isoform. *Inpp4bα* and *Inpp4bβ* are previously characterized splice isoforms generated due to alternative splicing of the terminal exon of *Inpp4b* exon 25, resulting in different terminal exons and 3' UTRs [106]. INPP4B α has a hydrophilic carboxy terminus while INPP4B β has a hydrophobic carboxy terminus. *Inpp4b* also has an alternative *Inpp4bα* isoform that lacks exon 5, however this isoform is not expressed in the brain [106].

Given these results, I also wanted to determine whether the *Tgkd* insertion caused the generation of any novel splice isoforms of the gene *Inpp4b* in addition to its effect on *Inpp4bα* and *Inpp4bβ*. Transcripts from E13.5 embryonic brain from wildtype and homozygous (*Tgkd/Tgkd*) were ideal for this analysis as *Tgkd/Tgkd* brains should show an enrichment for any potential *Tgkd* induced splice isoforms. To investigate the existence of novel splice isoforms, RNA from a *Tgkd/Tgkd* and wildtype E13.5 brain was converted to cDNA. A series of PCRs after reverse transcription (RT-PCRs) were performed spanning the entire cDNA sequence of the

gene. The PCR primers were designed to generate 1kb amplicons and successive PCR products had overlap regions of at least 200bp. The PCR amplified amplicons were sequenced and the sequence from wildtype and *Tgkd/Tgkd* embryos were compared. Overlap regions were designed in PCR products to ensure sequencing of the entire *Inpp4b* cDNA sequence. Further if the loss of sequence in potential novel isoforms were in the region of the forward or reverse primer, then PCR amplification of that amplicon would not take place.

I designed 7 sets of primers to span the entire 3.23kb and 4.39kb *Inpp4b* α and β cDNA sequence respectively. The primer sequence for each amplicon is provided in Appendix B. I obtained successful PCR amplification of similar size for all sets of primers in both wildtype and *Tgkd/Tgkd* E13.5 brains indicating no major loss or gain of sequence in *Tgkd/Tgkd* E13.5 brains. DNA sequencing of the cloned RT-PCR products revealed no sequence differences or novel splice isoforms between wildtype and *Tgkd/Tgkd* embryonic brains (Data not shown). In summary, the insertion of *Tgkd* did not alter the sequence or generate novel isoforms of *Inpp4b*.

5.7 CONCLUSIONS

In this chapter, I have determined that the *Tgkd* transgene is inserted on chromosome 8 between the *Inpp4b* and *Il15* genes [101]. The *Tgkd* insertion is closest to the 3' end of *Inpp4b*. Allele specific expression studies revealed that the hemizygous *Tgkd* transgene had effects on the transcript levels of *Inpp4b*, *Zfp330* and *Rnfl50* genes. However the highest decrease induced by the *Tgkd* insertion was on the *Inpp4b* gene and this suppression was caused by the methylated maternal *Tgkd* transgene. *Inpp4b* transcript levels were examined in wildtype embryos prior to the perinatal lethality observed in *Tgkd/Tgkd* mice. *Inpp4b* was not expressed in E9.5 embryos,

however the levels of *Inpp4b* were high in both E13.5 and E16.5 brains. On further examination of E13.5 brains, homozygous *Tgkd/Tgkd* embryos showed the largest decrease in *Inpp4b* levels specifically in the *Inpp4b β* isoform compared to wildtype embryos. Embryos with maternal inheritance of *Tgkd* (*Tgkd(m)/+*) mimic *Inpp4b* expression patterns in *Tgkd/Tgkd* embryos while *Tgkd(p)/+* embryos have wildtype *Inpp4b* levels. On examination of INPP4B protein in E13.5 brains, a significant decrease in INPP4B protein was observed only in homozygous *Tgkd/Tgkd* embryos compared to wildtype levels. The *Tgkd* insertion did not alter the sequence or cause generations of novel splice isoforms of *Inpp4b* in *Tgkd/Tgkd* E13.5 brains. Therefore *Tgkd* mainly caused transcriptional suppression of *Inpp4b* levels in hemizygous and homozygous *Tgkd* E13.5 brains, which manifested as a significant decrease in INPP4B protein in *Tgkd/Tgkd* embryonic brains.

6.0 ES CELL MODEL TO STUDY EFFECT OF *Tgkd* ON INPP4B AND DOWNSTREAM SIGNAL TRANSDUCTION PATHWAYS

6.1 AIMS OF THESE STUDIES

The effect of the *Tgkd* transgene in decreasing the levels of INPP4B was demonstrated in the previous chapter by allele specific expression in adult brain and real time PCR studies in embryonic brain. Recent studies have shown that the tumor suppressor *Inpp4b* is a negative regulator of PI3-Kinase/AKT (PI3K/AKT) signaling pathway through degradation of PI(3,4)P₂ to PI(3)P [111, 112]. An increase in PI(3,4)P₂ levels promotes increased phosphorylation of AKT; therefore by degrading PI(3,4)P₂, *Inpp4b* acts as a suppressor of the PI3K/AKT pathway. To study the role of *Tgkd* in OT formation, I decided to examine its role on the PI3K/AKT pathway.

I did not perform PI3K/AKT activation studies in the adult or embryonic brain as the levels of phospho-AKT (P-AKT) were very low (Data not shown) and the stimulation experiments to study AKT activation kinetics on embryonic brain seemed difficult and unconnected to the process of OT formation from oocytes. *Inpp4b* expression and PI3K/AKT studies in oocytes were also challenging due to the limited amount of oocyte material. Therefore to develop an in vitro model closer to the oocyte developmental time point, we decided to use ES cells as a model to study *Tgkd* induced effects on *Inpp4b* levels and the activation of the

PI3K/AKT pathway. The ES cell model offered a number of advantages as a tool to study the effect of *Tgkd* on the PI3K/AKT pathway. INPP4B is expressed in ES cells and ES cells are derived from an early embryonic time point (E3.5 blastocysts), which is a closer developmental time point to oocytes. They provide an unlimited amount of material to study AKT activation kinetics and AKT phosphorylation can be modulated easily in ES cells through serum starvation and subsequent stimulation with the hormone IGF1. Further, since ES cells are derived from E3.5 blastocysts, we should be able to derive wildtype (+/+), hemizygous (*Tgkd*(m)/+ and *Tgkd*(p)/+) and homozygous *Tgkd/Tgkd* ES cell lines to perform a 4-way comparison on the effect of the *Tgkd* transgene on *Inpp4b* expression and subsequent PI3K/AKT activation in this model.

These factors rendered the *Tgkd* ES cell model as an attractive model to study signaling alterations in the PI3K/AKT pathway caused by the transgene, which can be subsequently confirmed in *Tgkd* oocytes that lead to OT formation.

6.2 DEVELOPMENT OF THE *Tgkd* ES CELL MODEL AND METHYLATION STATUS OF *Tgkd* IN ES CELLS

To develop the *Tgkd* ES cell model, I derived ES cell lines from E3.5 blastocysts by previously established methods [89]. I decided to derive ES cell lines from blastocysts of the 129 strain as these blastocysts depict a higher potential to give rise to ES cell lines than blastocysts from other mouse strains [113]. The FVB strain is permissive to OT development and the 129 strain is not OT permissive in the presence of the *Tgkd* transgene. However, the gene/genes linked to the FVB strain specific OT phenotype was linked to a region on chromosome 6 independent of the

Tgkd transgene insertion on chromosome 8. This observation led us to assume that the cis-acting effects of *Tgkd* on the surrounding genes on chromosome 8 in the 129 strain would be identical to that observed in the FVB-*Tgkd* strain. However additional strain specific alleles on chromosome 6 also are required for OT development. Hence, the effect of *Tgkd* on *Inpp4b* levels and its effects on the PI3K/AKT pathway were examined in 129 ES cells with the *Tgkd* transgene (129-*Tgkd* ES cells) and these effects were considered similar to that observed in FVB-*Tgkd* ES cells.

To develop 129 wildtype, hemizygous and homozygous *Tgkd* ES cell lines, I set up the following crosses to obtain blastocysts for ES cell derivation (Table 6). About 40% of the blastocysts collected from matings gave rise to ES cell lines. Homozygous *Tgkd* (*Tgkd/Tgkd*) ES cell lines could be derived from a cross between a hemizygous 129-*Tgkd* female and 129-*Tgkd* male (Table 6). The homozygous *Tgkd* lines were obtained at a lower frequency as approximately 1 out of 4 ES cell lines derived from the above cross were *Tgkd/Tgkd* lines according to Mendelian ratios. Further I could derive hemizygous *Tgkd* lines that inherit the transgene maternally (*Tgkd(m)/+*) or paternally (*Tgkd(p)/+*), thereby altering the methylation state of *Tgkd* in the ES cell lines (Table 6). 129 wildtype lines were derived from 129 blastocysts obtained from all the above crosses.

Table 6: Derivation of *Tgkd* ES cell lines and expected methylation state

The following crosses were set up in order to collect E3.5 blastocysts for derivation of *Tgkd* ES cell lines. Crosses between 129-*Tgkd* and 129 mice were set up such that the blastocyst inherited the transgene either from the mother (*Tgkd*(m)/+) or the father (*Tgkd*(p)/+). The maternally inherited *Tgkd* was expected to be more highly methylated than paternally inherited *Tgkd* in these ES cell lines. Homozygous *Tgkd*/*Tgkd* ES cell lines were derived from crosses between hemizygous 129-*Tgkd* mice and were expected to have an intermediate methylation due to *Tgkd* methylation from both the maternal and paternal allele. Number of lines indicates the number of ES cell lines derived from these crosses, which were used for further analysis.

Cross (Female X Male)	<i>Tgkd</i> inheritance	Expected <i>Tgkd</i> methylation state	Number of lines
129- <i>Tgkd</i> X 129	Maternal	Highly methylated	3
129 X 129- <i>Tgkd</i>	Paternal	Relatively Unmethylated	3
129- <i>Tgkd</i> X 129- <i>Tgkd</i>	Homozygous	Intermediate methylation	2
All the above crosses give rise to 129 (+/+) lines			2

The crosses detailed in Table 6 allowed us to derive ES cell lines to perform a 4-way comparison analysis between $+/+$, $Tgkd(m)/+$, $Tgkd(p)/+$ and $Tgkd/Tgkd$ ES cell lines. This allowed me to study the effect of *Tgkd* methylation on *Inpp4b* levels and on the PI3K/AKT pathway. Furthermore the derivation of the homozygous $Tgkd/Tgkd$ ES cell lines helped me analyze whether 2 copies of *Tgkd* had a larger effect on *Inpp4b* suppression and on the PI3K/AKT pathway, as observed in $Tgkd/Tgkd$ E13.5 brains (Figure 19). I derived 3 $Tgkd(m)/+$, 3 $Tgkd(p)/+$ and 2 $Tgkd/Tgkd$ ES cell lines from the above crosses (Table 6). Several wildtype lines were obtained from all 3 crosses out of which 2 lines were used for further analysis.

The ES cell lines were genotyped by the PCR assay described in Figure 7B and a representative genotyping assay from the ES cell lines is depicted in Figure 20A. The wildtype band is absent in homozygous $Tgkd/Tgkd$ ES cell lines (Lane 1,2 - Figure 20A) while hemizygous *Tgkd* lines have a wildtype and a *Tgkd* PCR band (Lane 3-16 - Figure 20A). Maternal and paternal inheritance of *Tgkd* cannot be distinguished in the PCR genotyping of hemizygous *Tgkd* ES cell lines (Lane 3-16 - Figure 20A). The *Tgkd* PCR product was absent in wildtype ES cell lines (Data not shown).

After derivation of the 4 groups of ES cell lines, I wanted to first examine whether the methylation status of the transgene *Tgkd* is maintained in the independently derived lines. *Tgkd* is a maternally imprinted transgene and maternal imprints are established in the oocyte, maintained in the early embryo and undergo erasure only in the PGCs [100]. Therefore, I expected the maternal $Tgkd(m)/+$ lines to possess higher *Tgkd* methylation than paternal $Tgkd(p)/+$ lines and $Tgkd/Tgkd$ lines to depict intermediate levels of *Tgkd* methylation (Table 6). However, on examining the levels of *Tgkd* methylation using Southern blot analysis, I found that independently derived *Tgkd* lines of the same category depicted a wide range of *Tgkd*

methylation (Figure 20B). The upper band in the Southern blot in Figure 20B indicates methylated *Tgkd* band (M), while the lower band constitutes the unmethylated *Tgkd* band (UM). The extent of *Tgkd* methylation was determined in each of the ES cell lines by calculating a methylation (M/UM) ratio by dividing the signal from the methylated band by the unmethylated band. I expected a highly methylated *Tgkd* transgene to have ratio of greater than 1 and unmethylated *Tgkd* to have a ratio much lower than 1. Homozygous *Tgkd/Tgkd* lines were expected to show a ratio close to 1 due to the contribution of the maternal and paternal copies of *Tgkd*.

In the methylation analysis of the *Tgkd* ES cell lines, both of the homozygous *Tgkd/Tgkd* lines showed very high *Tgkd* methylation (Methylation Ratio=1.9 & 1.4), which were very different from the expected methylation ratio of 1 (Figure 20B). The 3 independently derived maternal *Tgkd(m)/+* lines depicted the highest range of variability in *Tgkd* methylation (Ratio range = 0.4-3.2) with *Tgkd(m)/+* lines depicting high *Tgkd* transgene methylation (Ratio=3.2), intermediate *Tgkd* methylation (Ratio=1) and low levels of *Tgkd* methylation (Ratio=0.4) (Figure 20B). The paternal *Tgkd(p)/+* lines showed variability in the levels of *Tgkd* methylation between the 3 independently derived lines but all the lines showed low levels of *Tgkd* methylation (Ratio range = 0.3-0.7) (Figure 20B).

In summary, independently derived *Tgkd* ES cell lines depicted a wide variation in *Tgkd* transgene methylation, which did not depend on the parental inheritance of the transgene. The process of in vitro ES cell derivation from the inner cell mass may have led to an instability in the maintenance of *Tgkd* methylation. ES cells are able to survive in the undifferentiated state with very low levels of genomic DNA methylation [114]. This ability to survive in the absence of proper genomic imprints may have removed the selection pressure for appropriate *Tgkd*

methylation. Further factors in the ES cell media, which maintain the undifferentiated state could affect the levels of *Tgkd* transgene methylation.

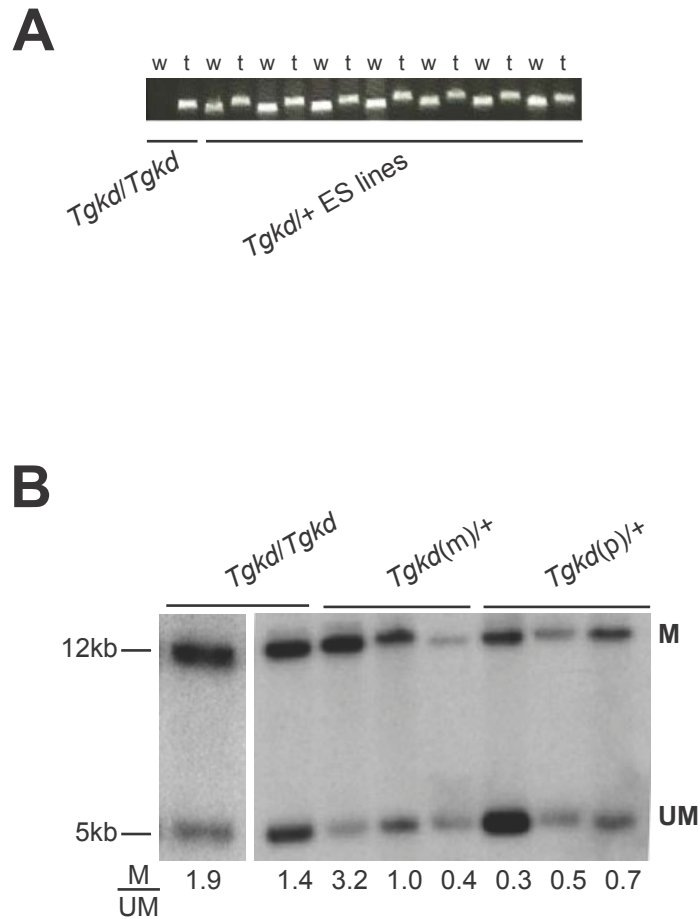


Figure 20: PCR genotyping of ES cell lines and maintenance of *Tgkd* methylation

ES cell lines were established from matings described in Table 6 to derive homozygous (*Tgkd/Tgkd*), hemizygous (*Tgkd/+*) and wildtype (+/+) ES cell lines. Panel (A) describes the PCR genotyping procedure used to assay for *Tgkd/Tgkd* and *Tgkd/+* ES cell lines. w - PCR band obtained for the wildtype allele in the absence of the *Tgkd* insertion and t - *Tgkd* transgene PCR product. The wildtype (w) band is absent in homozygous (*Tgkd/Tgkd*) ES cell lines and the both the wildtype (w) and *Tgkd* (t) band are present in hemizygous *Tgkd/+* ES cell lines. (B) Southern analysis on ES cell DNA digested with the methylation sensitive enzyme BstUI with the *Ca*

probe located in the *Tgkd* transgene (Described in methods section). M - Methylated *Tgkd* band and UM - Unmethylated *Tgkd* band. M/UM ratio calculates extent of methylation by dividing the signal from the methylated band to the unmethylated band. M/UM ratio for each ES cell lines is indicated below the respective lane.

6.3 EFFECT OF *Tgkd* ON INPP4B IN ES CELLS

The methylation of the *Tgkd* transgene in the ES cell lines did not match the predicted pattern of *Tgkd* methylation observed in somatic tissues. However I also wanted to determine the effect of the *Tgkd* transgene on INPP4B levels in undifferentiated ES cells and whether the inheritance or methylation of *Tgkd* affects INPP4B levels.

To study *Tgkd* induced effects on INPP4B levels, I compared INPP4B (I) protein levels, normalized to the housekeeping gene Actin (A) between different groups of ES cell lines. I used 2 wildtype ES cell lines obtained during ES cell derivation and 1 previously available wildtype ES line W9.5 as controls. I compared the levels of INPP4B (normalized to Actin) in the *+/+* lines to 3 *Tgkd(m)/+*, 3 *Tgkd(p)/+* and 2 *Tgkd/Tgkd* ES cell lines (Figure 21A). The levels of INPP4B were expressed as the fold change of expression relative to INPP4B levels in a single wildtype ES cell lines generated in the experiment (Figure 21A, Lane 5, I/A=1) and statistical significance of differences in the ES cell lines was assessed by comparison to the same wildtype ES line.

The wildtype line W9.5 expressed very high levels of INPP4B compared to the other 2 wildtype lines derived in the experiment (I/A=3.7 fold compared to 1 & 1.3). The 3 independent *Tgkd(m)/+* lines showed decreased levels of INPP4B compared to all the wildtype lines, however this difference was not statistically significant. The *Tgkd(p)/+* lines however depicted widely variable INPP4B levels (I/A=2.7 - 0.7) with 1 ES line upregulating INPP4B and the 2 other *Tgkd(p)/+* lines having decreased levels of INPP4B. The levels of INPP4B in the 2 homozygous *Tgkd/Tgkd* ES cell lines derived in the experiment were different from each other (I/A=0.7 & 1.1) with only one of the *Tgkd/Tgkd* ES cell lines showing a significant decrease in levels of INPP4B compared to the wildtype line (Figure 21A). These results led us to conclude that INPP4B levels were variable even in independently derived wildtype ES cell lines, which did not contain the *Tgkd* transgene. There was variation in INPP4B levels between *Tgkd* ES cell lines of the same group in paternal *Tgkd(p)/+* and homozygous (*Tgkd/Tgkd*) ES cell lines. INPP4B levels seemed to be more similar between the maternal *Tgkd(m)/+* lines; however, these lines represent a small sample size (n=3) and variation in INPP4B levels might be present in additional lines.

Inpp4b transcript levels were also measured in the 4 groups of ES cell lines and the fold changes in transcript levels are similar to INPP4B protein expression levels. *Inpp4b α* is the only isoform of *Inpp4b* expressed in ES cells. The β isoform of *Inpp4b* could not be detected in ES cells (Figure 21B).

In conclusion, the ES cell model cannot accurately map the effect of the *Tgkd* transgene on INPP4B expression due to the wide variation in INPP4B levels independent of the transgene. These differences did not correlate with the extent of ES cell *Tgkd* methylation (Figure 20B). The reason for this wide variation in INPP4B levels in ES cells is not known. ES cell lines mainly consist of undifferentiated cells but a small subset of ES cell undergo differentiation in

culture. This proportion of differentiated cells may differ from cell line to cell line and may cause the variation in INPP4B levels. These results led us to conclude that ES cell lines were not suitable as a model system to study the effect of the *Tgkd* transgene on the *Inpp4b* gene.

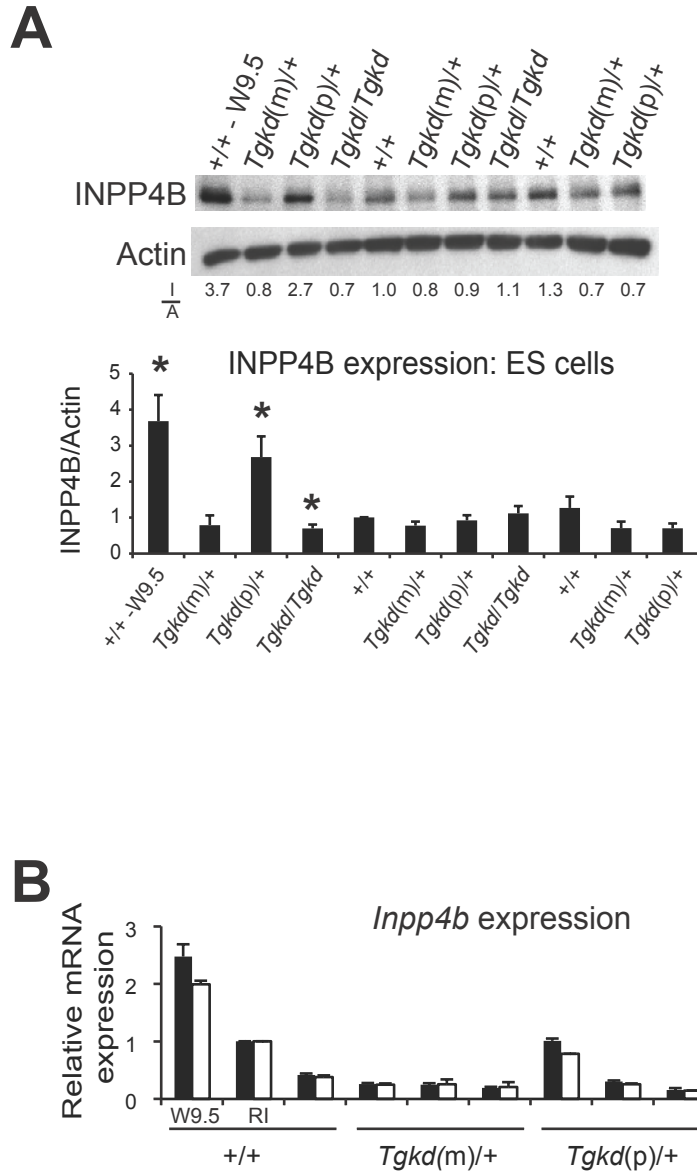


Figure 21: *Tgkd* induced effects on *Inpp4b* levels in ES cells

The effect of the *Tgkd* insertion on the gene *Inpp4b* was measured in ES cells by measuring (A) Protein levels of INPP4B in +/+, *Tgkd(m)/+*, *Tgkd(p)/+* and *Tgkd/Tgkd* ES cell lines. INPP4B (I) levels are normalized to the levels of the housekeeping gene Actin (A). The levels of INPP4B are

represented relative to the INPP4B/Actin (I/A) ratio observed in the +/+ ES line in lane 5. Immunoblot data is quantified in the graph below. * - $p < 0.05$ **(B)** The levels of *Inpp4b* transcript were also measured in the 4 groups of ES cell lines. The α isoform was the only *Inpp4b* isoform present in ES cells. *Inpp4b* levels were normalized to the housekeeping gene TBP and fold changes were expressed relative to the RI wildtype ES line.

6.4 EFFECT OF *Tgkd* ON PI3-KINASE/AKT ACTIVATION IN ES CELLS

The primary purpose for developing the *Tgkd* ES cell model was to evaluate *Tgkd* induced effects on INPP4B levels and the regulation of PI3K/AKT signaling. On checking the levels of INPP4B in wildtype, hemizygous and homozygous *Tgkd* ES cells lines, I found that the levels of INPP4B were highly variable between lines of the same group and there was no consistent effect of the *Tgkd* transgene on INPP4B in any group. However I still wanted to evaluate whether changes in the levels of INPP4B observed are sufficient to alter the kinetics of PI3K/AKT pathway in these ES cell lines.

The activation kinetics of the pathway was measured using a well-established protocol of serum starvation for 34 hours followed by stimulation with IGF1 for indicated time points [115]. Activation of the pathway was quantified through phosphorylation of the AKT1 protein measured by ELISA and normalized to the total levels of AKT1 in each ES cell lines. AKT1 is the main isoform expressed in ES cell lines with minimal expression of AKT2 and AKT3.

Therefore, we assumed AKT1 phosphorylation represented all, or the majority, of AKT phosphorylation in ES cells [116].

The first 4 ES cell lines in Figure 21A represent lines with the expected INPP4B levels based on the E13.5 embryo data. The maternal *Tgkd(m)/+* (I/A=0.8) and homozygous *Tgkd/Tgkd* (I/A=0.7) ES line have lower levels of INPP4B compared to the wildtype W9.5 (I/A=3.7) and paternal *Tgkd(p)/+* ES line (I/A=2.7). I used these lines in the preliminary experiment to assess whether the alterations in INPP4B levels affect AKT phosphorylation in ES cell lines.

On stimulating the ES cell lines with IGF1 after 34 hours of serum starvation, an increase in the level of AKT1 phosphorylation (PAKT1/AKT1) was observed in all 4 ES cell lines, which peaked at about 30 minutes after IGF1 stimulation (Figure 22). The levels of AKT1 phosphorylation remained steady and began to decline after 90 minutes of IGF1 stimulation. However, I observed no differences in the kinetics of AKT phosphorylation at any time points between the *+/+*, *Tgkd(m)/+*, *Tgkd(p)/+* and *Tgkd/Tgkd* ES cell lines (Figure 22). The differences in INPP4B levels between the various ES cell lines had no effect on the AKT activation kinetics on IGF1 stimulation following serum starvation. The presence of the *Tgkd* transgene had no significant effect on the regulation of the PI3K/AKT pathway in *Tgkd* ES cells.

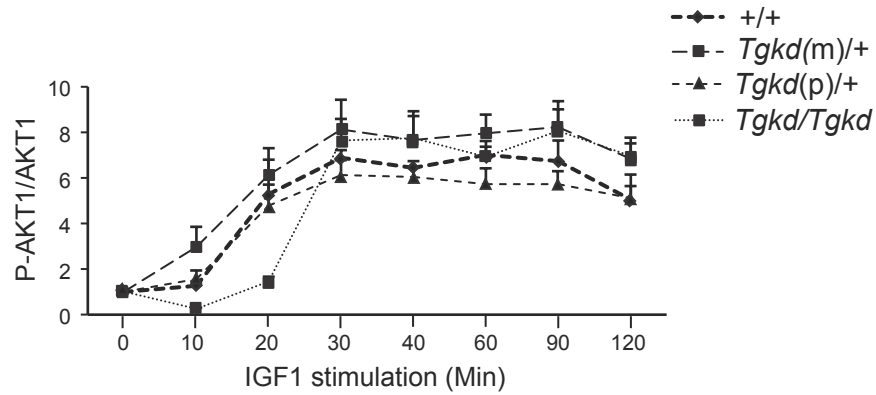


Figure 22: Kinetics of the PI3-Kinase/AKT pathway in *Tgkd* ES cell lines

Kinetics of AKT phosphorylation in +/+ (W9.5), *Tgkd(m)/+*, *Tgkd(p)/+* and *Tgkd/Tgkd* ES cell lines were during IGF1 stimulation following serum starvation of the ES cells. AKT phosphorylation was represented as a PAKT1/AKT1 ratio. PAKT1 was the level of phosphorylated AKT1 and AKT1 was the total level of AKT1 measured by ELISA.

6.5 ASSESSING THE RELEVANCE OF INPP4B IN ES CELLS

In the previous section, I found that the presence of the *Tgkd* transgene did not alter INPP4B levels sufficiently enough to alter the activation kinetics of the PI3K/AKT pathway during IGF1 stimulation. These results could also indicate that the tumor suppressor *Inpp4b* is not a major entity in controlling AKT1 phosphorylation in mouse ES cells. Other suppressors of the PI3K/AKT pathway such as PTEN, SHIP1/2 or protein phosphatase PP2A could play a more prominent role in ES cells [117, 118]. I decided to address this by examining PI3/AKT pathway activation in ES cells during IGF1 stimulation after shRNA-mediated downregulation of *Inpp4b*.

To assess the effect of INPP4B on IGF1-induced signaling in ES cells, I electroporated 2 independent shRNA constructs to the *Inpp4b* gene and one control shRNA construct into wildtype RI ES cells. Electroporation led to stable integration of the constructs into ES cell genome and stable clones were selected using puromycin selection. Both shRNA constructs to *Inpp4b* led to a stable downregulation of the INPP4B protein to 50% of the levels measured in RI ES cells with the shRNA control (Figure 23A). When the 3 ES cell lines were stimulated with IGF1 after 34 hours of serum starvation, the 2 ES cell lines with shRNA constructs to *Inpp4b* depicted a significantly increased and prolonged phosphorylation of AKT1 (P-AKT1/AKT1) compared to the control shRNA ES line (Figure 23B).

This result led me to conclude that *Inpp4b* was an important negative regulator of the PI3K/AKT pathway in mouse ES cells as the shRNA mediated decrease of *Inpp4b* levels led to an increase in AKT1 phosphorylation during IGF1 stimulation. The absence of AKT1 phosphorylation differences between *Tgkd* and wildtype ES cell lines could be due to the adaption of the ES cell lines to changes in INPP4B levels during the process of ES cell derivation, while the shRNA experiment involved a more sudden decrease in INPP4B levels

possibly not allowing for adaptation by other negative regulators of the PI3K/AKT pathway. Further the shRNA-mediated downregulation of *Inpp4b* was performed in a single parent ES line while the independently derived ES cell lines were more heterogeneous in nature. Mouse ES cell lines requires an active PI3K/AKT pathway in order to maintain pluripotency, therefore independent ES cell lines may have adapted during the process of derivation to be resist changes in AKT1 phosphorylation [118]. In summary, the ES cell model may not be suitable to study the effect of *Tgkd* on the PI3K/AKT pathway, even though INPP4B regulates AKT1 phosphorylation in mouse ES cells.

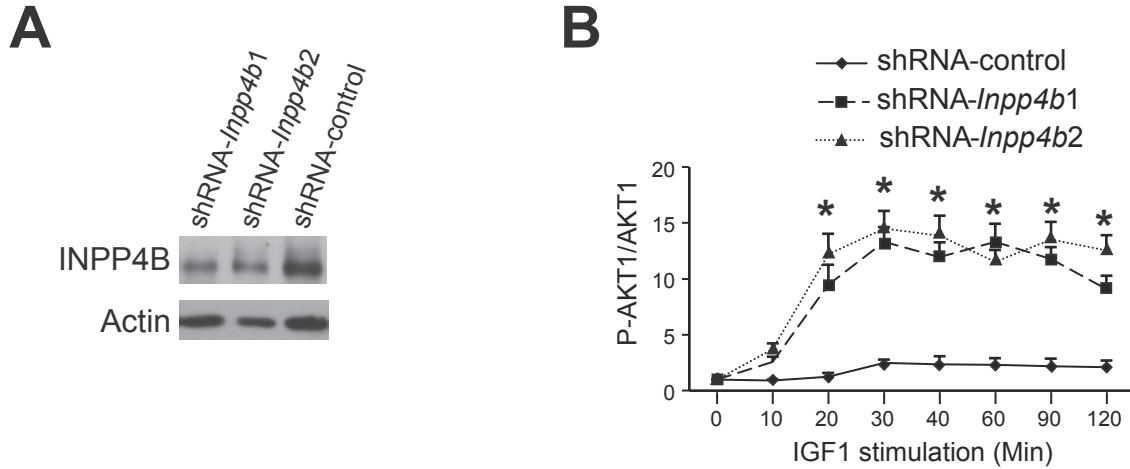


Figure 23: shRNA-mediated downregulation of *Inpp4b* in mouse ES cells

Inpp4b levels were specifically depleted in wildtype RI mouse ES cells using 2 independent shRNA constructs. Panel (A) depicts the decrease in INPP4B levels in the 2 ES cell lines electroplated with shRNA constructs to the *Inpp4b* gene (shRNA-*Inpp4b1* and shRNA-*Inpp4b2*) compared to the ES line with the shRNA control construct. (B) Phosphorylation of AKT1 on IGF1 stimulation was measured by ELISA in all 3 ES cell lines and normalized to the total levels of AKT1. PAKT1/AKT1 levels were significantly higher in the ES cell lines depicting shRNA-mediated INPP4B downregulation. *- p<0.05

6.6 EFFECT OF *Tgkd* ON METHYLATION OF SURROUNDING GENES

The *Tgkd* transgene is inserted as multiple copies in head-head, tail-tail or head-tail orientation in chromosome 8 (Figure 13). Therefore, the insertion of the methylated *Tgkd* transgene creates a large area of CpG methylation on chromosome 8. This CpG methylation could cause large scale epigenetic silencing through alterations of chromatin modifications in the region or cause CpG methylation spreading on chromosome 8. As a preliminary study on the effect of *Tgkd* CpG methylation, I decided to examine whether the methylated *Tgkd* transgene alters methylation of CpG islands in a 2Mb region surrounding the insertion (Figure 24A).

I used the ES cell model for this methylation study and chose the heavily methylated *Tgkd(m)/+* (Figure 20B-Lane 3) ES line, the unmethylated *Tgkd(p)/+* (Figure 20B-Lane 6) and the wildtype RI ES line for this study. I analyzed the methylation of 10 CpG islands on chromosome 8, which were identified by the program CpG island searcher in a 2Mb region surrounding the *Tgkd* insertion (<http://www.uscnorris.com/cpgislands2/cpg.aspx>) (Figure 24A). I analyzed the methylation status of these CpG islands using the HpaII-McrBC methylation-sensitive PCR method [119] with minor modifications to the protocol. The genomic DNA from these 3 ES cell lines was first digested with the restriction enzyme AseI, which was not present in any of the CpG islands, to digest the genomic DNA into smaller fragments. One portion of the AseI digested DNA was subsequently digested with the HpaII enzyme and the other with McrBC enzyme followed by PCR amplification across the CpG island. HpaII is methylation sensitive and cuts only unmethylated CpG islands at CCGG sites while McrBC digests methylated alleles at R^mCN_{40~80}R^mC sites. Therefore, a completely methylated region would be digested only by the McrBC enzyme and HpaII would fail to digest this region, hence amplification would be successful only from the HpaII digested template (Figure 24B). Conversely a completely

unmethylated CpG island would be digested only with HpaII not McrBC resulting in PCR amplification from the McrBC digested template. In principle the technique can distinguish between 4 different kinds of CpG island methylation (Figure 24B). PCR amplification was performed on just the AseI digested genomic DNA as a positive control and on AseI+MspI digested DNA as a negative control. The enzyme MspI digests CpG rich regions at the site CCGG irrespective of their methylation status. The *Tgkd(m)/+*, *Tgkd(p)/+* and RI (+/+) ES cell lines were analyzed for successful PCR amplifications after these enzymatic digests.

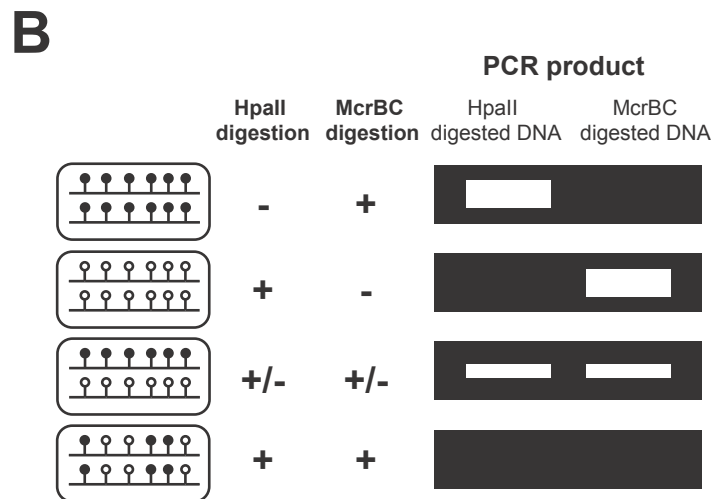
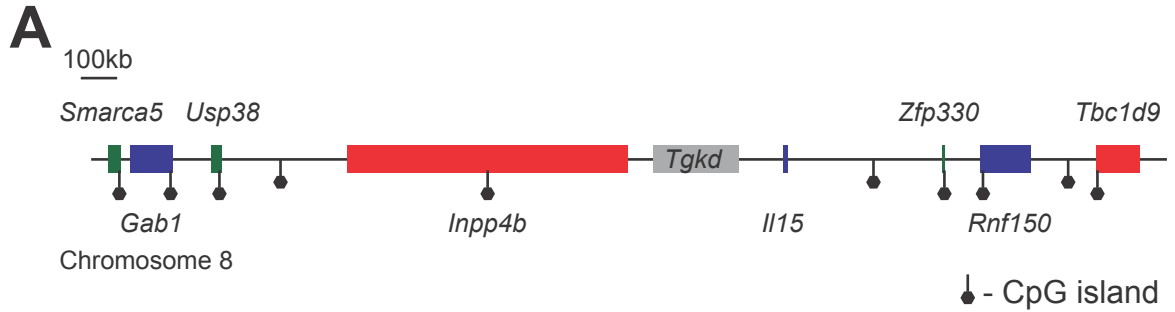


Figure 24: CpG islands examined by HpaII-McrBC PCR

The methylation state of each CpG island was analyzed by the HpaII-McrBC PCR. Panel (A) indicates the position of each of the 10 CpG islands in a 1Mb region centromeric and a 1Mb region telomeric of the *Tgkd* insertion. Schematic (B) illustrates the 4 possible methylation states that can be distinguished by the HpaII-McrBC method and the amplification result in each case.

On examining the 10 CpG islands by the above method, I found that most CpG islands (CpGi) were unmethylated in +/+, *Tgkd(m)/+* and *Tgkd(p)/+* ES cell lines (Figure 25). The CpG island CpG9i had an unmethylated and a methylated allele according to the schematic in Figure 24B with an identical methylation pattern in all 3 ES cell lines. The CpG islands CpG5i and CpG6i, which were closest to the *Tgkd* insertion also depicted a methylated and unmethylated allele in the *Tgkd(m)/+* and *Tgkd(p)/+* ES cell lines (Figure 25). However these PCR reactions did not work in the RI (+/+) ES cell line even in the control samples possibly due to SNP differences in the region. However, since I did not see a difference in CpG island methylation between the highly methylated *Tgkd(m)/+* line and the relatively unmethylated *Tgkd(p)/+* line in the CpG islands closest to the insertion site, I concluded that the *Tgkd* transgene does not cause aberrant methylation of unmethylated CpG islands surrounding the insertion site in ES cell lines. The effect of *Tgkd* on surrounding genomic methylation may be different in different tissues. Alternatively the *Tgkd* transgene may mediate transcriptional repression of the gene *Inpp4b* through altered chromatin configuration or disruption of a distal enhancer.

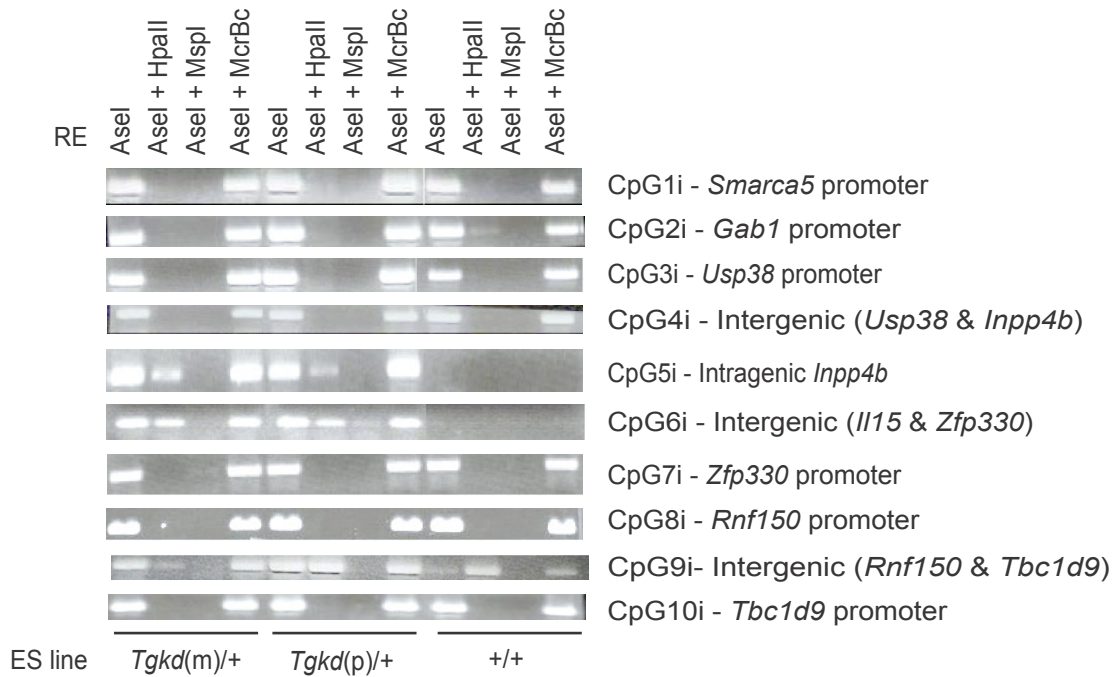


Figure 25: CpG island methylation in *Tgkd* ES cell lines

The methylation state of 10 CpG islands surrounding the *Tgkd* insertion was analyzed by PCR amplification after digestion with the methylation sensitive enzymes HpaII and McrBC in the methylated *Tgkd(m)/+*, unmethylated *Tgkd(p)/+* and *+/+* ES cell lines. The location of each CpG island (CpGi) on chromosome 8 is indicated and the restriction enzyme (RE) digest before PCR amplification is indicated above.

6.7 CONCLUSIONS

In the ES cell model to study *Tgkd* induced effects on *Inpp4b*, I managed to derive maternal, paternal and homozygous *Tgkd* ES cell lines on the 129 strain background. The methylation of the *Tgkd* transgene in these lines were not consistent between lines of the same genotype and did not match the expected pattern of *Tgkd* methylation observed in somatic tissues. Further there was a variation in INPP4B expression between independently derived ES cell lines, which did not correlate with the presence or absence of the transgene. On analyzing PI3K/AKT activation in wildtype and *Tgkd* ES cell lines, I found no significant changes in the kinetics of AKT phosphorylation between wildtype, hemizygous and homozygous ES cell lines. shRNA mediated downregulation of *Inpp4b* resulted in increased AKT phosphorylation in the +/+ RI ES line indicating that a sudden and severe decrease in *Inpp4b* may be required to alter AKT activation kinetics in ES cells. The insertion of the *Tgkd* transgene did not alter the methylation state of CpG islands surrounding the transgene in *Tgkd(m)/+* and *Tgkd(p)/+* ES cell lines compared to the wildtype line. In summary, *Tgkd* ES cells do not show a decrease in the level of INPP4B and augmented effects on PI3K/AKT signaling following IGF1 stimulation.

7.0 EFFECT OF *Tgkd* TRANSGENE ON INPP4B AND DOWNSTREAM PI3-KINASE/AKT PATHWAY IN TGKD OVARIES

7.1 AIMS OF THESE STUDIES

The results of the previous sections (Chapter 5) indicate that the *Tgkd* transgene causes transcriptional suppression of the nearby gene *Inpp4b* leading to a decrease in the levels of *Inpp4b* transcript and protein in embryonic FVB E13.5 *Tgkd* brains. I was unable to show a consistent association between the *Tgkd* insertion and decreased INPP4B levels in mouse ES cells and the alterations in INPP4B levels due to *Tgkd* did not affect PI3K/AKT signaling in ES cells (Chapter 6).

Since OTs arise from mature oocytes in the ovary, which have completed meiosis I, we decided to investigate the effect of the *Tgkd* transgene on the nearby inositol phosphatase *Inpp4b* in FVB and FVB-*Tgkd* (*Tgkd*) ovaries. As described in chapter 4, *Tgkd* ovaries show defects in follicular maturation (trapped oocytes) and a high rate of oocyte parthenogenesis. Therefore, *Tgkd* induced effects on *Inpp4b* could be in *Tgkd* oocytes or in the surrounding somatic GCs of the ovarian follicle or both. This led me to first examine *Inpp4b* expression in wildtype and *Tgkd* oocytes and GCs. Further *Inpp4b* levels have been previously shown to be responsive to the levels of androgens in prostate cancer cells, hence I examined whether *Inpp4b* levels in the ovary were affected during gonadotrophin (FSH and LH) stimulation [112].

The PI3K/AKT pathway is an essential pathway in the ovary involved both in resumption of oocyte meiosis and various steps of follicular maturation [41, 43, 44, 120]. As stated before, INPP4B is a negative regulator of the PI3K/AKT pathway; therefore I examined the effect of the *Tgkd* transgene on AKT phosphorylation and subsequent downstream steps of the pathway in both GCs and oocytes. The functional consequences of the signaling alterations caused by the *Tgkd* transgene were also studied, which could explain the follicular defects observed in *Tgkd* ovaries. In summary, I worked to dissect out the molecular and signaling alterations in *Tgkd* ovaries that could explain the route to OT formation.

7.2 INPP4B EXPRESSION IN THE OVARY

Since OTs were shown to arise from mature oocytes that have completed meiosis I, I first examined the expression of INPP4B protein in MII oocytes that have completed meiosis I. INPP4B protein expression could not be detected in wildtype (+/+, n=68) or *Tgkd* (*Tgkd*+, n=75) mature MII oocytes, whereas high levels of INPP4B were expressed in the adult mouse brain (Figure 26A) (Experiment performed by Dr. M.C. Cirio). However, INPP4B expression was detected in the ovary at numerous developmental stages in embryonic (E13.5, E16.5 and E17.5) and adult ovary lysate (Figure 26B). These results suggested that *Inpp4b* may be expressed and dysregulated at an earlier stage of oocyte development than the metaphase II stage but oocytes need to complete meiosis I before OT formation. In the adult mouse ovary, oocytes in different follicles (primordial versus antral) are at different stages of oocyte development. Therefore, it difficult to isolate a pool of oocytes from the ovary from a single stage before advanced stages of oogenesis. Alternatively *Inpp4b* may not be expressed in oocytes at any stage

and may be expressed in other ovarian cells, which promote OT formation through paracrine mechanisms.

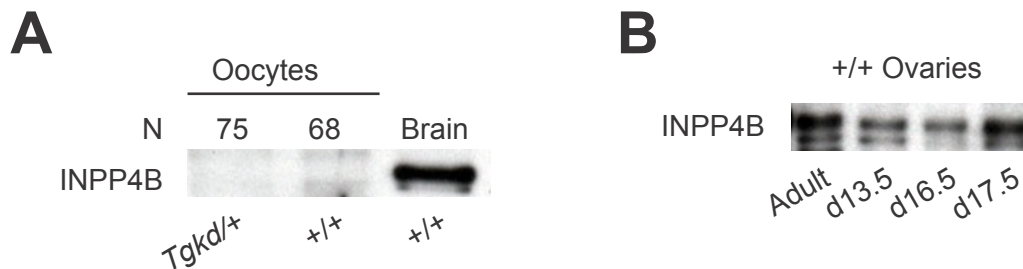


Figure 26: INPP4B expression in the ovary

INPP4B expression was examined in (A) Wildtype (+/+) and *Tgkd* MII oocytes. Adult brain lysate was used as a positive control for INPP4B expression. N= number of oocytes. (B) Total ovary lysates from embryonic (E13.5, E16.5 and E17.5) and adult ovaries in wildtype females. INPP4B expression was seen in total ovary lysates but not in MII oocytes.

To sample *Inpp4b* expression in oocytes at several follicular stages, RNA *in situ* hybridization (ISH) was used to determine the location of *Inpp4b* transcripts in the adult ovary. This adult mammalian ovary contains follicles of all stages within the ovary; therefore RNA ISH of ovarian sections would enable identification of the specific developmental stage and ovarian cells with *Inpp4b* expression.

RNA ISH experiments on adult ovaries from 7-week old females showed that *Inpp4b α* , but not the *Inpp4b β* isoform was expressed in the ovary and this expression was confined to the GCs of the ovary (Figure 27). No expression was observed in oocytes at any stage of ovarian follicle development. These findings were confirmed in measurements of individual *Inpp4b* transcripts by real-time PCR in GCs and oocytes from PD30 wildtype and *Tgkd* mice (Figure 28). The surprising finding that ovarian *Inpp4b* expression is confined to GCs raises the possibility that the *Tgkd* insertion facilitates OT formation primarily by altering INPP4B expression in GCs, which in turn alters follicular development and possibly normal GC-oocyte interactions.

Slc39a10



Inpp4ba



Inpp4ba



Inpp4bβ



Inpp4bβ



Inpp4bβ

Figure 27: *Inpp4b* expression in the adult wildtype ovary

Inpp4b α and β isoform expression in the ovarian follicle was measured by *in situ* hybridization in 7-week old wildtype ovaries. Top right panel: Oocyte specific probe: *Slc39a10* to depict oocyte specific staining. Lower right panel: Small Intestine as positive control for *Inpp4b β* probe. Other panels: *Inpp4b α* and *Inpp4b β* isoform expression in ovarian follicles.

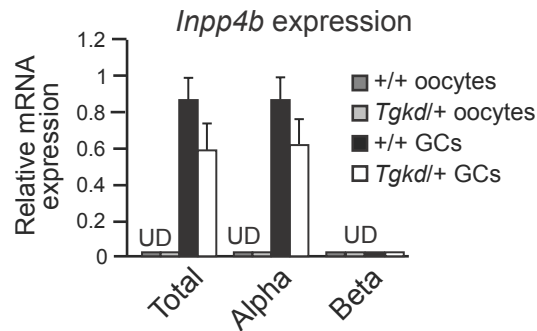


Figure 28: *Inpp4b* expression in oocyte and GCs of PD30 ovaries

Real-time PCR quantitation of *Inpp4b* in GCs and oocytes isolated from PD30 wildtype and *Tgkd* ovaries. *Inpp4b* levels were normalized to the housekeeping gene TBP. Fold changes was expressed relative to wildtype *Inpp4b* levels in GCs. UD – Undetected.

7.3 REGULATION OF INPP4B IN *Tgkd* OVARIES DURING GONADOTROPHIN STIMULATION

Inpp4b is expressed primarily in the GCs of the ovarian follicle. With this result in hand, we hypothesized that *Tgkd* induced effects on *Inpp4b* levels in GCs during follicular maturation may lead to the maturation defects such as trapped oocytes. *Inpp4b* expression is known to be induced by the androgen receptor in prostate cancer cells [112]. Therefore, I wanted to evaluate whether *Inpp4b* levels vary during female gonadotrophin stimulation with FSH (PMSG) and LH (HCG).

For these reasons, the effect of *Tgkd* on *Inpp4b* levels was examined in ovarian cells exposed to hormonal stimuli. *Inpp4b α* is the only isoform expressed in the ovary (Figure 27 & 28). No difference in expression of *Inpp4b* was observed between immature PD23 wildtype and *Tgkd* ovaries (Figure 29A). Synchronized *in vivo* maturation of wildtype and *Tgkd* ovarian follicles was initiated with gonadotrophins (one-time IP injection of PMSG), followed by induction of ovulation with a one-time injection of HCG. Levels of *Inpp4b* transcript in wildtype mice fluctuated over the 48-hour time course of PMSG stimulation and 2 hours of HCG stimulation. The *Tgkd* ovaries show a 20% decrease in the level of *Inpp4b* transcript compared to the wildtype mice at 24 and 38 hours after PMSG stimulation (Figure 29A). A slightly larger difference was seen between wildtype and *Tgkd* ovaries 48 hours after PMSG stimulation, where *Tgkd* ovaries expressed 70% of wildtype levels of *Inpp4b*.

The *Tgkd* transgene also affected levels of ovarian INPP4B protein. INPP4B levels in lysates of whole ovaries fluctuated slightly during the time course of PMSG stimulation. *Tgkd* ovaries expressed approximately 70% of wildtype levels at 14 ($p < 0.05$) and 24 hours after PMSG stimulation (Figure 29B). The largest difference, a 50% decrease of INPP4B in *Tgkd* ovaries ($p < 0.05$), was recorded 38 hours after PMSG stimulation (Figure 29B). At other time

points during PMSG stimulation, the levels of INPP4B were comparable in wildtype and *Tgkd* mice. I did not examine INPP4B levels in wildtype and *Tgkd* ovaries after HCG stimulation, as no differences were observed in *Inpp4b* transcript levels (Figure 29A).

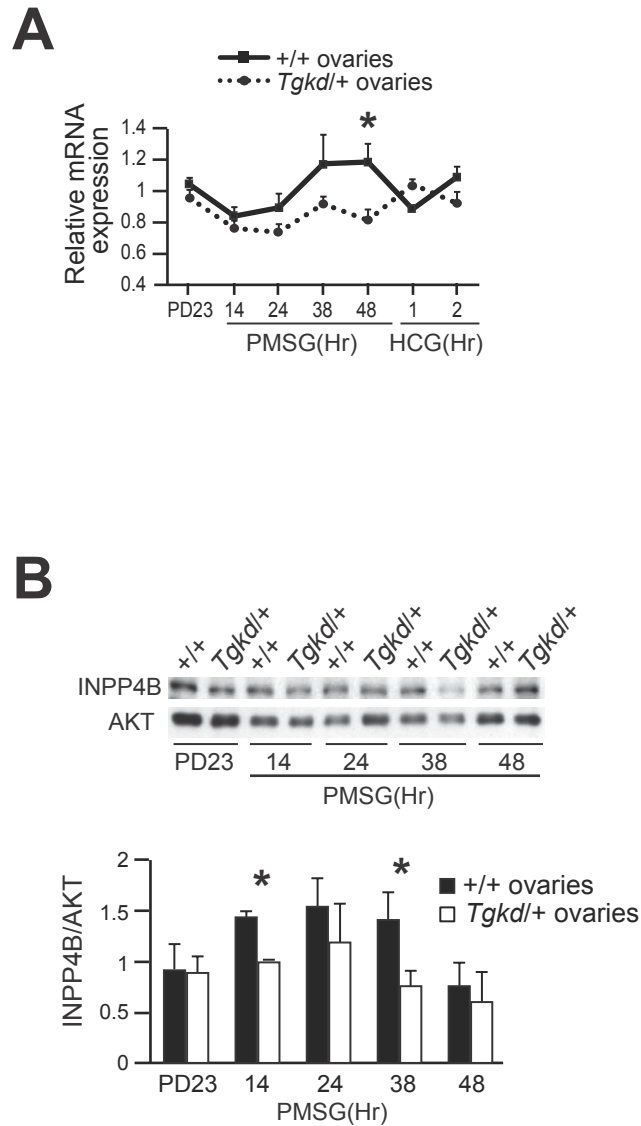
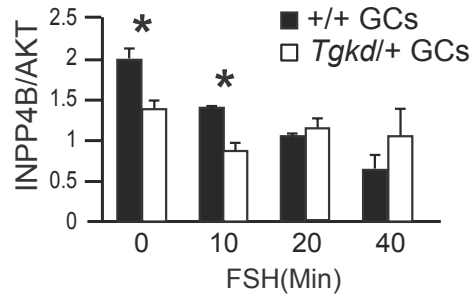
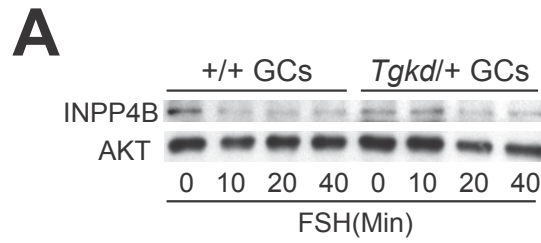


Figure 29: *Inpp4b* transcript and protein levels in wildtype and *Tgkd* ovaries

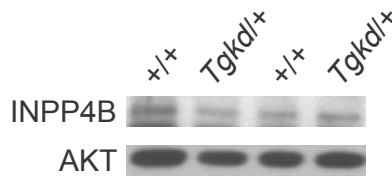
(A) Real-time PCR quantitation of *Inpp4b* (*Inpp4ba*) in wildtype and *Tgkd* ovaries during the time course of PMSG and HCG stimulation (n>3 mice/time point). *Inpp4b* levels were normalized to the housekeeping gene GUSB and fold changes were expressed relative to

wildtype PD23 ovaries. **(B)** INPP4B protein levels in wildtype and *Tgkd* ovaries during PMSG stimulation (n=3). *-p<0.05.

A more pronounced effect of the transgene on INPP4B expression was observed in purified and *in-vitro* cultured GCs. INPP4B was significantly downregulated to a higher extent even in cultured unstimulated PD23 *Tgkd* GCs (70% of wildtype GCs) and following 10 minutes of FSH administration (Figure 30A). This method of enriching for GCs excluded the ovarian capsule and stroma, which expressed low levels of *Inpp4b* (Figure 30B and C). The levels of INPP4B in the ovary after removal of GCs are similar in wildtype and *Tgkd* ovaries. These results indicate that the *Tgkd* GCs have lower levels of INPP4B than wildtype GCs even in immature PD23 ovaries. However during PMSG stimulation, there is extensive GC proliferation causing the number of GCs to exponentially increase [14]. This proliferation dramatically increases the contribution of GCs in the ovary lysate resulting in larger INPP4B differences between wildtype and *Tgkd* ovaries under PMSG stimulation than in the immature PD23 state. In summary, the *Tgkd* transgene causes decrease in INPP4B levels specifically in *Tgkd* GCs.



B



C

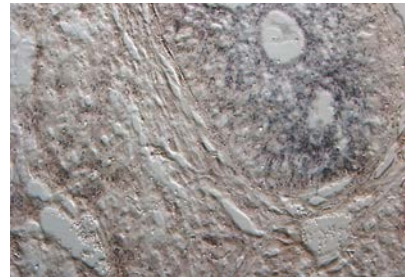


Figure 30: INPP4B expression in wildtype and *Tgkd* GCs

INPP4B levels were specifically measured in GCs to exclude the low levels expressed in the tunica and stroma of the ovary (A) Measurement of INPP4B protein on enriching the GCs in culture (n=3). * - p value <0.05. (B) Residual INPP4B expression in the tunica after removal of

the somatic follicle cells and oocytes. (C) Minimal expression of *Inpp4b* outside the ovarian follicle.

7.4 REGULATION OF PI3-KINASE/AKT PATHWAY IN *Tgkd* OVARIES ON GONADOTROPHIN STIMULATION

Inpp4b is a recently identified suppressor of the PI3K/AKT signal transduction pathway that has not been studied previously in the ovary [111, 112, 121]. *Inpp4b* is an inositol-polyphosphate-4-phosphatase, whose main substrate is phosphatidylinositol 3,4 bisphosphate (PI(3,4)P₂), which *Inpp4b* dephosphorylates to phosphatidylinositol-3-phosphate PI(3)P (Figure 31). Because PI(3,4)P₂ stimulates AKT phosphorylation, a decrease in *Inpp4b* levels has been linked to increased AKT activation and the progression of breast, ovarian and prostate cancer [111, 112, 121]. Since *Inpp4b* is a suppressor of AKT phosphorylation, I decided to investigate whether the *Tgkd* transgene alters the kinetics of AKT phosphorylation during gonadotrophin stimulation. I also examined whether downstream components of the PI3K/AKT pathway were affected by the decrease in INPP4B levels. The downstream signaling molecules of the PI3K/AKT pathway were chosen based on their relevance to GC proliferation and follicular maturation described previously in literature (Figure 31) [48, 122].

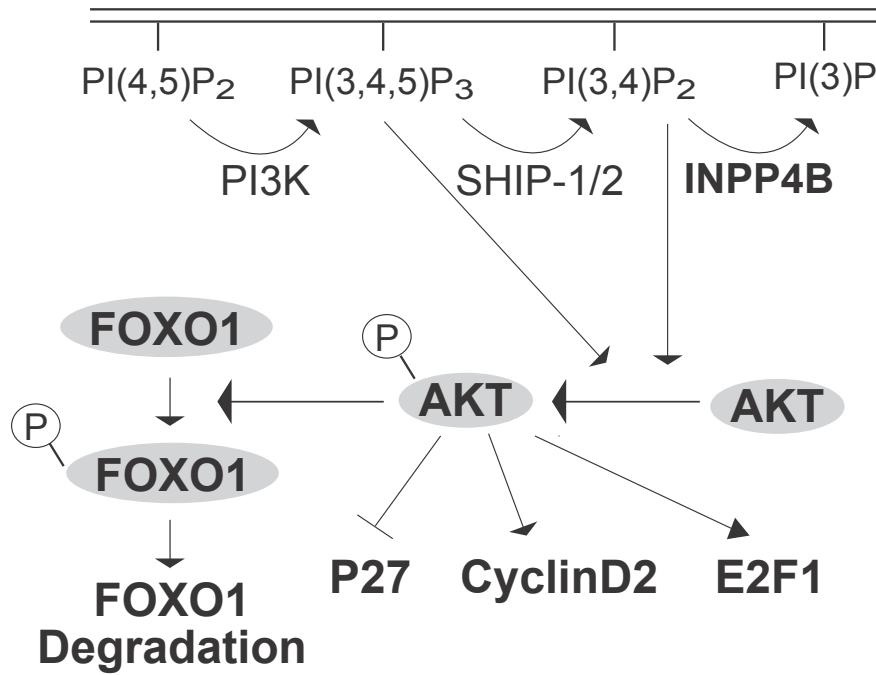


Figure 31: Role of INPP4B in regulation of the PI3K/AKT pathway

The function of INPP4B in regulating AKT phosphorylation is depicted in the pathway. The downstream signaling molecules affected by AKT phosphorylation, which were examined in the ovary during gonadotrophin stimulaton are shown in the pathway diagram.

Whole ovaries were collected at different time points following *in-vivo* hormonal stimulation, and the time course of phosphorylated AKT (P-AKT), an indication of PI3K/AKT pathway activation, and its downstream effects were measured. P-AKT levels were roughly similar in immature PD23 wildtype and *Tgkd* ovaries prior to administration of exogenous hormones, but significant differences were evident following 14 and 24 hours of PMSG stimulation ($p < 0.05$) (Figure 32A; Quantified in Figure 32B). Corresponding differences in levels of phosphorylated FOXO1 (P-FOXO1), a downstream target of P-AKT (Figure 31) specifically in GCs, was also evident (Figure 32A&B) [122]. Time courses of changes in total FOXO1, E2F1, CyclinD2 and P27 were similar between wildtype and *Tgkd* ovaries (Figure 32).

Following administration of a single dose of HCG 48 hours after PMSG stimulation, P-AKT and P-FOXO1 concentrations declined at a much faster rate in *Tgkd* compared to wildtype ovaries (Figure 33A; Quantified in Figure 33B). An accentuated rate of decline in the level of FOXO1 and an accentuated rate of increase in CyclinD2 levels in *Tgkd* ovaries at specific time points following HCG stimulation were also evident (Figure 33A). Time courses of changes in E2F1, CyclinD2 and P27 were similar between wildtype and *Tgkd* ovaries (Figure 33A&B). From these results, 2 types of *Tgkd* induced effects on the PI3K/AKT pathway were observed. One is a proximal premature and increased phosphorylation of AKT and FOXO1 during PMSG stimulation and a distal effect, where the AKT and FOXO1 phosphorylation are attenuated early after HCG stimulation.

I conclude from these experiment that the presence of the *Tgkd* transgene 3' of the *Inpp4b* gene augments the response of mature ovarian follicles to stimuli known to mimic endogenous ovulatory stimuli, leading to premature phosphorylation of the AKT protein and activation of downstream effectors of the PI3K/AKT signaling pathway.

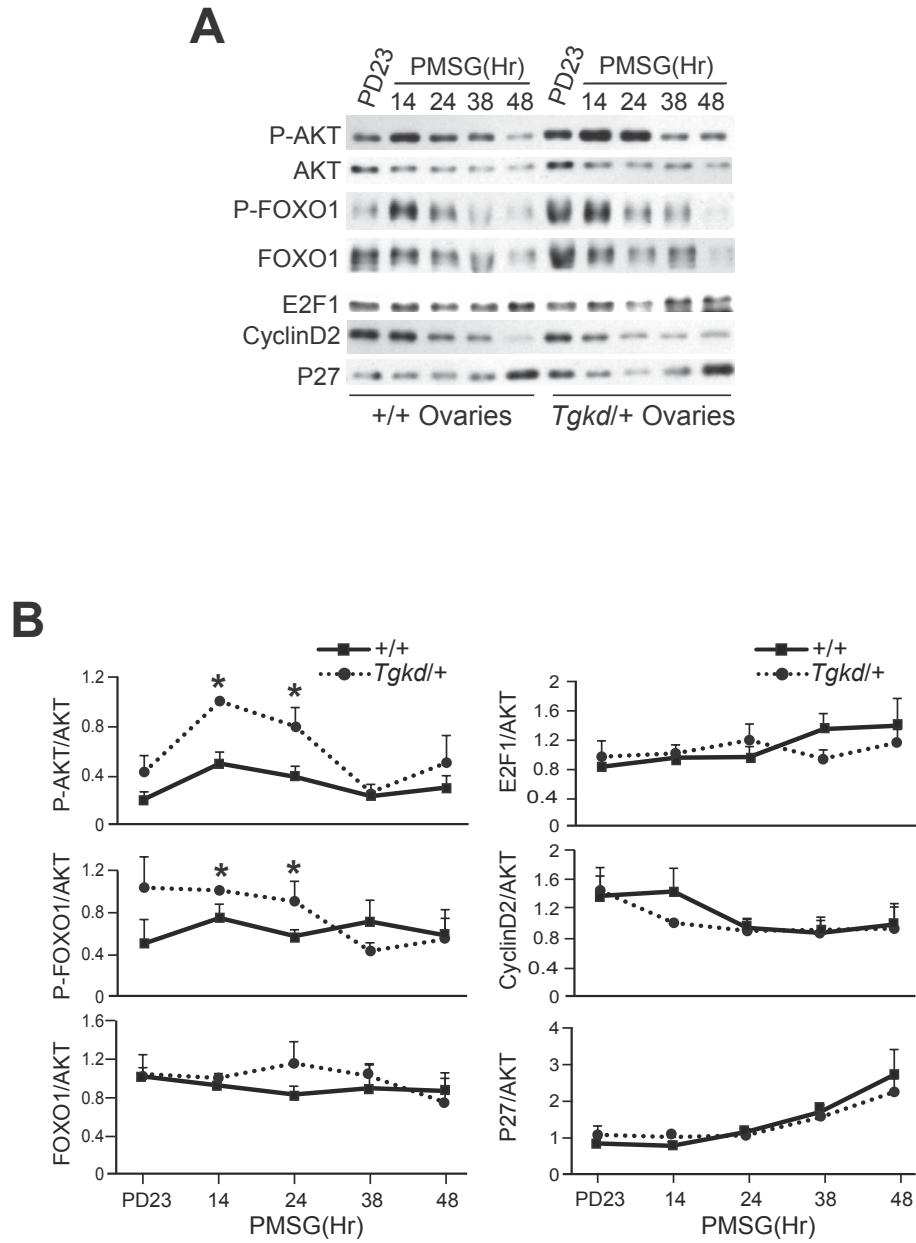


Figure 32: Activation of PI3K/AKT pathway in *Tgkd* ovaries on PMSG stimulation

(A) Dynamics of the PI3K/AKT pathway was measured in wildtype and *Tgkd* ovaries in immature mice and on PMSG stimulation by investigating the levels of P-AKT, P-FOXO1, FOXO1, E2F1, Cyclin D2 and P27 (ovaries from single female per lane). (B) Quantification of

P-AKT, P-FOXO1, FOXO1 E2F1, Cyclin D2 and P27 levels in wildtype and *Tgkd* ovaries on PMSG stimulation (n=3 mice/time point). *- p<0.05

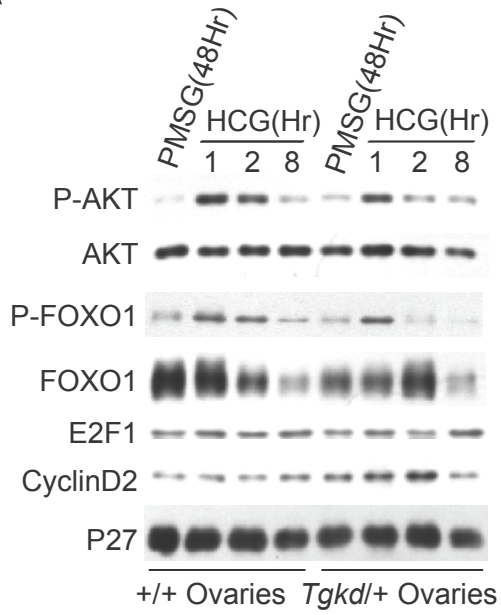
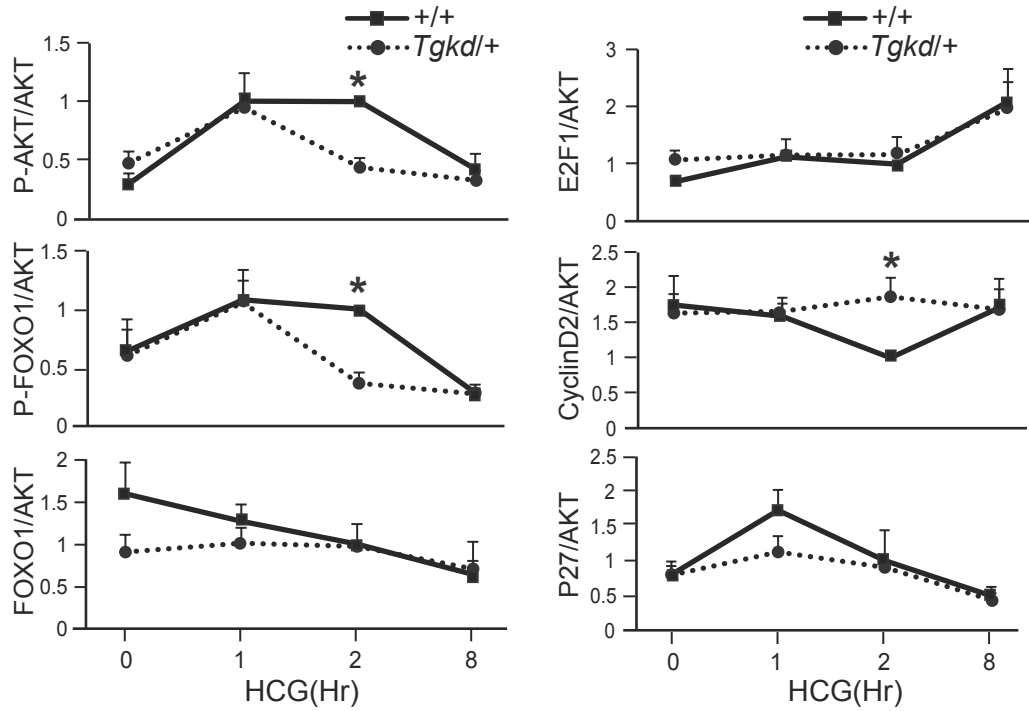
A**B**

Figure 33: Activation of PI3K/AKT pathway in *Tgkd* ovaries on HCG stimulation

- (A) After 48 hours of PMSG stimulation; the mice were injected with HCG and the activation of the PI3K/AKT pathway was measured in wildtype and *Tgkd* ovaries by investigating the levels of P-AKT, P-FOXO1, FOXO1, E2F1, Cyclin D2 and P27 (ovaries from single female per lane).
- (B) Quantification of P-AKT, P-FOXO1, FOXO1 E2F1, Cyclin D2 and P27 levels in wildtype and *Tgkd* ovaries on HCG stimulation (n=3 mice/time point). *- p<0.05

The pattern of P-AKT activation following gonadotropin administration was then investigated in wildtype and *Tgkd* oocytes. There was no difference in the P-AKT activation and phosphorylation of its downstream target FOXO3A between wildtype and *Tgkd* oocytes during the time course of gonadotrophin stimulation (Figure 34A). These findings are consistent with the observed absence of *Inpp4b* expression in fully-grown oocytes (Figure 27&28). Collectively, the observed effects of the *Tgkd* transgene on ovarian and oocyte AKT signaling are consistent with effects of *Tgkd* on PI3K/AKT signaling in GCs.

To directly test this postulate, I obtained purified GC pools and stimulated them with FSH. *Tgkd* GCs from PD23 ovaries had a lower level of INPP4B than wildtype GCs (Figure 30A). *Tgkd* GCs also had a slightly higher level of P-AKT and P-FOXO1 after overnight culture in medium containing 10% FBS (Figure 34B, Quantified in Figure 34C). *Tgkd* GCs did not show the decline in P-AKT levels seen in wildtype GCs after 40 minutes of FSH stimulation (Figure 34B, Quantified in Figure 34C). These results indicate that the *Tgkd* transgene induced

decrease in INPP4B specifically in GCs is associated with hyperactivated PI3K/AKT activation in GCs not oocytes.

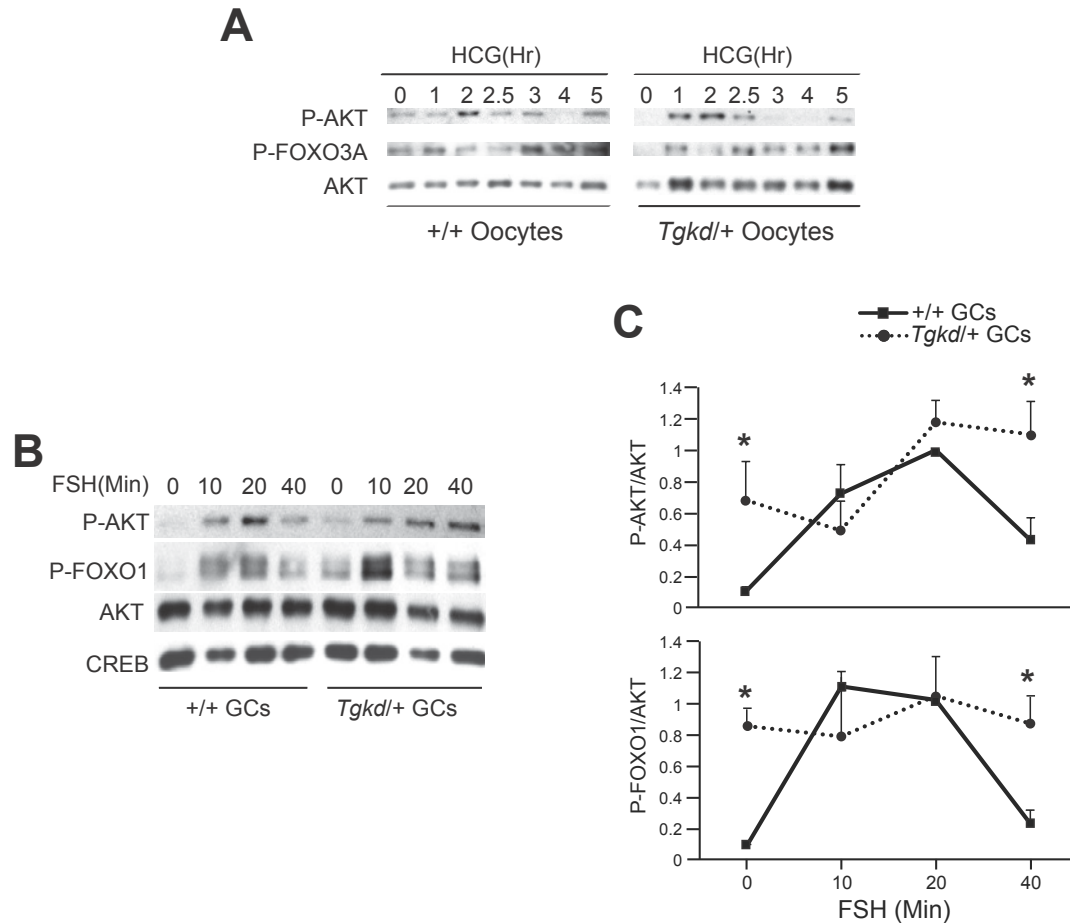


Figure 34: Kinetics of PI3K/AKT activation in *Tgkd* oocytes and GCs

(A) The dynamics of AKT and FOXO3A phosphorylation was examined in wildtype and *Tgkd* oocytes (20 oocytes/lane). (B) P-AKT and P-FOXO1 activation were measured after FSH stimulation in cultured GCs from wildtype and *Tgkd* mice. (C) Quantification of the levels of P-AKT and P-FOXO1 in wildtype and *Tgkd* GCs upon FSH stimulation (n=3).

I independently investigated this inverse relationship between INPP4B levels and AKT pathway activation in GCs infected with lentiviruses expressing shRNAs to the mouse *Inpp4b* gene. Two independent shRNA constructs were used, and expression of both constructs resulted in 50% reduction in the levels of INPP4B compared to control uninfected wildtype GCs (Figure 35). Corresponding increases in the levels of P-AKT and P-FOXO1 were seen prior to and 40 minutes after FSH administration (Figure 35). These results confirm the inverse relationship between INPP4B and PI3K/AKT signaling observed in *Tgkd* GCs. A decrease in INPP4B due to the *Tgkd* insertion is associated with augmented effects on PI3K/AKT signaling in GCs following gonadotrophin stimulation.

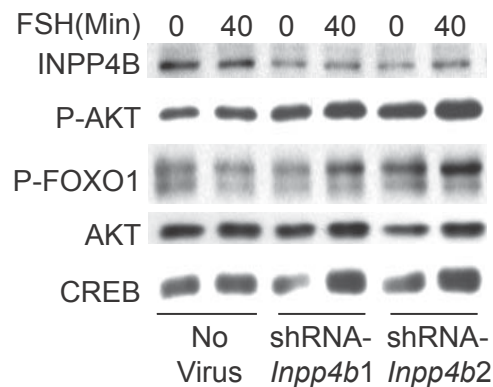


Figure 35: shRNA-mediated downregulation of INPP4B in wildtype GCs

Lentiviral mediated shRNA downregulation of *Inpp4b* in wildtype GCs led to increased levels of AKT and FOXO1 phosphorylation before and after 40 minutes of FSH stimulation similar to that observed in *Tgkd* GCs (n=3).

7.5 FUNCTIONAL CONSEQUENCES OF HYPERACTIVATION OF PI3-KINASE/AKT SIGNALING IN *Tgkd* OVARIES

The results of the previous section show that *Tgkd* GCs are associated with a decrease in INPP4B levels and hyper-activated PI3K/AKT signaling. I wanted to investigate the functional consequences of the signaling pathway alterations observed in GCs. Downstream effectors of AKT activation have been shown to induce cell proliferation and block apoptosis [123]. There was also a previous report, where the knockout of the mouse *Pten* gene specifically in GCs caused an increase in the rate of GC proliferation and decrease in GC apoptosis [48]. Furthermore, the females with *Pten*^{-/-} GCs showed defective clearance of corpora lutea causing persistence of many non-functional corpora lutea after ovulation. Since *Inpp4b* is a negative regulator of the PI3K/AKT pathway similar to *Pten* and the levels of P-AKT and downstream targets FOXO1 and Cyclin D2 in the ovary were observed to be influenced by *Tgkd* (Figure 32&33), The rates of GC proliferation and apoptosis in preantral and antral follicles were compared in *Tgkd* and wildtype female mice [48, 124]. I measured GC proliferation and apoptosis in large preantral and antral follicles as these stages had defects in folliculogenesis in *Tgkd* ovaries (Figure 8A) and these follicle stages were FSH dependent [8, 125].

The rate of GC proliferation was measured by using bromodeoxyuridine (BrdU) IHC as proliferating cells in the S phase incorporate BrdU into the newly synthesized DNA. The number of proliferating (BrdU+) GCs was divided by the total number of GCs in each ovarian follicle to measure the percentage of proliferating cells in each follicle. There was a significant 1.8-fold increase in the rate of GC proliferation in PD30 *Tgkd* ovaries compared to wildtype ovaries (Figure 36).

I also measured apoptosis in *Tgkd* GCs as apoptosis plays a major role in follicular selection and atresia, and FOXO1 is a pro-apoptotic protein that is affected in *Tgkd* GCs [126]. Apoptosis was measured by activated or cleaved caspase-3 (CC3 staining), which is activated in cells during early stages of apoptosis and the number of apoptotic (CC3+) GCs was divided by the total number of GCs per follicle to measure the percentage of apoptotic cells in each follicle. The rate of apoptosis in *Tgkd* GCs was also significantly reduced to approximately 50% of the rate seen in wildtype ovaries at 2 hours after HCG stimulation (Figure 37).

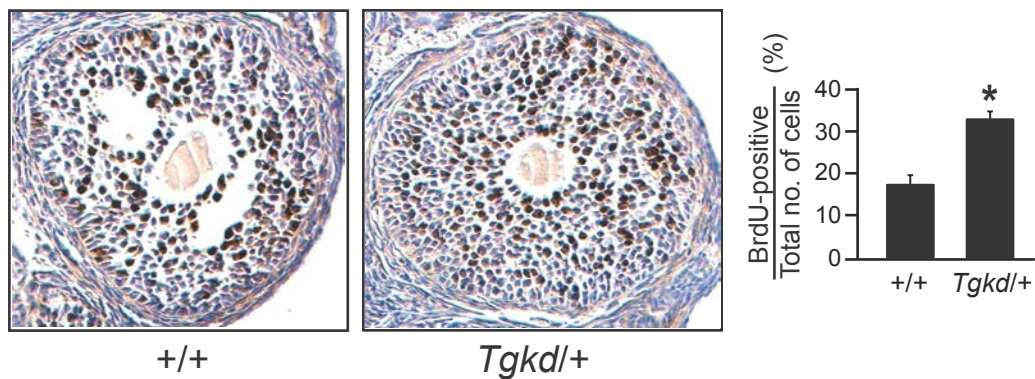


Figure 36: Comparison of GC proliferation in wildtype and *Tgkd* ovaries

Representation and quantification of rate of GC proliferation in PD30 wildtype and *Tgkd* follicles measured by bromodeoxyuridine (BrdU) staining (n=25 follicles). * - p value <0.05.

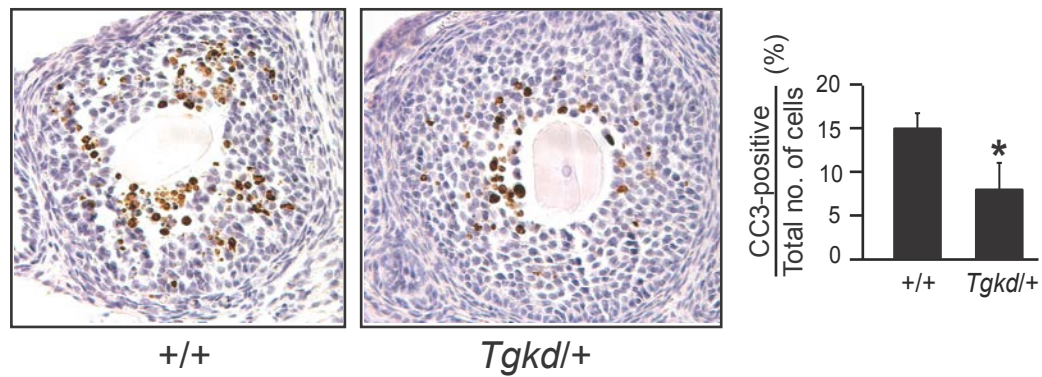


Figure 37: Comparison of apoptosis in wildtype and *Tgkd* ovaries

Quantification of rate of GC apoptosis in wildtype and *Tgkd* follicles measured by Cleaved Caspase 3 (CC3) staining (n=25 follicles). Apoptosis was measured after hormonal stimulation of PD23 wildtype and *Tgkd* mice with PMSG for 48 hours followed by HCG for 2 hours. * - p value <0.05.

In mice with *Pten*^{-/-} GCs, the ovaries showed an abundance of corpora lutea due to defective clearance and persistence of non-functional corpora lutea, which did not express the LH receptor [48]. To examine the lifespan of the corpora lutea in the *Pten*^{-/-} GC model, the authors injected immature PD23 mice with a superovulatory regime of PMSG for 48 hours followed by a one-time injection of HCG to induce synchronized follicle maturation, ovulation and corpora lutea formation. The study showed that while corpora lutea was present in both sets of ovaries after 4 days of HCG stimulation, the corpora lutea persisted in the ovaries with *Pten*^{-/-} GCs after 7 days of HCG stimulation when corpora lutea had disappeared in wildtype ovaries

[48]. Since *Inpp4b* is a negative regulator of PI3K/AKT signaling similar to the *Pten* gene, I hypothesized that the decrease in INPP4B levels in *Tgkd* GCs could affect the rate of corpus luteum clearance.

To determine *Tgkd* effects on clearance of corpora lutea, the same superovulatory regimen was followed by injecting PD23 immature mice with PMSG for 48 hours followed by a single dose of HCG. On examining the ovaries of wildtype and *Tgkd* mice 7 days after HCG injection, I found that both groups had regressing corpora lutea (*) of a similar small size (Figure 38). The rate of corpora lutea regression was similar in wildtype and *Tgkd* ovaries. The presence of corpora lutea in wildtype FVB ovaries 7 days after HCG stimulation could be due to strain specific differences as the mice with the *Pten*^{-/-}GCs were on the B6 strain background. I concluded from this experiment that there is no difference in the rate of corpora lutea clearance between wildtype and *Tgkd* ovaries (Figure 38).

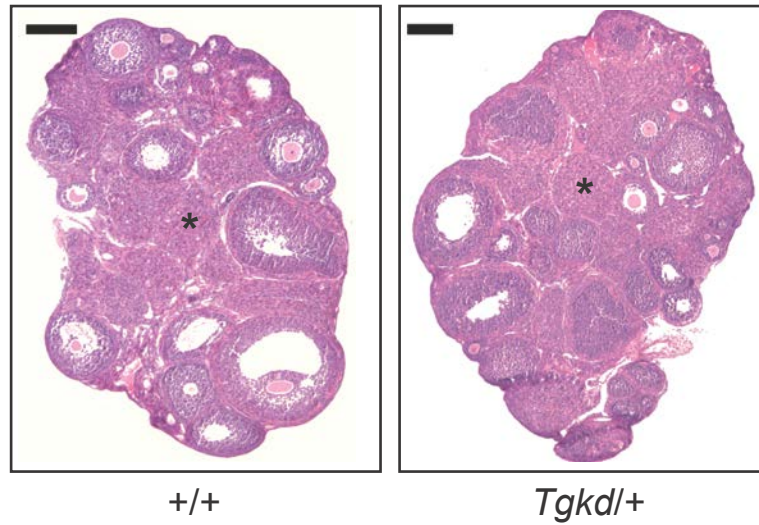


Figure 38: Persistence of corpora lutea in wildtype and *Tgkd* ovaries

Corpora lutea persistence in wildtype and *Tgkd* mice was examined using a superovulatory regime of PMSG and HCG. Corpora lutea clearance was measured 7 days after HCG injection (Scale bar: 200 μ m). * - Corpus luteum

One of the main changes observed between wildtype and *Tgkd* GCs in the PI3K/AKT pathway was an increase in AKT and FOXO1 phosphorylation. FOXO1 is a pro-apoptotic protein known to play a major role in GC apoptosis and follicle survival in the ovary [46, 48]. FOXO1 is primarily expressed in GCs of preantral and antral follicles but is undetectable in luteal cells of fully developed corpus luteum [48, 83]. I wanted to examine whether the alterations in FOXO1 phosphorylation and degradation in *Tgkd* GCs led to a mislocalization of FOXO1 to different follicular stages than those observed in wildtype ovaries. On examining wildtype and *Tgkd* postpubertal PD30 ovaries for FOXO1 expression, I found that FOXO1 localization was similar in wildtype and *Tgkd* PD30 ovaries. FOXO1 was localized in GCs of preantral and antral follicles and completely absent in the luteal cells of the corpora lutea (Figure 39).

These results indicate that the hyperactivation of the PI3K/AKT pathway in *Tgkd* GCs due to the decrease in INPP4B levels is associated with an increase in GC proliferation and a decrease in GC apoptosis. The signaling changes in *Tgkd* GCs did not alter the rate of corpora lutea clearance or cause mislocalization of the pro-apoptotic protein FOXO1.

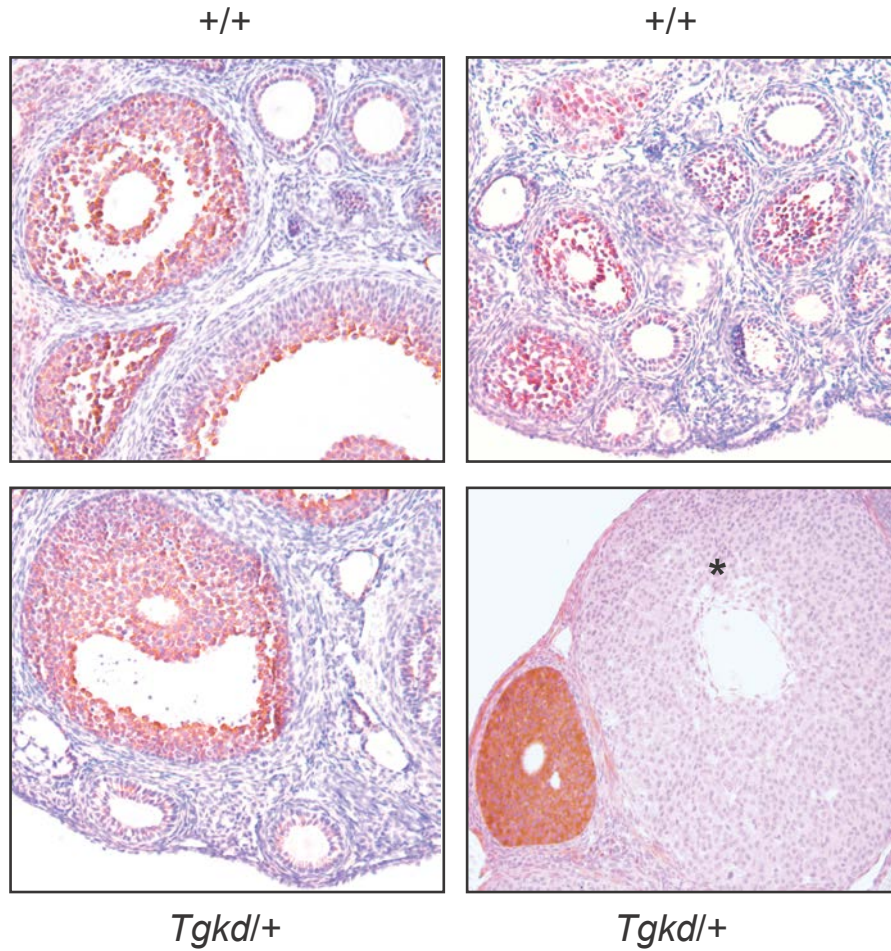


Figure 39: FOXO1 localization in wildtype and *Tgkd* PD30 ovaries

FOXO1 localization in wildtype and *Tgkd* PD30 ovaries. FOXO1 is highly expressed in GCs of preantral and antral follicles and absent in luteal cells. * - Corpus luteum with trapped oocyte.

7.6 CONCLUSIONS

In this chapter, I have demonstrated that *Inpp4b* is expressed in the GCs of the ovarian follicle and not in the oocyte. The *Tgkd* transgene insertion is associated with reduced expression of INPP4B in GCs. *Tgkd* ovaries depict enhanced activation of the PI3K/AKT pathway in terms of increased phosphorylation of AKT and FOXO1, which is specific to *Tgkd* GCs not oocytes. Increased activation of the PI3K/AKT pathway in *Tgkd* GCs is associated with an increase in proliferation and decrease in apoptosis of GCs. Corpora lutea clearance and FOXO1 localization was not affected in *Tgkd* GCs. The imbalance in the proliferation/apoptosis ration in GCs may cause the follicular defects such as oocytes trapped within corpus lutea, which ultimately promote ovarian teratoma formation [101].

8.0 DISCUSSION AND FUTURE DIRECTIONS

8.1 EFFECT OF THE *Tgkd* TRANSGENE ON OT DEVELOPMENT

In this study, I have established a link between PI3K/AKT signaling and OT development in *Tgkd* mice by showing that lower levels of the inositol phosphatase *Inpp4b* in follicular GCs leads to the development of OTs [101]. Specifically the results demonstrated that the insertion of the *Tgkd* transgene 3' of the *Inpp4b* gene results in a decrease in *Inpp4b* levels in GCs. This decrease in INPP4B levels is associated with hyperactivation of the PI3K/AKT pathway during gonadotrophin stimulation, which is reflected by an increase in AKT phosphorylation and subsequent FOXO1 phosphorylation in *Tgkd* GCs. The hyperactivation of the PI3K/AKT pathway is accompanied by an increase in proliferation and decrease in apoptosis in *Tgkd* GCs. These changes lead to multiple defects in folliculogenesis in the ovary including an increase in preantral follicles and premature appearance of corpora lutea in *Tgkd* mice. Moreover, a subset of luteinized follicles in *Tgkd* ovaries contains mature oocytes trapped within them. The oocytes of the FVB strain were found to have a high parthenogenetic activation rate, which is independent of the *Tgkd* transgene. The OTs in *Tgkd* mice were independently verified to arise from mature oocytes, which had completed meiosis I. These results led us to postulate that the combination of luteinized unruptured follicles observed in the *Tgkd* strain resulting from *Inpp4b*

reduction in GCs and the high innate parthenogenetic activation rate of FVB oocytes predispose *Tgkd* mice to OT formation.

8.2 INPP4B AND REGULATION OF PI3K/AKT PATHWAY

Inpp4b is a recently identified suppressor of the PI3K/AKT signal transduction pathway that has not been studied previously in the ovary. *Inpp4b* is an inositol polyphosphate-4-phosphatase, which was shown to catalyze the hydrolysis of the D4-position phosphate on phosphatidylinositol PI(3,4)P₂, inositol I(1,3,4)P₃ and I(3,4)P₂ [127, 128]. The enzyme INPP4B was shown to have a much higher activity towards PI(3,4)P₂, which it degrades to PI(3)P [111, 129]. The lipids PI(3,4)P₂ and PI(3,4,5)P₃ promote activation of the PI3K/AKT pathway by causing phosphorylation of the downstream protein AKT at the Serine-473 (Ser-473) and Threonine-309 (Thr-309) positions respectively [130]. Therefore by decreasing the levels of cellular PI(3,4)P₂, *Inpp4b* acts as a negative regulator of AKT phosphorylation. A decrease in *Inpp4b* has been previously shown to increase AKT phosphorylation in human mammary epithelial cells (HMEC) and LNCaP prostate adenocarcinoma cells and *Inpp4b* loss has been positively correlated with the progression of breast and prostate cancer [111, 112].

In this study I observed a decrease in *Inpp4b* levels in E13.5 brain and ovarian GCs from *Tgkd* mice. The decrease in *Tgkd* E13.5 brains was higher in homozygous *Tgkd/Tgkd* brains and a greater decrease of *Inpp4b* transcript levels was also detected in hemizygous *Tgkd/+* brain by allele specific expression studies on the chromosome 8 copy with the *Tgkd* transgene (Figure 16D, Figure 19). These data indicate that the effect of *Tgkd* on *Inpp4b* is a cis-acting effect. In the ovary, *Inpp4b* was surprisingly not expressed in the oocytes that give rise to OTs, but was

expressed in follicular GCs. *Inpp4b* levels in wildtype GCs fluctuate during induced follicular maturation by gonadotrophin stimulation similar to the protein PTEN, which is another well-known suppressor of the PI3K/AKT pathway (Figure 31) [131]. The PI3K/AKT pathway plays an extremely important role in follicular maturation. Hence, the levels of these regulators during gonadotrophin stimulation may help orchestrate the kinetics of activation of AKT and other downstream molecules during the different phases of follicular maturation. A decrease in *Inpp4b* levels was observed in immature *Tgkd* GCs and this difference was more apparent in *Tgkd* ovaries after PMSG stimulation. The *Tgkd*-induced *Inpp4b* decrease in ovaries may become more evident after PMSG (FSH) gonadotrophin stimulation, as FSH induces exponential proliferation in GCs increasing their cellular contribution to the ovary [15]. INPP4B levels in *Tgkd* GCs were reduced to approximately 70% of wildtype levels (Figure 30A). This decrease was associated with increased activation of AKT and its downstream target FOXO1 (Figure 34B). The consequence of *Inpp4b* downregulation was tested independently in wildtype GCs using shRNA constructs to *Inpp4b* and found that a decrease in *Inpp4b* levels resulted in increased AKT phosphorylation on FSH stimulation (Figure 35). These data collectively suggest that *Inpp4b* is a gonadotrophin responsive gene and a decrease in *Inpp4b* levels alters the kinetics of PI3K/AKT activation in *Tgkd* GCs.

8.3 ALTERED KINETICS OF THE PI3K/AKT PATHWAY LEADS TO OT DEVELOPMENT

The decrease in *Inpp4b* is associated with enhanced activation of the PI3K/AKT pathway, measured by increased phosphorylation of AKT and FOXO1 in *Tgkd* GCs. The PI3K/AKT

pathway is an essential signal transduction pathway in the ovary, involved in primordial follicle recruitment and induction of many important FSH-mediated follicular maturation events including GC proliferation, differentiation, cumulus cell expansion, and meiotic resumption of oogenesis [15, 41-44, 120]. Studies of mouse PTEN, a better characterized suppressor of the PI3K/AKT pathway than INPP4B, nicely illustrate the diverse cellular roles of this important intracellular signaling pathway in the ovary. Ablation of the *Pten* gene in oocytes leads to premature follicle recruitment and ovarian failure leading to infertility in early adulthood, while loss of *Pten* in fully-grown oocytes has no effect on oocyte development or fertility [40, 132]. Deletion of both *Pten* alleles in GCs results in enhanced GC proliferation, decreased GC apoptosis, persistence of multiple corpora lutea and unexpected increases in litter size [48]. These studies illustrate the cell and stage specific role of the PI3K/AKT pathway in the ovary. *Pten* and *Inpp4b* suppress the PI3K/AKT pathway by degrading PI(3,4,5)P₃ and PI(3,4)P₂ respectively, the chief activators of AKT (Figure 31) [111, 128, 133]. *Tgkd* GCs with decreased *Inpp4b* levels show a similar increase in proliferation and decrease in apoptosis to that observed in GCs depleted of PTEN, but the rate of corpora lutea clearance in *Tgkd* ovaries was unaffected by the decrease in *Inpp4b* levels (Figure 38).

Molecular events both upstream and downstream of follicular AKT activation have been previously implicated in OT development. Forced expression of a constitutively active form of the FSH receptor from a transgene (*mFshr^{D580H}*) in GCs causes OTs in 20% of transgene carriers and FSH receptor signaling is associated with activation of the PI3K/AKT pathway in a protein kinase A (PKA) dependent manner [84, 134, 135]. Furthermore, a reduction in FOXO3A activity, a downstream effect of increased AKT activation is associated with OT development [81]. FOXO3A is primarily expressed in oocytes, not GCs and is phosphorylated by activated

AKT, causing its nuclear exclusion, degradation and loss of its transcriptional activation [83, 126]. Interestingly, a missense mutation in the mouse *Foxo3a* gene in the *MommeR1* mouse strain directly decreases its transcriptional activation, mimicking the effect of increased oocyte PI3K/AKT pathway activity on FOXO3A, which causes one out of every six homozygous mutant *MommeR1* female mice to develop OTs [81]. In summary, the *mFshr^{D580H}* and *Tgkd* transgenes illustrate the relationship between hyperactivation of the GC PI3K/AKT pathway and OT formation, while the *MommeR1* strain illustrates the same relationship, but in oocytes.

8.4 EFFECT OF INPP4B LEVELS ON OT PHENOTYPE

Ovarian phenotypes appear to be exquisitely sensitive to the cell type and/or extent of gene disruption. For example, whereas a decrease in *Foxo3a* activity in *MommeR1* mice causes OTs, complete loss of oocyte FOXO3A activity is associated with premature ovarian failure, without the occurrence of OTs [81, 136]. Similarly, the level of ovarian transgene expression of *mFshr^{D580H}* correlates with the severity of the ovarian phenotype [84]. The studies in this thesis indicate that a small decrease in GC INPP4B in *Tgkd* mice is sufficient to alter AKT activation kinetics in GCs during hormonal stimulation, leading to a variety of abnormal ovarian phenotypes including OTs. I have specifically observed that a 30% decrease in the levels of tumor suppressor INPP4B can cause a 2-fold increase in P-AKT levels during certain time points after PMSG stimulation. This data is in agreement with previous studies, where a 20% reduction in the levels of tumor suppressor PTEN in mammary epithelial cells is sufficient to increase P-AKT levels by 2-4 fold compared to *Pten* wildtype cells [137]. This data supports a continuum model of tumor suppression, where small alterations in the level of tumor suppressors cause

larger downstream effects possibly by disturbing the homeostasis of the signaling pathway, which causes associated secondary effects [138]. One can speculate that lesser or greater degrees of INPP4B defects would produce a different and unique collection of abnormal ovarian phenotypes, including ones that might preclude OT formation.

Recently an *Inpp4b* knockout mouse has been generated through the *Cre* mediated deletion of exon 11 [139]. Adult *Inpp4b*^{-/-} mice are reported to be viable and do not develop OTs or spontaneous cancers, even though *Inpp4b* reduction has been previously linked to the etiology of breast and prostate cancer [111, 112, 121]. Sustained loss of INPP4B in *Inpp4b*^{-/-} mice may have led to adaptation by other suppressors of the PI3K/AKT pathway. Further, the mechanism by which the *Tgkd* transgene causes a decrease in *Inpp4b* levels is currently unknown. The insertion could have disrupted an enhancer or changed local chromatin configuration, which leads to sudden or cell-specific changes, preventing adaptation by other components of the pathway. The insertion could have affected other genes on chromosome 8, but a preliminary screen by allele specific expression analysis did not detect a decrease in transcript levels in genes in a 2Mb region surrounding the *Tgkd* transgene. I also have not identified any sequence changes in the body of the *Tgkd*-linked *Inpp4b* gene nor novel splice isoforms of *Inpp4b* mRNAs in homozygous *Tgkd* E13.5 brains. I was able to correlate the decrease in *Inpp4b* levels with an increase in phosphorylation of AKT, which reinforced the hypothesis that the *Tgkd* insertion caused OT formation primarily by decreasing *Inpp4b* levels in GCs.

8.5 EFFECT OF *Tgkd* ON INPP4B IN THE ES CELL MODEL

To assess the effect of *Tgkd* on *Inpp4b* levels and on PI3K/AKT signaling, I initially developed an ES cell model as in vitro cell culture system prior to focusing on studies in the ovary. In this model, wide variability and no clear differences were observed in *Tgkd* methylation and INPP4B levels between wildtype (+/+), hemizygous and homozygous *Tgkd* ES cell lines derived on the 129 strain background (Figure 20B, Figure 21A). The kinetics of phosphorylation of AKT1 was also not significantly different between wildtype and *Tgkd* ES cell lines on IGF1 stimulation (Figure 22). This experiment led me to examine whether *Inpp4b* functioned as a suppressor in ES cell lines by using shRNA-mediated downregulation of *Inpp4b*. Electroporation of shRNA constructs to *Inpp4b* led to an increase in AKT1 phosphorylation on IGF1 stimulation, indicating that *Inpp4b* acted as a PI3K/AKT pathway suppressor in ES cells (Figure 23). The absence of a consistent effect of *Tgkd* on INPP4B levels and AKT phosphorylation in ES cells could be due to a few reasons. *Tgkd* may not alter INPP4B levels in ES cells sufficiently to alter AKT phosphorylation. ES cells require an activated PI3K/AKT pathway to maintain pluripotency; hence they may compensate during the process of ES cell derivation and prevent alterations in AKT phosphorylation [140]. The shRNA-mediated decrease in *Inpp4b* levels is induced in a wildtype ES cell line after the derivation stage and is a more rapid change, which may prevent compensatory alterations by other suppressors in the pathway. Further the shRNA experiment is performed in a homogenous wildtype ES cell line, while innate differences among independently derived wildtype and *Tgkd* ES cell lines are likely to be found. This led me to conclude that independently derived wildtype and *Tgkd* ES cell lines do not serve as a good model to study the effects of the transgene on *Inpp4b* and the PI3K/AKT pathway.

8.6 CELL AUTONOMOUS AND NON-AUTONOMOUS ORIGINS OF OTS

OT mouse models have provided a good insight into the pathways that contribute to OT development. The genetic defects leading to OT formation could be cell autonomous confined to the oocyte, or the OT could have a non-cell autonomous origin where the surrounding GCs in the ovarian follicle provide an environment conducive to OT formation. The *c-mos*^{-/-} and the *MommeR1* mice are considered cell autonomous models of OT, as both proteins are solely expressed in the oocyte [82, 83]. OTs in the LT/Sv mice have been shown to have a cell autonomous origin as oocytes in the LT/Sv related LTXBO strain show a high rate of parthenogenetic activation in chimeric reaggregated ovaries, when LTXBO oocytes are reaggregated with GCs from an OT non-permissive strain [141].

There are also other OT models that are considered non cell-autonomous OT models. Constitutive signaling through FSH receptor (*mFshr*^{D580H}) in GCs specifically, predispose the oocytes towards OT formation [84]. A decrease in GC GATA4 leads to 10% of the mice developing OTs [86]. Overexpression of anti-apoptotic protein *Bcl-2* in GCs also leads to the development of OTs [85]. These models indicate that in non-cell autonomous OT models, the genetic modifications alter signaling pathways in the GCs, which disturb follicle maturation driving the oocyte towards parthenogenesis and OT development.

The above results indicate that the primary defect in *Tgkd* ovaries is non-cell autonomous, where a decrease in *Inpp4b* levels in *Tgkd* GCs is associated with signaling alterations in the PI3K/AKT pathway and follicular defects such as oocytes trapped in corpora lutea. *Inpp4b* is expressed only in GCs and not in oocytes, and the signaling alterations in the PI3K/AKT pathway are confined to *Tgkd* GCs not oocytes. However OTs are not observed in all mouse models with luteinized unruptured follicles [3]. A high rate of parthenogenetic activation

was observed in oocytes of the FVB strain, which is independent of the *Tgkd* insertion. Oocyte parthenogenetic activation has been postulated to be necessary but not sufficient for OT formation and the oocyte parthenogenesis rate of OT permissive strains such as the LT/SV strain (18%) are reported to be higher than the OT non-permissive B6 strain (3%) [78]. The high frequency of metaphase I arrested oocytes seen in the LT/Sv strain (90%) was not observed in FVB (44%) or FVB-*Tgkd* (51%) oocytes [78]. These results indicate that the *Tgkd* OT model has a non-cell autonomous component leading to trapped oocytes and a cell-autonomous component of high oocyte parthenogenesis, both of which contribute to OT formation.

8.7 STRAIN SPECIFICITY OF THE OT PHENOTYPE

A common feature of many mouse strains developing OTs is the FVB strain background; therefore, one must consider the possibility that these influences on OT development are determined by FVB alleles of other genes. The *Tgkd*, *mFshr*^{D580H}, *Inhα-bcl2* and *MommeR1* strains have been reported to develop OTs on the FVB background [81, 84, 85, 88]. OTs are not observed in *Tgkd* females on the 129 background or in F1 (FVB-*Tgkd* X B6) females with the *Tgkd* transgene (Table 3). Similarly, OTs have been reported to absent in *MommeR1* compound heterozygotes (FVB/129/B6) or *MommeR1* mice backcrossed to the B6 strain for 10 generations [81].

In this study, FVB oocytes were found to possess a high parthenogenetic activation rate, which is required for OT formation (Figure 10) [78]. In this regard, an FVB-specific OT modifier locus (*Ots2*) has been mapped to chromosome 6, within a region that overlaps a previously mapped LT/Sv strain-specific OT modifier allele (*Ots1*) (Eicher et al., manuscript in

preparation, [79]. On crossing FVB-*Tgkd* mice to LT/Sv mice, F1 *Tgkd* females develop OTs at a much higher frequency (90%) than either of the parent strains indicating that the *Ots1* region and *Ots2* region may involve the same gene/genes which enhance oocyte parthenogenesis (Table 3) [63, 88]. The effect of LT/Sv derived *Ots1* appears to be much stronger than FVB *Ots2* and the frequency of the OT phenotype is further increased by *Tgkd* induced effects on *Inpp4b* on chromosome 8. Identification of candidate genes within this region that contribute to the OT phenotype would help better understand the multifactorial processes involved in the generation of teratomas. The effect of the FVB strain background may also explain the lack of the OT phenotype in the *Inpp4b*^{-/-} mice, which were studied in the B6 strain background [139].

8.8 OT DEVELOPMENT IS A MULTIFACTORIAL PROCESS

OT formation has been linked to signaling defects in either oocytes or in the surrounding follicular GCs. Other OT mouse models, particularly those with defects in GCs, share aspects of *Tgkd* ovarian pathology. The intentional genetic defects in the *mFshr*^{D580H}, *Inhα-bcl2* and *siGata4* mouse lines are all confined to GCs [84-86]. Interestingly the *mFshr*^{D580H} model shows an increase in GC proliferation, while *Inhα-bcl2* ovaries display a decrease in GC apoptosis. Luteinized follicles containing trapped oocytes are seen in *mFshr*^{D580H} mice [84]. All of these processes are affected in female *Tgkd* mice, which have a high incidence of OTs, suggesting that the collective influence of many altered follicular processes greatly enhances the likelihood of OT formation.

Further FVB strain modifier alleles play a major role in promoting OT formation in *Tgkd* mice and many other OT models [81, 84, 85, 88]. The FVB modifier locus has been mapped to a

region on chromosome 6 that overlaps with the previously characterized OT susceptibility locus *Ots1*. This locus on chromosome 6 may promote oocyte parthenogenesis in OT susceptible strains such as LT/Sv and FVB mice. High rates of metaphase I arrest and parthenogenetic activation have been reported to be necessary but not sufficient for development of OTs [78]. The OT phenotype in both LT/Sv mice and *Tgkd* mice is clearly a polygenic trait with several different developmental abnormalities contributing to OT development both in GCs and oocytes. The *Tgkd* OT model serves as a valuable model to understand the etiology of OT development as the insertion of the *Tgkd* transgene at a single site on chromosome 8 converts the OT-free FVB females to OT-susceptible FVB-*Tgkd* females. Further, our studies are able to link the transgene insertion with an effect on the nearby gene *Inpp4b* and the downstream PI3K/AKT pathway. I was also able to establish a connection between altered GC proliferation and apoptosis and the presence of luteinized unruptured follicles with OT development. In this model, hemizygous *Tgkd* mice develop malignant OTs at a frequency of 15-20% by 12-22 weeks of age [88]. This frequency may appear to be low compared to other OT mouse models such as the LT/Sv strain, which are reported to develop OTs at a frequency of 50% by 3 months of age. However, the LT/Sv strain is an inbred strain, which spontaneously develops OTs [63]. Several cell cycle abnormalities have been reported in LT/Sv oocytes but the primary genetic lesions responsible for OT formation are not known [53, 142, 143]. On the other hand, most OT models with a defined single gene defect such as *mFshr^{D580H}*, *Inh α -bcl2*, *siGata4*, *MommeR1* and *Tgkd* mice develop OTs a frequency between 10-20% [81, 84-86, 88].

On speculating on the mechanism of OT formation in the *Tgkd* strain, we can evaluate the contribution of the cell (oocyte) and non-cell (GC) autonomous component of OT formation. The effect of the decrease in GC INPP4B and associated increase in P-AKT levels may cause a

dramatic increase in the number of follicular GCs during the FSH/PMSG mediated follicular growth phase. This increase in GC number may cause a delay or failure of antrum formation and uncoupling of oocyte growth from ovarian follicle growth in a subset of recruited follicles. Hence, the oocyte is unable to undergo successful ovulation from these follicles either due to the structure of the overgrown follicle or due disruption of oocyte-GC communication. The follicle is however competent for luteinization of GCs after the LH surge, hence forms a corpus luteum after an unsuccessful ovulation. A subset of trapped oocytes in the FVB strain may initiate parthenogenetic activation but may need to grow rapidly to form an OT before clearance of the surrounding corpora lutea. Oocytes that initiate malignant OT development in the *Tgkd* strain may possess this selective growth advantage and the increased activation of the PI3K/AKT pathway may further accelerate this process.

In summary, altered regulation of the PI3K/AKT pathway caused by a decrease in *Inpp4b* in *Tgkd* GCs during follicle maturation leads to a dramatic increase in the number of GCs. This is associated with several follicular defects including oocytes trapped within luteinized follicles. The trapped oocytes caused by the *Tgkd* transgene combined with the parthenogenetic oocytes of the FVB strain predispose *Tgkd* mice to OT development (Figure 40).

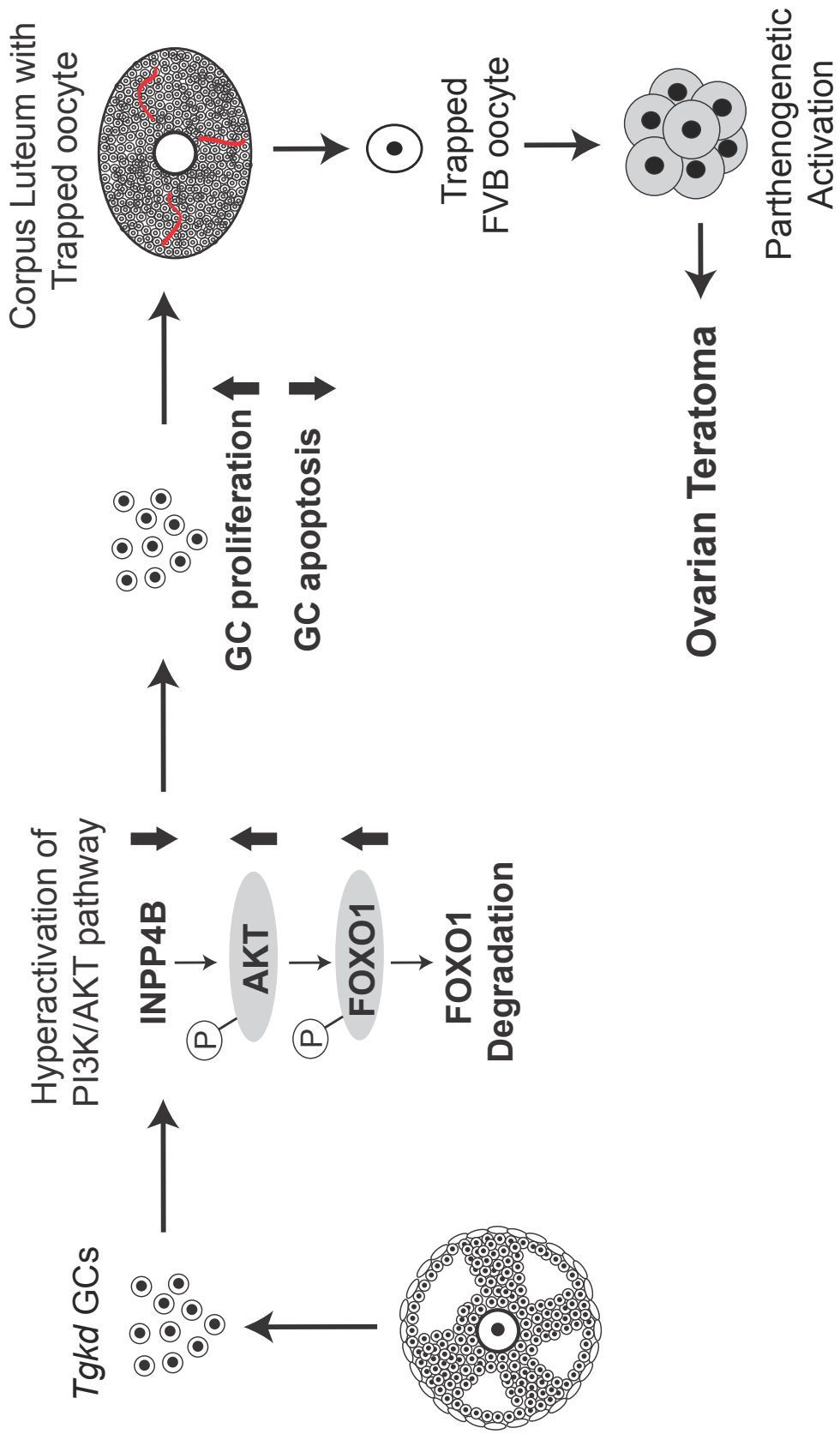


Figure 40: Model of *Tgkd* induced OT formation

OT formation is a multifactorial process in the *Tgkd* OT model with GCs and oocytes playing a role in the development of OTs. The *Tgkd* transgene causes a decrease in INPP4B levels in *Tgkd* GCs resulting in hyperactivation of the PI3K/AKT pathway. This signaling alteration is associated increased proliferation and decreased apoptosis of *Tgkd* GCs and follicular defects such as trapped oocytes in corpora lutea. The combination of trapped oocytes and high FVB oocyte parthenogenesis may predispose the *Tgkd* females to OT formation.

8.9 FUTURE DIRECTIONS

In the *Tgkd* OT model, I have demonstrated a decrease in the levels of *Inpp4b* in combination with FVB strain specific modifier alleles leads to OT formation. In future studies, we plan to independently verify this observation using *Inpp4b*^{loxP/loxP} mice, which were used to generate *Inpp4b*^{-/-} mice [139]. We have obtained *Inpp4b*^{loxP/loxP} mice from Dr. Vacher, where the loxP sites are designed to flank exon 11 of the *Inpp4b* gene. We plan to cross the *Inpp4b*^{loxP/loxP} mice with transgenic mice carrying *Sox2* promoter-mediated Cre recombinase (*Sox2*-Cre mice). This would generate *Inpp4b*^{loxP/loxP}; *Sox2*-Cre mice similar to the *Inpp4b*^{-/-} mice with loss of INPP4B protein in the epiblast and subsequently all tissues of the embryo [144]. We would also cross the *Inpp4b*^{loxP/loxP} mice with transgenic mice carrying a granulosa cell promoter-mediated Cre recombinase (GC-Cre) in order to generate *Inpp4b*^{loxP/loxP}; GC-Cre mice with a tissue specific

knockout of *Inpp4b* in GCs to reduce the timespan for adaptation. We plan to use the cytochrome P450, family 19 promoter (*Cyp19*-Cre) and anti-Müllerian hormone promoter (AMH-Cre) strains of mice to generate GC specific knockouts of *Inpp4b* [48, 145]. We plan to backcross the *Inpp4b*^{loxP/loxP}; *Sox2*-Cre and *Inpp4b*^{loxP/loxP}; GC-Cre mice into the FVB background for at least 10 generations and then evaluate whether the females develop OTs. Since ovarian phenotypes are sensitive to the extent of gene downregulation, we plan to also cross *Inpp4b*^{loxP/+} with transgenic mice expressing Cre recombinase and then backcross the resulting *Inpp4b*^{loxP/+}; *Sox2*-Cre and *Inpp4b*^{loxP/+}; GC-Cre mice into the FVB background for several generations. We would verify the loss of INPP4B in each of these strains of mice and examine whether there are alterations in the PI3K/AKT pathway. These experiments would help us directly address the role of *Inpp4b* and the extent of downregulation required for OT formation.

We are also planning to further pursue studies on the role of the FVB background on OT formation. Linkage analysis has already identified the FVB strain specific modifier locus in *Tgkd* females, designated *Ots2* to be located between 20-50cM on chromosome 6 (Eicher et al., manuscript in preparation). Congenic mouse strains have been generated on the B6 background, which possess small genomic regions from the FVB strain on chromosome 6 overlapping *Ots2*. One of congenic lines Line B is on the B6 strain background but contains the 20-50cM region of chromosome 6 from the FVB strain. Line B mice with the *Tgkd* transgene develop OTs at a high frequency, when crossed to OT susceptible LT/Sv mice (Eicher et al., manuscript in preparation). Creating a number of congenic lines with small specific subintervals of *Ots2* from the FVB background may help us specify the location of the FVB modifier gene involved in the OT phenotype to a 1-2 cM resolution for effective positional cloning and evaluation of candidate genes.

One interesting candidate in the *Ots2* region is the gene inositol 1,4,5-trisphosphate receptor 1 *Itp1* (49.74 cM), which plays a role in calcium release post fertilization. The binding of inositol (1,4,5) triphosphate (IP3) to *Itp1* post fertilization initiates a series of calcium oscillations, which promote egg activation involving completion of meiosis II and subsequent mitotic cleavage [146]. Recent studies have shown an increase in ITPR1 sensitivity and levels with oocyte maturation, which peaks after completion of meiosis I and is subsequently downregulated after fertilization [147-149]. Calcium ionophores that increase intracellular calcium levels in mature oocytes promote oocyte parthenogenesis [150]. Therefore, alterations in the cDNA sequence or protein levels of ITPR1 may lower the threshold for calcium release and alter the rate of oocyte parthenogenetic activation between OT susceptible and OT non-permissive strains. Further, we also plan to analyze whether *Tgkd* alters PI3K/AKT activation kinetics in GCs and is associated with luteinized unruptured follicles in OT non-permissive strains. These studies would help us determine whether the strain permissiveness of the FVB strain is limited to the modifier locus on chromosome 6 or involves many other FVB strain specific effects on ovarian follicular maturation.

APPENDIX A

PERICENTRIC AND DISTAL SNPS ANALYZED IN SPLEEN AND OTS TO DETERMINE LAST STAGE OF MEIOSIS OF OTS

SNP genotyping for spleen and teratoma, used to determine the last stage of meiosis completed by oocyte before initiating OT formation. Single nucleotide polymorphisms (SNPs) that are documented to be different between B6 and FVB were chosen for this analysis. One pericentric and distal SNP were chosen per chromosome and analyzed in spleen (Spl) and OT pairs from OT positive *Tgkd* females from the backcross between (FVB-*Tgkd* X B6) and FVB mice. The chromosomal location of each SNP and their nucleotide status in the spleen and OT are stated in the below figure.

Tgkd ovarian teratoma

Chromosome (No.-position(bp))	Nucleotide B6 FVB	Chromosomal Location	1		2		3		4		5		6		7	
			OT	Spl												
1-008110094	G	T	G	G/T	T	G/T	G	G/T	G/T	G/T	T	G/T	G/T	G/T	T	T
1-191804699	A	T	A/T	A/T	T	A/T	A/T	A/T	T	T	T	T	A/T	A/T	T	T
2-011117260	G	C	G	G/C	C	G/C	G	G/C	G	G/C	C	C	C	C	C	C
2-176114999	G	T	G	G/T	T	T	T	T	G/T	G/T	T	T	T	T	G	G/T
3-009298864	C	T	T	C/T	C	C/T	T	C/T	NI	C/T	T	T	T	T	T	T
3-155372777	T	C	T/C	T/C	C	C	NI	NI	C	C	C	C	T/C	T/C	NI	T/C
4-006370062	A	G	G	G	G	G	G	G	C	C	G	A/G	G	G	G	G
4-151168886	G	T	NI	G/T	G/T	G/T	T	T	T	T	T	T	G/T	G/T	T	T
5-008305854	C	T	C	C/T	T	T	T	C/T	C	C/T	T	T	T	C/T	T	C/T
5-149044358	C	A	A	A	A	A	A	A	A	A	A	A	C	C/A	C	C/A
6-004259021	C	T	T	C/T	T	C/T	T	C/T	T	C/T	C	C/T	T	T	T	T
6-148400389	G	A	A	A	G/A	G/A	G/A	G/A	A	A	A	A	A	A	A	A
7-004201219	A	G	A/G	A/G	A	A/G	G	G	G	G	G	G	G	G	A	A
7-135345950	A	G	NI													
8-015199792	T	C	C	C	C	C	C	C	C	C	C	C	C	C	C	C
8-119264649	C	T	T	T	T	T	T	T	T	T	T	T	T	T	T	T
9-018952877	C	A	C/A	C/A	A	A	C/A	C/A	C	C/A	A	C/A	C	C/A	A	A
9-123708875	G	A	G/A	G/A	G/A	G/A	A	A	A	A	G/A	G/A	A	A	G/A	G/A
10-006360048	G	A	A	A	A	A	A	A	A	A	A	A	A	A	A	A
10-129117100	G	A	A	A	A	A	A	A	A	A	A	A	A	A	A	A
11-004367508	G	A	A	A	A	A	A	A	A	A	A	A	A	A	A	A
11-117212076	A	G	G	G	G	G	G	G	A/G	A/G	A	A/G	A/G	A/G	A	A
12-009581325	G	T	G/T	T	T	T	T	G/T	T	T	T	T	T	T	T	T
12-110383990	C	T	NI													
13-003966099	A	G	A/G	A/G	G	A/G	G	A/G	A	A/G	G	A/G	G	G	G	A/G
13-115141257	C	A	NI													
14-005055006	T	A	A	A	A	T/A	A	A	A	T/A	A	A	A	A	A	T/A
14-114403652	C	T	T	T	C/T	C/T	C/T	C/T	T	T	T	T	NI	C/T	C/T	C/T
15-010120073	T	C	C	C	T	T/C	C	T/C	C	C	C	T/C	T	T/C	C	C
15-096231715	T	G	G	G	T/G	T/G	G	G	G	G	T/G	T/G	G	G	G	G
16-003310511	G	A	A	G/A	A	G/A	A	G/A	G/A	G/A	A	A	G	G/A	G	G/A
16-096070057	C	T	C/T	C/T	C/T	C/T	C/T	C/T	T	T	NI	C/T	C/T	C/T	T	T
17-019783711	T	G	T/G	T/G	T	T/G	G	T/G	G	T/G	T	T/G	G	G	T	T/G
17-092673068	T	G	T/G	T/G	G	G	G	G	G	G	T/G	T/G	G	G	T/G	T/G
18-010953833	A	G	A	A/G	A	A/G	A	A/G	A	A/G	G	G	G	G	G	G
18-089124391	A	G	G	A/G	A/G	A/G	G	G	A/G	A/G	G	G	G	G	G	G
19-007376322	T	C	C	T	T/C	C	T/C	C	T	T/C	C	C	C	T/C	C	C
19-060030696	A	G	A/G	A/G	G	G	G	G	G	G	G	G	A/G	A/G	A/G	A/G
X-016114535	C	A	A	A	A	A	A	A	A	A	A	A	C	C/A	C	C/A
X-143466659	A	C	C	C	C	C	A/C	A/C	C	C	C	C	NI	A/C	A/C	A/C

APPENDIX B

PRIMER SEQUENCES USED IN EXPERIMENTS

Primer name	Primer sequence
Genotyping of wildtype and <i>Tgkd</i> mice	
WT-F	TGCAGTGAAGACAATGGGTATTGTG
WT-R	CACAACAAAGACAGCTTGTGGAC
<i>Tgkd</i> -F	CTATTCCAGCCTAGTCTGCT
<i>Tgkd</i> -R	AGTCAGAAGCTACGGAGCCT
Primer sequences for <i>Tgkd</i> genotyping	
BS- <i>Tgkd</i> -F	GTATTGAAATTGAGTTTGAAGTGG
BS- <i>Tgkd</i> -R	ATACTCTAAATAACCTAAAAAATCC
BS- <i>Tgkd</i> -nested-F	GTATTGAAATTGAGTTTGAAGTGG
BS- <i>Tgkd</i> -nested-R	TATCTTCACCTAAAAACCCTCCAC
HpaII-McrBC methylation sensitive PCR	

CpGi-1F	AGGTGGTTCAACAGCGAATC
CpGi-1R	ACCTTTTCCCCTCGGTGTAG
CpGi-2F	CTTCTTGCGTCCACAGTTCA
CpGi-2R	CCGATCGAGTTCCTCTTCAG
CpGi-3F	GAGTGGTAGCCCTGCTGAAG
CpGi-3R	ACCCAGGGCGACTTTTAACT
CpGi-4F	GAGCTACCTTCTCACATCCT
CpGi-4R	ATTCACCCATCCTCACCCTC
CpGi-5F	CCAGAAGCTGTGTTGTTTTG
CpGi-5R	CACCCTATTGTACTGCTGTC
CpGi-6F	GATGAGGAAGGCAGAAATGG
CpGi-6R	CCTGTGCAGACTAAAATCCT
CpGi-7F	TGGAGTTTGTTCACACA
CpGi-7R	TGTGGGCTCGTCTTTCTTTT
CpGi-8F	GCTGCTTTCCTTTTGTTCG
CpGi-8R	GGA CT TCTCAGCCAGAGGTG
CpGi-9F	TCTGGTGTTTGGACCTCCTC
CpGi-9R	CAGCTTTGAAGTGTGCATCC
CpGi-10F	CAGTACCTCCTCCGGATTCA
CpGi-10R	TGACAAGTTTAGCGCGTGAC
<i>Inpp4b</i> cDNA overlapping PCR products	
<i>Inpp4b</i> -cDNA-1F	CTGAGCTCGCCGCTATAAAT

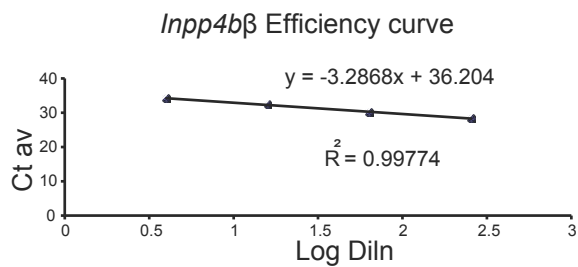
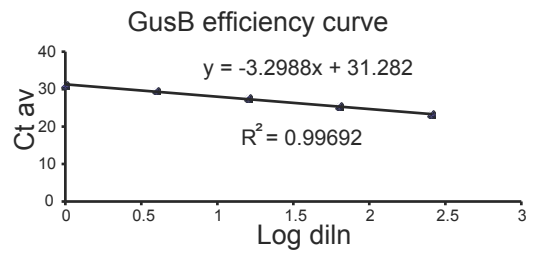
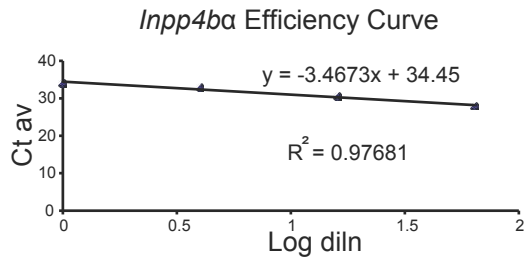
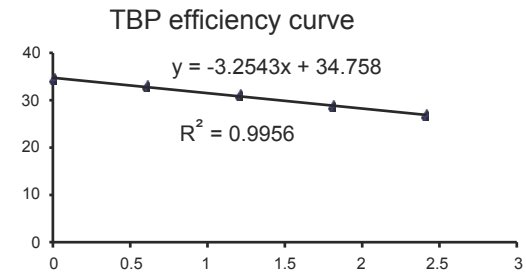
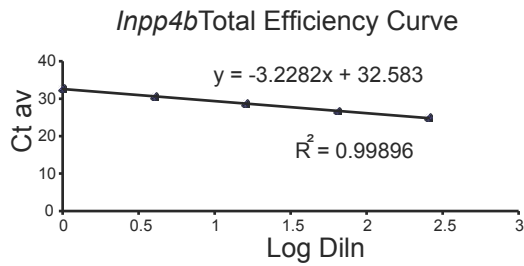
<i>Inpp4b</i> -cDNA-1R	CCCTGCACATCTGTTGTGAT
<i>Inpp4b</i> -cDNA-2F	ATTCGAACCAGTGTCCCTTCC
<i>Inpp4b</i> -cDNA-2R	GCAGCAGGTCTGCATGAGT
<i>Inpp4b</i> -cDNA-3F	AGCAGCAGCAAAGGAGAGAA
<i>Inpp4b</i> -cDNA-3R	AGCGCCTGACTGAAGACAAT
<i>Inpp4b</i> -cDNA-4F	TCACAACGAAGAAGGTGCTG
<i>Inpp4b</i> -cDNA-4R	TGTTCCAGTGTCCACCGACAT
<i>Inpp4b</i> -cDNA-5F (α only)	GAAATTGGAATGCTGGAGGA
<i>Inpp4b</i> -cDNA-5R (α only)	CAAAGCTCAGTGTATTTGTGTTCC
<i>Inpp4b</i> -cDNA-6F (β only)	TTGGACAATCTCCACCAAAA
<i>Inpp4b</i> -cDNA-6R (β only)	AACAGAAATAGCCATTCTTTCCA
<i>Inpp4b</i> -cDNA-7F (β only)	ACCTCCTCTTCCCAGGTCAT
<i>Inpp4b</i> -cDNA-7R (β only)	TTGTTCAATGCAGAGTTGCAG
SNuPE RT-PCR and extension primer	
<i>Smarca5</i> -RTPCR-F	CGGGTCTTCATAAGATGTGC
<i>Smarca5</i> -RTPCR-R	TGCTTCAGGGTCTCCAGTTT
<i>Smarca5</i> -SNuPE	ATAATTTTCTATGCATATTT
<i>Gab1</i> -RTPCR-F	TCCGGAGGAGTTTCAGAGAA
<i>Gab1</i> -RTPCR-R	CAGACGGTGACCTGACCTG
<i>Gab1</i> -SNuPE	CAGTTCTGGGCTCCCTGTCC
<i>Usp38</i> -RTPCR-F	TCCAGACCTCCGTGGTTTAC
<i>Usp38</i> -RTPCR-R	AGCCCATCATCTTGAGCACT

<i>Usp38</i> -SNuPE	ACATCTGCTGCCTAAACTG
<i>Inpp4b</i> -RTPCR-F	GGTGTACCTGGCAAGAGAT
<i>Inpp4b</i> -RTPCR-R	TCACTGACAGGAGCCACAAG
<i>Inpp4b</i> -SNuPE	GGTACCATTTGAAAAAGACA
<i>Il15</i> -RTPCR-F	CGTGCTCTACCTTGCAAACA
<i>Il15</i> -RTPCR-R	GAAGCTTAGTTTGCCAGCA
<i>Il15</i> -SNuPE	ATCAACACGTCCTGACTGCA
<i>Zfp330</i> -RTPCR-F	AAATGTGTTTCCTGCAATCG
<i>Zfp330</i> -RTPCR-R	AAAACGGTGAACATGGCAAC
<i>Zfp330</i> -SNuPE	TGTAATGGGTAAAATTACCA
<i>Rnf150</i> -RTPCR-F	AAGACTGCGAGGAGGTGAAA
<i>Rnf150</i> -RTPCR-R	CTCGTACCCGTGGAATTCAT
<i>Rnf150</i> -SNuPE	CACTTGACTTCAGCCTCTCC
<i>Tbc1d9</i> -RTPCR-F	TACCTAAAACTCTGGACTGC
<i>Tbc1d9</i> -RTPCR-R	GTGCCTTACTTTGGGTTATC
<i>Tbc1d9</i> -SNuPE	AATTAACTATTTATTAGTACC
Real time PCR	
TBP-F	CTGACCCACCAGCAGTTCAGT
TBP-R	TCTGGGTTTGATCATTCTGTAGATTAA
GusB-F	CGTGGTCGGAGAGCTCATCT
GusB-R	TCAGCGGTGACTGGTTCGT
<i>Inpp4b</i> -F	GCTGGCAGCAACGATTTGT
<i>Inpp4b</i> -R	TCTTTGGCACTTTTACAGCAGGTA

<i>Inpp4b</i> α -F	AGAGCTTTAGATTGCATGAGAAGAGA
<i>Inpp4b</i> α -R	CCTCCTGCATTTGATATTCTTCAGT
<i>Inpp4b</i> β -F	GAGCTTTAGATTGCATGAGAAGCA
<i>Inpp4b</i> β -R	CAGGATCATCGGATTCATTCAA
Primers for In Situ probes	
<i>Slc39a10</i> -IS-F	GCGCCTCGAGCTGCCTGCTCTTACACCACTG
<i>Slc39a10</i> -IS-R	GCGCGAATTCCACACCAGCACCTTTTAGCA
<i>Inpp4b</i> α -IS-F	GCGCCTCGAGAGAAGGATGCCGCATAGAGA
<i>Inpp4b</i> α -IS-R	GCGCGAATTCCAAAG`CTCAGTGTATTTGTGTT CC
<i>Inpp4b</i> β -IS-F	GCGCCTCGAGTATCCTGTGCGCCTTGCTTCT
<i>Inpp4b</i> β -IS-R	GCGCGAATTCACCATTATTGCCTTCGGAAA

APPENDIX C

EFFICIENCY CURVES FOR REAL TIME PCR EXPERIMENTS



BIBLIOGRAPHY

1. Williams RH, Larsen PR. Williams textbook of endocrinology. 10th ed. Philadelphia, Pa.: Saunders; 2003. xxiii, 1927.
2. Leung PCK, Adashi EY. The ovary. 2nd ed. Amsterdam ; Boston: Elsevier; 2004. xviii, 664.
3. Edson MA, Nagaraja AK, Matzuk MM. The mammalian ovary from genesis to revelation. *Endocrine reviews*. 2009;30(6):624-712.
4. McGee EA, Hsueh AJ. Initial and cyclic recruitment of ovarian follicles. *Endocrine reviews*. 2000;21(2):200-14.
5. Camp TA, Rahal JO, Mayo KE. Cellular localization and hormonal regulation of follicle-stimulating hormone and luteinizing hormone receptor messenger RNAs in the rat ovary. *Mol Endocrinol*. 1991;5(10):1405-17.
6. Zheng W, Magid MS, Kramer EE, Chen YT. Follicle-stimulating hormone receptor is expressed in human ovarian surface epithelium and fallopian tube. *The American journal of pathology*. 1996;148(1):47-53.
7. Eppig JJ, Wigglesworth K, Pendola FL. The mammalian oocyte orchestrates the rate of ovarian follicular development. *Proc Natl Acad Sci U S A*. 2002;99(5):2890-4.
8. Dierich A, Sairam MR, Monaco L, Fimia GM, Gansmuller A, LeMeur M, et al. Impairing follicle-stimulating hormone (FSH) signaling in vivo: targeted disruption of the FSH receptor leads to aberrant gametogenesis and hormonal imbalance. *Proc Natl Acad Sci U S A*. 1998;95(23):13612-7.
9. Halpin DM, Charlton HM. Effects of short-term injection of gonadotrophins on ovarian follicle development in hypogonadal (hpg) mice. *Journal of reproduction and fertility*. 1988;82(1):393-400.
10. Wang XN, Greenwald GS. Hypophysectomy of the cyclic mouse. I. Effects on folliculogenesis, oocyte growth, and follicle-stimulating hormone and human chorionic gonadotropin receptors. *Biol Reprod*. 1993;48(3):585-94.

11. Van Cappellen WA, Meijs-Roelofs HM, Kramer P, Van den Dungen HM. Ovarian follicle dynamics in immature rats treated with a luteinizing hormone-releasing hormone antagonist (Org. 30276). *Biol Reprod.* 1989;40(6):1247-56.
12. Diaz FJ, Wigglesworth K, Eppig JJ. Oocytes determine cumulus cell lineage in mouse ovarian follicles. *Journal of cell science.* 2007;120(Pt 8):1330-40.
13. Solc P, Schultz RM, Motlik J. Prophase I arrest and progression to metaphase I in mouse oocytes: comparison of resumption of meiosis and recovery from G2-arrest in somatic cells. *Molecular human reproduction.* 2010;16(9):654-64.
14. Rao MC, Midgley AR, Jr., Richards JS. Hormonal regulation of ovarian cellular proliferation. *Cell.* 1978;14(1):71-8.
15. Robker RL, Richards JS. Hormone-induced proliferation and differentiation of granulosa cells: a coordinated balance of the cell cycle regulators cyclin D2 and p27Kip1. *Mol Endocrinol.* 1998;12(7):924-40.
16. Pedersen T, Peters H. Proposal for a classification of oocytes and follicles in the mouse ovary. *Journal of reproduction and fertility.* 1968;17(3):555-7.
17. Achermann JC, Jameson JL. Fertility and infertility: genetic contributions from the hypothalamic-pituitary-gonadal axis. *Mol Endocrinol.* 1999;13(6):812-8.
18. Adashi EY, Leung PCK. *The Ovary.* New York: Raven Press; 1993. xv, 687.
19. Knobil E, Neill JD. *Knobil and Neill's physiology of reproduction.* 3rd ed. Amsterdam ; Boston: Elsevier; 2006. 2 v. (xxix, 3230).
20. Southworth MB, Matsumoto AM, Gross KM, Soules MR, Bremner WJ. The importance of signal pattern in the transmission of endocrine information: pituitary gonadotropin responses to continuous and pulsatile gonadotropin-releasing hormone. *The Journal of clinical endocrinology and metabolism.* 1991;72(6):1286-9.
21. Belchetz PE, Plant TM, Nakai Y, Keogh EJ, Knobil E. Hypophysial responses to continuous and intermittent delivery of hypothalamic gonadotropin-releasing hormone. *Science.* 1978;202(4368):631-3.
22. Wildt L, Hausler A, Marshall G, Hutchison JS, Plant TM, Belchetz PE, et al. Frequency and amplitude of gonadotropin-releasing hormone stimulation and gonadotropin secretion in the rhesus monkey. *Endocrinology.* 1981;109(2):376-85.
23. Haisenleder DJ, Dalkin AC, Ortolano GA, Marshall JC, Shupnik MA. A pulsatile gonadotropin-releasing hormone stimulus is required to increase transcription of the gonadotropin subunit genes: evidence for differential regulation of transcription by pulse frequency in vivo. *Endocrinology.* 1991;128(1):509-17.

24. Zeleznik AJ, Schuler HM, Reichert LE, Jr. Gonadotropin-binding sites in the rhesus monkey ovary: role of the vasculature in the selective distribution of human chorionic gonadotropin to the preovulatory follicle. *Endocrinology*. 1981;109(2):356-62. Epub 1981/08/01.
25. Evans AC, Fortune JE. Selection of the dominant follicle in cattle occurs in the absence of differences in the expression of messenger ribonucleic acid for gonadotropin receptors. *Endocrinology*. 1997;138(7):2963-71.
26. Hillier SG, Whitelaw PF, Smyth CD. Follicular oestrogen synthesis: the 'two-cell, two-gonadotrophin' model revisited. *Molecular and cellular endocrinology*. 1994;100(1-2):51-4.
27. Zeleznik AJ, Hutchison JS, Schuler HM. Interference with the gonadotropin-suppressing actions of estradiol in macaques overrides the selection of a single preovulatory follicle. *Endocrinology*. 1985;117(3):991-9.
28. Zeleznik AJ, Midgley AR, Jr., Reichert LE, Jr. Granulosa cell maturation in the rat: increased binding of human chorionic gonadotropin following treatment with follicle-stimulating hormone in vivo. *Endocrinology*. 1974;95(3):818-25.
29. Xia L, Van Vugt D, Alston EJ, Luckhaus J, Ferin M. A surge of gonadotropin-releasing hormone accompanies the estradiol-induced gonadotropin surge in the rhesus monkey. *Endocrinology*. 1992;131(6):2812-20.
30. Fritz MA, McLachlan RI, Cohen NL, Dahl KD, Bremner WJ, Soules MR. Onset and characteristics of the midcycle surge in bioactive and immunoactive luteinizing hormone secretion in normal women: influence of physiological variations in periovulatory ovarian steroid hormone secretion. *The Journal of clinical endocrinology and metabolism*. 1992;75(2):489-93.
31. Stocco C, Telleria C, Gibori G. The molecular control of corpus luteum formation, function, and regression. *Endocrine reviews*. 2007;28(1):117-49.
32. Hawkins SM, Matzuk MM. The menstrual cycle: basic biology. *Annals of the New York Academy of Sciences*. 2008;1135:10-8.
33. Nillni YI, Toufexis DJ, Rohan KJ. Anxiety sensitivity, the menstrual cycle, and panic disorder: a putative neuroendocrine and psychological interaction. *Clinical psychology review*. 2011;31(7):1183-91.
34. Silver LM. *Mouse genetics : concepts and applications*. New York: Oxford University Press; 1995. xiii, 362.
35. Fowler RE, Edwards RG. Induction of superovulation and pregnancy in mature mice by gonadotrophins. *The Journal of endocrinology*. 1957;15(4):374-84.

36. Richards JS, Pangas SA. The ovary: basic biology and clinical implications. *The Journal of clinical investigation*. 2010;120(4):963-72.
37. Hunzicker-Dunn M, Maizels ET. FSH signaling pathways in immature granulosa cells that regulate target gene expression: branching out from protein kinase A. *Cell Signal*. 2006;18(9):1351-9.
38. Farini D, La Sala G, Tedesco M, De Felici M. Chemoattractant action and molecular signaling pathways of Kit ligand on mouse primordial germ cells. *Dev Biol*. 2007;306(2):572-83.
39. Morita Y, Manganaro TF, Tao XJ, Martimbeau S, Donahoe PK, Tilly JL. Requirement for phosphatidylinositol-3'-kinase in cytokine-mediated germ cell survival during fetal oogenesis in the mouse. *Endocrinology*. 1999;140(2):941-9.
40. Reddy P, Liu L, Adhikari D, Jagarlamudi K, Rajareddy S, Shen Y, et al. Oocyte-specific deletion of Pten causes premature activation of the primordial follicle pool. *Science*. 2008;319(5863):611-3.
41. Shimada M, Ito J, Yamashita Y, Okazaki T, Isobe N. Phosphatidylinositol 3-kinase in cumulus cells is responsible for both suppression of spontaneous maturation and induction of gonadotropin-stimulated maturation of porcine oocytes. *The Journal of endocrinology*. 2003;179(1):25-34.
42. Hoshino Y, Yokoo M, Yoshida N, Sasada H, Matsumoto H, Sato E. Phosphatidylinositol 3-kinase and Akt participate in the FSH-induced meiotic maturation of mouse oocytes. *Mol Reprod Dev*. 2004;69(1):77-86.
43. Kalous J, Solc P, Baran V, Kubelka M, Schultz RM, Motlik J. PKB/AKT is involved in resumption of meiosis in mouse oocytes. *Biology of the cell / under the auspices of the European Cell Biology Organization*. 2006;98(2):111-23.
44. Zeleznik AJ, Saxena D, Little-Ihrig L. Protein kinase B is obligatory for follicle-stimulating hormone-induced granulosa cell differentiation. *Endocrinology*. 2003;144(9):3985-94.
45. Alam H, Maizels ET, Park Y, Ghaey S, Feiger ZJ, Chandel NS, et al. Follicle-stimulating hormone activation of hypoxia-inducible factor-1 by the phosphatidylinositol 3-kinase/AKT/Ras homolog enriched in brain (Rheb)/mammalian target of rapamycin (mTOR) pathway is necessary for induction of select protein markers of follicular differentiation. *J Biol Chem*. 2004;279(19):19431-40.
46. Park Y, Maizels ET, Feiger ZJ, Alam H, Peters CA, Woodruff TK, et al. Induction of cyclin D2 in rat granulosa cells requires FSH-dependent relief from FOXO1 repression coupled with positive signals from Smad. *J Biol Chem*. 2005;280(10):9135-48.

47. Sicinski P, Donaher JL, Geng Y, Parker SB, Gardner H, Park MY, et al. Cyclin D2 is an FSH-responsive gene involved in gonadal cell proliferation and oncogenesis. *Nature*. 1996;384(6608):470-4.
48. Fan HY, Liu Z, Cahill N, Richards JS. Targeted disruption of Pten in ovarian granulosa cells enhances ovulation and extends the life span of luteal cells. *Mol Endocrinol*. 2008;22(9):2128-40.
49. Mehlmann LM. Stops and starts in mammalian oocytes: recent advances in understanding the regulation of meiotic arrest and oocyte maturation. *Reproduction*. 2005;130(6):791-9.
50. Conti M, Andersen CB, Richard F, Mehats C, Chun SY, Horner K, et al. Role of cyclic nucleotide signaling in oocyte maturation. *Molecular and cellular endocrinology*. 2002;187(1-2):153-9.
51. Oh JS, Han SJ, Conti M. Wee1B, Myt1, and Cdc25 function in distinct compartments of the mouse oocyte to control meiotic resumption. *J Cell Biol*. 2010;188(2):199-207.
52. Pirino G, Wescott MP, Donovan PJ. Protein kinase A regulates resumption of meiosis by phosphorylation of Cdc25B in mammalian oocytes. *Cell Cycle*. 2009;8(4):665-70.
53. Hampl A, Eppig JJ. Analysis of the mechanism(s) of metaphase I arrest in maturing mouse oocytes. *Development*. 1995;121(4):925-33.
54. Sagata N, Watanabe N, Vande Woude GF, Ikawa Y. The c-mos proto-oncogene product is a cytostatic factor responsible for meiotic arrest in vertebrate eggs. *Nature*. 1989;342(6249):512-8.
55. Madgwick S, Jones KT. How eggs arrest at metaphase II: MPF stabilisation plus APC/C inhibition equals Cytostatic Factor. *Cell division*. 2007;2:4.
56. Colledge WH, Carlton MB, Udy GB, Evans MJ. Disruption of c-mos causes parthenogenetic development of unfertilized mouse eggs. *Nature*. 1994;370(6484):65-8.
57. Hashimoto N, Watanabe N, Furuta Y, Tamemoto H, Sagata N, Yokoyama M, et al. Parthenogenetic activation of oocytes in c-mos-deficient mice. *Nature*. 1994;370(6484):68-71.
58. Saunders CM, Larman MG, Parrington J, Cox LJ, Royse J, Blayney LM, et al. PLC zeta: a sperm-specific trigger of Ca(2+) oscillations in eggs and embryo development. *Development*. 2002;129(15):3533-44.
59. Linder D, McCaw BK, Hecht F. Parthenogenic origin of benign ovarian teratomas. *The New England journal of medicine*. 1975;292(2):63-6.
60. Ulbright TM. Germ cell tumors of the gonads: a selective review emphasizing problems in differential diagnosis, newly appreciated, and controversial issues. *Modern pathology* :

an official journal of the United States and Canadian Academy of Pathology, Inc. 2005;18 Suppl 2:S61-79.

61. Schmid-Braz AT, Cavalli LR, Cornelio DA, Wuicik L, Ribeiro EM, Bleggi-Torres LF, et al. Comprehensive cytogenetic evaluation of a mature ovarian teratoma case. *Cancer Genet Cytogenet.* 2002;132(2):165-8.
62. Howlader N, Noone AM, Krapcho M, Neyman N, Aminou R, Waldron W, et al. SEER Cancer Statistics Review, 1975-20082011.
63. Stevens LC, Varnum DS. The development of teratomas from parthenogenetically activated ovarian mouse eggs. *Dev Biol.* 1974;37(2):369-80.
64. Surti U, Hoffner L, Chakravarti A, Ferrell RE. Genetics and biology of human ovarian teratomas. I. Cytogenetic analysis and mechanism of origin. *American journal of human genetics.* 1990;47(4):635-43.
65. Carritt B, Parrington JM, Welch HM, Povey S. Diverse origins of multiple ovarian teratomas in a single individual. *Proc Natl Acad Sci U S A.* 1982;79(23):7400-4.
66. Deka R, Chakravarti A, Surti U, Hauselman E, Reefer J, Majumder PP, et al. Genetics and biology of human ovarian teratomas. II. Molecular analysis of origin of nondisjunction and gene-centromere mapping of chromosome I markers. *American journal of human genetics.* 1990;47(4):644-55.
67. Muretto P, Chilosi M, Rabitti C, Tommasoni S, Colato C. Biovularity and "coalescence of primary follicles" in ovaries with mature teratomas. *International journal of surgical pathology.* 2001;9(2):121-5.
68. Hoffner L, Shen-Schwarz S, Deka R, Chakravarti A, Surti U. Genetics and biology of human ovarian teratomas. III. Cytogenetics and origins of malignant ovarian germ cell tumors. *Cancer Genet Cytogenet.* 1992;62(1):58-65.
69. Parrington JM, West LF, Povey S. The origin of ovarian teratomas. *Journal of medical genetics.* 1984;21(1):4-12.
70. Blake KI, Gerrard MP. Malignant germ cell tumours in two siblings. *Medical and pediatric oncology.* 1993;21(4):299-300.
71. Brenner SH, Wallach RC. Familial benign cystic teratomata. *International journal of gynaecology and obstetrics: the official organ of the International Federation of Gynaecology and Obstetrics.* 1983;21(2):167-9.
72. Indinnimeo M, Cichini C, Larcinese A, Kanakaki S, Ricci F, Mingazzini PL. Two twins with teratoma of the ovary. An unusual association: case report. *European journal of gynaecological oncology.* 2003;24(2):199-201.

73. Plattner G, Oxorn H. Familial incidence of ovarian dermoid cysts. *Canadian Medical Association journal*. 1973;108(7):892-3.
74. Simon A, Ohel G, Neri A, Schenker JG. Familial occurrence of mature ovarian teratomas. *Obstetrics and gynecology*. 1985;66(2):278-9.
75. Stettner AR, Hartenbach EM, Schink JC, Huddart R, Becker J, Pauli R, et al. Familial ovarian germ cell cancer: report and review. *American journal of medical genetics*. 1999;84(1):43-6.
76. Eppig JJ, Kozak LP, Eicher EM, Stevens LC. Ovarian teratomas in mice are derived from oocytes that have completed the first meiotic division. *Nature*. 1977;269(5628):517-8.
77. O'Neill GT, Kaufman MH. Ovulation and fertilization of primary and secondary oocytes in LT/Sv strain mice. *Gamete research*. 1987;18(1):27-36.
78. Eppig JJ, Wigglesworth K, Varnum DS, Nadeau JH. Genetic regulation of traits essential for spontaneous ovarian teratocarcinogenesis in strain LT/Sv mice: aberrant meiotic cell cycle, oocyte activation, and parthenogenetic development. *Cancer Res*. 1996;56(21):5047-54.
79. Lee GH, Bugni JM, Obata M, Nishimori H, Ogawa K, Drinkwater NR. Genetic dissection of susceptibility to murine ovarian teratomas that originate from parthenogenetic oocytes. *Cancer Res*. 1997;57(4):590-3.
80. de Foy KA, Gayther SA, Colledge WH, Crockett S, Scott IV, Evans MJ, et al. Mutation analysis of the c-mos proto-oncogene in human ovarian teratomas. *British journal of cancer*. 1998;77(10):1642-4.
81. Youngson NA, Vickaryous N, van der Horst A, Epp T, Harten S, Fleming JS, et al. A missense mutation in the transcription factor Foxo3a causes teratomas and oocyte abnormalities in mice. *Mammalian genome : official journal of the International Mammalian Genome Society*. 2011;22(3-4):235-48.
82. Goldman DS, Kiessling AA, Millette CF, Cooper GM. Expression of c-mos RNA in germ cells of male and female mice. *Proc Natl Acad Sci U S A*. 1987;84(13):4509-13.
83. John GB, Gallardo TD, Shirley LJ, Castrillon DH. Foxo3 is a PI3K-dependent molecular switch controlling the initiation of oocyte growth. *Dev Biol*. 2008;321(1):197-204.
84. Peltoketo H, Strauss L, Karjalainen R, Zhang M, Stamp GW, Segaloff DL, et al. Female mice expressing constitutively active mutants of FSH receptor present with a phenotype of premature follicle depletion and estrogen excess. *Endocrinology*. 2010;151(4):1872-83.
85. Hsu SY, Lai RJ, Finegold M, Hsueh AJ. Targeted overexpression of Bcl-2 in ovaries of transgenic mice leads to decreased follicle apoptosis, enhanced folliculogenesis, and increased germ cell tumorigenesis. *Endocrinology*. 1996;137(11):4837-43.

86. Thurisch B, Liang SY, Sarioglu N, Schomburg L, Bungert J, Dame C. Transgenic mice expressing small interfering RNA against Gata4 point to a crucial role of Gata4 in the heart and gonads. *Journal of molecular endocrinology*. 2009;43(4):157-69.
87. Heikinheimo M, Ermolaeva M, Bielinska M, Rahman NA, Narita N, Huhtaniemi IT, et al. Expression and hormonal regulation of transcription factors GATA-4 and GATA-6 in the mouse ovary. *Endocrinology*. 1997;138(8):3505-14.
88. Fafalios MK, Olander EA, Melhem MF, Chaillet JR. Ovarian teratomas associated with the insertion of an imprinted transgene. *Mammalian genome : official journal of the International Mammalian Genome Society*. 1996;7(3):188-93.
89. Nagy A, Gertsenstein M, Vintersten K, Behringer R. *Manipulating the Mouse Embryo: A Laboratory Manual*. Third ed. Cold Spring Harbor, New York: Cold Spring Harbor Laboratory Press; 2003.
90. Escamilla-Hernandez R, Little-Ihrig L, Orwig KE, Yue J, Chandran U, Zeleznik AJ. Constitutively active protein kinase A qualitatively mimics the effects of follicle-stimulating hormone on granulosa cell differentiation. *Mol Endocrinol*. 2008;22(8):1842-52.
91. Clark SJ, Harrison J, Paul CL, Frommer M. High sensitivity mapping of methylated cytosines. *Nucleic Acids Res*. 1994;22(15):2990-7.
92. Chaillet JR, Bader DS, Leder P. Regulation of genomic imprinting by gametic and embryonic processes. *Genes & development*. 1995;9(10):1177-87.
93. Singer-Sam J, LeBon JM, Dai A, Riggs AD. A sensitive, quantitative assay for measurement of allele-specific transcripts differing by a single nucleotide. *PCR methods and applications*. 1992;1(3):160-3.
94. Pfaffl MW. A new mathematical model for relative quantification in real-time RT-PCR. *Nucleic Acids Res*. 2001;29(9):e45.
95. Cirio MC, Ratnam S, Ding F, Reinhart B, Navara C, Chaillet JR. Preimplantation expression of the somatic form of Dnmt1 suggests a role in the inheritance of genomic imprints. *BMC developmental biology*. 2008;8:9.
96. Barak Y, Nelson MC, Ong ES, Jones YZ, Ruiz-Lozano P, Chien KR, et al. PPAR gamma is required for placental, cardiac, and adipose tissue development. *Molecular cell*. 1999;4(4):585-95.
97. Swain JL, Stewart TA, Leder P. Parental legacy determines methylation and expression of an autosomal transgene: a molecular mechanism for parental imprinting. *Cell*. 1987;50(5):719-27.

98. Kirsch IR, Ravetch JV, Kwan SP, Max EE, Ney RL, Leder P. Multiple immunoglobulin switch region homologies outside the heavy chain constant region locus. *Nature*. 1981;293(5833):585-7.
99. Bourc'his D, Xu GL, Lin CS, Bollman B, Bestor TH. Dnmt3L and the establishment of maternal genomic imprints. *Science (New York, NY)*. 2001;294(5551):2536-9.
100. Chaillet JR, Vogt TF, Beier DR, Leder P. Parental-specific methylation of an imprinted transgene is established during gametogenesis and progressively changes during embryogenesis. *Cell*. 1991;66(1):77-83.
101. Balakrishnan A, Chaillet JR. Role of the inositol polyphosphate-4-phosphatase type II *Inpp4b* in the generation of ovarian teratomas. *Dev Biol*. 2012. Epub 2012/10/20.
102. Kennedy MK, Glaccum M, Brown SN, Butz EA, Viney JL, Embers M, et al. Reversible defects in natural killer and memory CD8 T cell lineages in interleukin 15-deficient mice. *The Journal of experimental medicine*. 2000;191(5):771-80.
103. Fehniger TA, Suzuki K, Ponnappan A, VanDeusen JB, Cooper MA, Florea SM, et al. Fatal leukemia in interleukin 15 transgenic mice follows early expansions in natural killer and memory phenotype CD8⁺ T cells. *The Journal of experimental medicine*. 2001;193(2):219-31.
104. Zouridis H, Deng N, Ivanova T, Zhu Y, Wong B, Huang D, et al. Methylation subtypes and large-scale epigenetic alterations in gastric cancer. *Science translational medicine*. 2012;4(156):156ra40.
105. Dallosso AR, Oster B, Greenhough A, Thorsen K, Curry TJ, Owen C, et al. Long-range epigenetic silencing of chromosome 5q31 protocadherins is involved in early and late stages of colorectal tumorigenesis through modulation of oncogenic pathways. *Oncogene*. 2012;31(40):4409-19.
106. Ferron M, Vacher J. Characterization of the murine *Inpp4b* gene and identification of a novel isoform. *Gene*. 2006;376(1):152-61.
107. Lazzaro MA, Picketts DJ. Cloning and characterization of the murine Imitation Switch (ISWI) genes: differential expression patterns suggest distinct developmental roles for *Snf2h* and *Snf2l*. *Journal of neurochemistry*. 2001;77(4):1145-56.
108. Holgado-Madruga M, Emllet DR, Moscatello DK, Godwin AK, Wong AJ. A Grb2-associated docking protein in EGF- and insulin-receptor signalling. *Nature*. 1996;379(6565):560-4.
109. Leclercq G, Debacker V, de Smedt M, Plum J. Differential effects of interleukin-15 and interleukin-2 on differentiation of bipotential T/natural killer progenitor cells. *The Journal of experimental medicine*. 1996;184(2):325-36.

110. Bolivar J, Diaz I, Iglesias C, Valdivia MM. Molecular cloning of a zinc finger autoantigen transiently associated with interphase nucleolus and mitotic centromeres and midbodies. Orthologous proteins with nine CXXC motifs highly conserved from nematodes to humans. *J Biol Chem*. 1999;274(51):36456-64.
111. Gewinner C, Wang ZC, Richardson A, Teruya-Feldstein J, Etemadmoghadam D, Bowtell D, et al. Evidence that inositol polyphosphate 4-phosphatase type II is a tumor suppressor that inhibits PI3K signaling. *Cancer cell*. 2009;16(2):115-25.
112. Hodgson M, Shao L-J, Frolov A, Li R, Peterson L, Ayala G, et al. Decreased Expression and Androgen Regulation of the Tumor Suppressor Gene INPP4B in Prostate Cancer. *Cancer research*. 2011;71(2):572-82.
113. Brook FA, Gardner RL. The origin and efficient derivation of embryonic stem cells in the mouse. *Proc Natl Acad Sci U S A*. 1997;94(11):5709-12.
114. Li E, Bestor TH, Jaenisch R. Targeted mutation of the DNA methyltransferase gene results in embryonic lethality. *Cell*. 1992;69(6):915-26.
115. Sun H, Lesche R, Li DM, Liliental J, Zhang H, Gao J, et al. PTEN modulates cell cycle progression and cell survival by regulating phosphatidylinositol 3,4,5,-trisphosphate and Akt/protein kinase B signaling pathway. *Proc Natl Acad Sci U S A*. 1999;96(11):6199-204.
116. Stiles B, Gilman V, Khanzenon N, Lesche R, Li A, Qiao R, et al. Essential role of AKT-1/protein kinase B alpha in PTEN-controlled tumorigenesis. *Mol Cell Biol*. 2002;22(11):3842-51.
117. Zhang Q, Claret FX. Phosphatases: the new brakes for cancer development? *Enzyme research*. 2012;2012:659649.
118. Dyson JM, Fedele CG, Davies EM, Becanovic J, Mitchell CA. Phosphoinositide phosphatases: just as important as the kinases. *Sub-cellular biochemistry*. 2012;58:215-79.
119. Yamada Y, Watanabe H, Miura F, Soejima H, Uchiyama M, Iwasaka T, et al. A comprehensive analysis of allelic methylation status of CpG islands on human chromosome 21q. *Genome research*. 2004;14(2):247-66.
120. Han SJ, Vaccari S, Nedachi T, Andersen CB, Kovacina KS, Roth RA, et al. Protein kinase B/Akt phosphorylation of PDE3A and its role in mammalian oocyte maturation. *The EMBO journal*. 2006;25(24):5716-25.
121. Fedele C, Ooms L, Ho M, Vieuxseux J, O'Toole S, Millar E, et al. Inositol polyphosphate 4-phosphatase II regulates PI3K/Akt signaling and is lost in human basal-like breast cancers. *Proceedings of the National Academy of Sciences of the United States of America*. 2010;107(51):22231-6.

122. Richards JS, Sharma SC, Falender AE, Lo YH. Expression of FKHR, FKHRL1, and AFX genes in the rodent ovary: evidence for regulation by IGF-I, estrogen, and the gonadotropins. *Mol Endocrinol.* 2002;16(3):580-99.
123. Manning BD, Cantley LC. AKT/PKB signaling: navigating downstream. *Cell.* 2007;129(7):1261-74.
124. Fan HY, Shimada M, Liu Z, Cahill N, Noma N, Wu Y, et al. Selective expression of KrasG12D in granulosa cells of the mouse ovary causes defects in follicle development and ovulation. *Development.* 2008;135(12):2127-37.
125. Hsueh AJ, McGee EA, Hayashi M, Hsu SY. Hormonal regulation of early follicle development in the rat ovary. *Molecular and cellular endocrinology.* 2000;163(1-2):95-100.
126. Huang H, Tindall DJ. Dynamic FoxO transcription factors. *Journal of cell science.* 2007;120(Pt 15):2479-87.
127. Bansal VS, Caldwell KK, Majerus PW. The isolation and characterization of inositol polyphosphate 4-phosphatase. *J Biol Chem.* 1990;265(3):1806-11.
128. Norris FA, Atkins RC, Majerus PW. The cDNA cloning and characterization of inositol polyphosphate 4-phosphatase type II. Evidence for conserved alternative splicing in the 4-phosphatase family. *J Biol Chem.* 1997;272(38):23859-64.
129. Norris FA, Majerus PW. Hydrolysis of phosphatidylinositol 3,4-bisphosphate by inositol polyphosphate 4-phosphatase isolated by affinity elution chromatography. *J Biol Chem.* 1994;269(12):8716-20.
130. Ma K, Cheung SM, Marshall AJ, Duronio V. PI(3,4,5)P3 and PI(3,4)P2 levels correlate with PKB/akt phosphorylation at Thr308 and Ser473, respectively; PI(3,4)P2 levels determine PKB activity. *Cell Signal.* 2008;20(4):684-94.
131. Cannon JD, Cherian-Shaw M, Lovekamp-Swan T, Chaffin CL. Granulosa cell expression of G1/S phase cyclins and cyclin-dependent kinases in PMSG-induced follicle growth. *Molecular and cellular endocrinology.* 2007;264(1-2):6-15.
132. Jagarlamudi K, Liu L, Adhikari D, Reddy P, Idahl A, Ottander U, et al. Oocyte-specific deletion of Pten in mice reveals a stage-specific function of PTEN/PI3K signaling in oocytes in controlling follicular activation. *PLoS one.* 2009;4(7):e6186.
133. Maehama T, Dixon JE. The tumor suppressor, PTEN/MMAC1, dephosphorylates the lipid second messenger, phosphatidylinositol 3,4,5-trisphosphate. *J Biol Chem.* 1998;273(22):13375-8.
134. Gonzalez-Robayna IJ, Falender AE, Ochsner S, Firestone GL, Richards JS. Follicle-Stimulating hormone (FSH) stimulates phosphorylation and activation of protein kinase

- B (PKB/Akt) and serum and glucocorticoid-induced kinase (Sgk): evidence for A kinase-independent signaling by FSH in granulosa cells. *Mol Endocrinol.* 2000;14(8):1283-300.
135. Hunzicker-Dunn ME, Lopez-Biladeau B, Law NC, Fiedler SE, Carr DW, Maizels ET. PKA and GAB2 play central roles in the FSH signaling pathway to PI3K and AKT in ovarian granulosa cells. *Proc Natl Acad Sci U S A.* 2012.
 136. Castrillon DH, Miao L, Kollipara R, Horner JW, DePinho RA. Suppression of ovarian follicle activation in mice by the transcription factor Foxo3a. *Science.* 2003;301(5630):215-8.
 137. Alimonti A, Carracedo A, Clohessy JG, Trotman LC, Nardella C, Egia A, et al. Subtle variations in Pten dose determine cancer susceptibility. *Nat Genet.* 2010;42(5):454-8.
 138. Berger AH, Knudson AG, Pandolfi PP. A continuum model for tumour suppression. *Nature.* 2011;476(7359):163-9.
 139. Ferron M, Boudiffa M, Arsenault M, Rached M, Pata M, Giroux S, et al. Inositol polyphosphate 4-phosphatase B as a regulator of bone mass in mice and humans. *Cell metabolism.* 2011;14(4):466-77.
 140. Watanabe S, Umehara H, Murayama K, Okabe M, Kimura T, Nakano T. Activation of Akt signaling is sufficient to maintain pluripotency in mouse and primate embryonic stem cells. *Oncogene.* 2006;25(19):2697-707.
 141. Eppig JJ, Wigglesworth K, Hirao Y. Metaphase I arrest and spontaneous parthenogenetic activation of strain LTXBO oocytes: chimeric reaggregated ovaries establish primary lesion in oocytes. *Dev Biol.* 2000;224(1):60-8.
 142. Hupalowska A, Kalaszczynska I, Hoffmann S, Tsurumi C, Kubiak JZ, Polanski Z, et al. Metaphase I arrest in LT/Sv mouse oocytes involves the spindle assembly checkpoint. *Biol Reprod.* 2008;79(6):1102-10.
 143. Ciemerych MA, Kubiak JZ. Cytostatic activity develops during meiosis I in oocytes of LT/Sv mice. *Dev Biol.* 1998;200(2):198-211.
 144. Hayashi S, Lewis P, Pevny L, McMahon AP. Efficient gene modulation in mouse epiblast using a Sox2Cre transgenic mouse strain. *Gene expression patterns : GEP.* 2002;2(1-2):93-7.
 145. Lecureuil C, Fontaine I, Crepieux P, Guillou F. Sertoli and granulosa cell-specific Cre recombinase activity in transgenic mice. *Genesis.* 2002;33(3):114-8.
 146. Miyazaki S, Shirakawa H, Nakada K, Honda Y. Essential role of the inositol 1,4,5-trisphosphate receptor/Ca²⁺ release channel in Ca²⁺ waves and Ca²⁺ oscillations at fertilization of mammalian eggs. *Dev Biol.* 1993;158(1):62-78.

147. Jellerette T, He CL, Wu H, Parys JB, Fissore RA. Down-regulation of the inositol 1,4,5-trisphosphate receptor in mouse eggs following fertilization or parthenogenetic activation. *Dev Biol.* 2000;223(2):238-50.
148. Wakai T, Vanderheyden V, Yoon SY, Cheon B, Zhang N, Parys JB, et al. Regulation of inositol 1,4,5-trisphosphate receptor function during mouse oocyte maturation. *Journal of cellular physiology.* 2012;227(2):705-17.
149. Mehlmann LM, Mikoshiba K, Kline D. Redistribution and increase in cortical inositol 1,4,5-trisphosphate receptors after meiotic maturation of the mouse oocyte. *Dev Biol.* 1996;180(2):489-98.
150. Uranga JA, Pedersen RA, Arechaga J. Parthenogenetic activation of mouse oocytes using calcium ionophores and protein kinase C stimulators. *The International journal of developmental biology.* 1996;40(2):515-9.